



THE HONG KONG
POLYTECHNIC UNIVERSITY

香港理工大學

Pao Yue-kong Library

包玉剛圖書館

Copyright Undertaking

This thesis is protected by copyright, with all rights reserved.

By reading and using the thesis, the reader understands and agrees to the following terms:

1. The reader will abide by the rules and legal ordinances governing copyright regarding the use of the thesis.
2. The reader will use the thesis for the purpose of research or private study only and not for distribution or further reproduction or any other purpose.
3. The reader agrees to indemnify and hold the University harmless from and against any loss, damage, cost, liability or expenses arising from copyright infringement or unauthorized usage.

IMPORTANT

If you have reasons to believe that any materials in this thesis are deemed not suitable to be distributed in this form, or a copyright owner having difficulty with the material being included in our database, please contact lbsys@polyu.edu.hk providing details. The Library will look into your claim and consider taking remedial action upon receipt of the written requests.

The Hong Kong Polytechnic University

Department of Building Services Engineering

**Effect of Elastic Boundary Supports and Stiffening
Treatments on Vibroacoustic Response of Plate-like
Structures**

Ou Dayi

**A thesis submitted in partial fulfillment of the requirements for the
Degree of Doctor of Philosophy**

June 2011

Certificate of Originality

I hereby declare that this thesis is my own work and that, to the best of my knowledge and belief, it reproduces no material previously published or written, nor material that has been accepted for the award of any other degree or diploma, except where due acknowledgement has been made in the text. I also declare that the intellectual content of this thesis is the product of my own work, even though I may have received assistance from others on style, presentation and language expression.

_____ (Signed)

Ou Dayi _____ (Name of student)

Department of Building Services Engineering

The Hong Kong Polytechnic University

Hong Kong, China

June, 2011

Dedication

To my parents

Ou Jianzu and Wei Xiaoxiong

and my sister

Dana

who always provide me with unconditional love and support

To my wife

Pan Sensen

who fully supports my career with her love and has been waiting for this day
patiently

Abstract

Most of the complicated structures or systems in buildings or engineering industries can be modeled as thin plates. A better understanding of the vibroacoustic behavior of thin plates can be useful for improving the sound insulation of a practical structure. In this thesis, the vibroacoustic responses of unstiffened and stiffened, thin plates with arbitrary elastic boundary supports (or called “elastic boundary conditions”) were investigated. Both the steady-state and the transient vibroacoustic behaviors of the plate were studied. The aim of this thesis was to examine the effects of the elastic boundary supports and the stiffeners on the vibroacoustic performance of plate structures in order to provide guidance to the design and installation of plate-like structures for sound insulation.

A method was first developed to determine the actual boundary condition of the plate system; this was based on a coupled finite element and boundary element method (FEM/BEM) in frequency domain. The fluid loading effect was taken into account by coupling the acoustic equation with the elastic equation. This model was then improved and applied to predict the steady-state vibration and sound radiation (SVSR) of a stiffened plate; this allowed for an efficient computation of a plate with arbitrary boundary conditions and with arbitrarily located stiffeners. The effects of

the stiffeners on the sound transmission loss (STL) of a window were then studied in the parametric studies.

Another method was proposed to predict the transient vibration and sound radiation (TVSR) of a plate with arbitrary elastic boundary supports, which was based on the time-domain finite element method (TDFEM) and time-domain boundary element method (TDBEM). This model was then improved and applied to predict the TVSR of a stiffened plate. In parametric studies, the maximum acceleration and maximum radiated sound pressure were calculated to examine the effects of the boundary supports and the stiffeners.

Extensive experiments were carried out in two connected semi-anechoic chambers at The Hong Kong Polytechnic University; these included the STL measurements of unstiffened and stiffened plate structures and the transient sound radiation measurements of unstiffened and stiffened plate structures. The proposed boundary condition identification method was used to identify the actual boundary conditions of the plate structures used in the experiments. The measured results were used to validate the prediction methods. The predicted results agreed well with measured data.

Both the results of the experiments and the parametric studies clearly demonstrated the significant effects of the elastic boundary supports and the stiffeners on the vibroacoustic responses of a practical plate structure. It is believed that the sound insulation (or vibration isolation) performance of a plate structure can be improved through an appropriate use of the elastic boundary supports or stiffeners or both. The proposed prediction models can therefore be effective design tools for this purpose.

Publications Arising from the Thesis

Published and accepted journal papers

D.Y. Ou and C.M. Mak. Experimental validation of the sound transmission of rectangular baffled plates with general elastic boundary conditions. *Journal of the Acoustical Society of America* 129, EL274-EL279 (2011).

D.Y. Ou and C.M. Mak. The effects of elastic supports on the transient vibroacoustic response of a window caused by sonic booms. Accepted by *Journal of the Acoustical Society of America* (2010).

Conference papers

D.Y. Ou and C.M. Mak. The effects of stiffeners on the transient vibroacoustic response of a window. *Proceeding of Inter-noise 2011*, Osaka, Japan.

Papers under review

D.Y. Ou and C.M. Mak. Numerical and experimental study of sound transmission through a stiffened window with general elastic boundary supports. Submitted to *Journal of the Acoustical Society of America* (2011).

D.Y. Ou, C.M. Mak and S.M. Deng. Prediction of the sound transmission loss of a stiffened window. Submitted to *Building Services Engineering Research and Technology* (2011).

D.Y. Ou and C.M. Mak. Transient vibration and sound radiation of a stiffened window. Submitted to *Acta Acustica united with Acustica* (2011).

A paper in preparation

D.Y. Ou and C.M. Mak. Transient sound radiation of a stiffened plate with arbitrary elastic boundary conditions. In preparation.

Acknowledgements

I would like to express appreciation to my chief supervisor, Dr. Mak Cheuk-ming, who has provided an invaluable guidance and warm encouragement to me as well as a full support and a thoughtful consideration from the initial to the final stage to enable me to complete this study. He has my sincere gratitude and respect.

I would also like to express the gratitude to my Co-supervisor, Prof. Deng Shi-ming, for his valuable advice and help during my study.

Furthermore, I would like to thank all the members in our research group and all my friends for their kind help both in my study and in my life during the past years.

All works including numerical work and experimental work reported in this PhD thesis were entirely conducted in the Hong Kong Polytechnic University. Before I conducted and planned all works reported in this thesis, I had an attachment in Purdue University. I would like to thank Purdue University for providing me with this opportunity and thank Prof. K. M. Li for his kind help when I was in Purdue University.

Nomenclature

A_{\max}	Maximum value of the acceleration level
$\{B_s\}$	Strain matrix of the stiffener
c	Sound propagation speed
D	Flexural rigidity of the plate
$\{D\}$	Global damping of the plate system
$\{D_s\}$	Rigidity matrix of the stiffener
F	External force adding on the plate
f_1, f_2	Lower and upper frequencies of the given frequency range
h	Plate thickness
$\{H\}$	Global matrix formed by the “collocation” procedure in BEM
$\{K\}$	Global stiffness of the plate system
$\{K_p\}_e$	Stiffness matrices of the plate in the element
$\{K_b\}_e$	Stiffness matrices of the boundary support in the element
$\{K_s\}_e$	Stiffness matrices of the stiffener in the element
k	Stiffness (spring constant)
\bar{k}	Dimensionless forms of k
k_{tb}	Boundary stiffness (spring constant) in the transverse direction
k_{rb}	Boundary stiffness (spring constant) in the rotational direction
k_{nb}	Boundary stiffness (spring constant) in the in-plane direction normal to the edge
k_{mb}	Boundary stiffness (spring constant) in the in-plane direction tangential to the edge

k_{ts}	Stiffener stiffness (spring constant) in the transverse direction
k_{rs}	Stiffener stiffness (spring constant) in the rotational direction
L_x	Plate length
L_y	Plate width
l_s	Stiffener axis
$\{M\}$	Global mass of the plate system
$\{M_p\}_e$	Mass matrices of the plate in the element
$\{M_s\}_e$	Mass matrices of the stiffener in the element
$\{N\}$	Shape function vectors for the displacements
$\{N_w\}$	Shape function vectors for the lateral displacement field
$\{N_u\}, \{N_v\}$	Shape function vectors for the axial displacement field
\vec{n}	Unit normal direction on the integration area
\vec{n}_b	Unit normal vector of the element boundary contour
\vec{n}_r	Unit tangent vector of the element boundary contour
\vec{n}_s	Unit normal vector of the stiffener axis
p_0	Sound pressure of the incidence wave
p	Sound pressure
$\{P_0\}$	Sound pressure of the incidence wave in vector format
$\{P^+\}$	Sound pressures on the front plate surfaces
$\{P^-\}$	Sound pressures on the back plate surfaces
r_s	Radius of the stiffener

r	Distance function
$\{\mathcal{R}\}$	Transformation matrix converting the nodal displacement vector to the nodal transverse deflection vector
S	Integration area
S_b	Baffle area
S_p	Plate area
SPL_{\max}	Maximum value of radiated sound pressure level
STL_{overall}	Overall STL
ΔS	Area of the plate element
t	Time
Δt	Time step
$\{T_s\}, \{T'_s\}$	Transformation matrices relating the stiffener global and local axes
$\{\mathcal{T}\}$	Transformation matrix converting fluid pressure to point forces that act on the nodes of the plate
$\{U\}$	Global nodal displacement vector
$\{\dot{U}\}$	Global nodal velocity vector
$\{\ddot{U}\}$	Global nodal acceleration vector
$\{U\}_e$	Element nodal displacement vector
u, v	In-plane displacements
V^+	Source section in fluid medium
V^-	Receiver section in fluid medium
W^+	Sound power at the front plate surface
W^-	Radiated sound power at the back plate surface
w	Transverse deflection

x, y	Cartesian Coordinates
Γ_b	Boundary contour
θ	Angle between the global axis and the local axis of the stiffener
σ_s	Line density function describing the added-mass effect caused by the stiffener
η	Damping factor of the plate system
ω_0	Fundamental natural frequency of the plate system
α, γ	Standard Newmark parameters
σ	Fundamental pressure
σ^*	Fundamental flux
σ_H	Half-space fundamental pressure solution
δ	Dirac delta function
ρ_0	Fluid density

Table of Contents

Certificate of Originality	I
Dedication	II
Abstract.....	III
Publications Arising from the Thesis.....	VI
Acknowledgements.....	VII
Nomenclature.....	VIII
Table of Contents.....	XII
List of Figures	XVI
List of Tables.....	XX
Chapter 1.....	1
Introduction	1
1.1 Background	1
1.2 Objectives of the Study	3
1.3 Structure of the Thesis.....	4
Chapter 2.....	7
Literature Review.....	7
2.1 Thin Plate Structures	7
2.2 General Boundary Conditions.....	10
2.3 Stiffened Plate Structures	12
2.4 Finite Element Method and Boundary Element Method	15
Chapter 3.....	18
Boundary Condition Identification of a Single Plate System.....	18
3.1 Introduction.....	18
3.2 Boundary Condition Identification Method	19

3.2.1	<i>Description of the Problem</i>	19
3.2.2	<i>Characteristic Equation of the Plate System</i>	20
3.2.3	<i>Stiffness and Mass Matrices of the Plate System</i>	22
3.2.4	<i>Identification Procedure</i>	24
3.3	Identification of Practical Plate systems	26
3.3.1	<i>Experimental Setup</i>	26
3.3.2	<i>Modal Testing</i>	27
3.3.3	Identification Results and Discussion	29
3.4	Summary	31
Chapter 4	33
A Study of the Effects of Elastic Supports on the Transient Vibroacoustic Response of a Single Plate	33
4.1	Introduction	33
4.2	Theoretical Framework	35
4.2.1	<i>Description of the Problem</i>	35
4.2.2	<i>Time-domain Finite Element Method (TDFEM)</i>	35
4.2.3	<i>Time-domain Boundary Element Method (TDBEM)</i>	37
4.3	Experimental Validation	39
4.3.1	<i>Experimental Setup</i>	39
4.3.2	<i>Experimental Results and Discussion</i>	41
4.4	Parametric Studies	45
4.5	Summary	50
Chapter 5	52
A Study of the Effects of Spring-type Stiffeners on the Sound Transmission Loss of a Single Plate with General Elastic Boundary Conditions	52
5.1	Introduction	52
5.2	Theoretical Framework	54

5.2.1	<i>Description of the Problem</i>	54
5.2.2	<i>The Coupled Vibroacoustic Model (Coupled FEM/BEM)</i>	55
5.2.3	<i>Stiffness and Mass Matrices of the Whole Stiffened Plate System</i>	56
5.2.4	<i>Sound Transmission Loss (STL)</i>	58
5.3	Experimental Validation	59
5.3.1	<i>Experimental Setup</i>	59
5.3.2	<i>Parameters of the Boundary Supports and the Stiffener</i>	62
5.3.3	<i>Experimental Results and Discussion</i>	63
5.4	Parametric Studies	65
5.5	Summary	68
Chapter 6	70
	A Study of the Effects of Spring-type Stiffeners on the Transient Vibroacoustic	
	Response of a Single Plate with General Elastic Boundary Conditions	70
6.1	Introduction	70
6.2	Theoretical Framework	71
6.2.1	<i>Description of the Problem</i>	71
6.2.2	<i>Time-domain Vibroacoustic Model</i>	72
6.3	Experimental Validation	73
6.3.1	<i>Experimental Setup</i>	73
6.3.2	<i>Experimental Results and Discussion</i>	74
6.4	Parametric Studies	78
6.5	Summary	83
Chapter 7	85
	A Study of the Effects of Beam-type Stiffeners on the Sound Transmission Loss	
	of a Single Plate with General Elastic Boundary Conditions	85
7.1	Introduction	85
7.2	Theoretical Framework	87

7.3 Numerical Results and Discussion.....	91
7.3.1 Concentrically Stiffened Plate.....	91
7.3.2 Eccentrically Stiffened Plate.....	92
7.3.3 Stiffened Window Simulation.....	93
7.4 Summary.....	96
Chapter 8.....	98
A Study of the Effects of Beam-type Stiffeners on the Transient Vibroacoustic Response of a Single Plate with General Elastic Boundary Conditions.....	98
8.1 Introduction.....	98
8.2 Theoretical Framework.....	99
8.3 Numerical Results and Discussion.....	100
8.3.1 Comparisons with Existing Published Results.....	100
8.3.2 Parametric Studies.....	102
8.4 Summary.....	107
Chapter 9.....	109
Conclusions and Suggestions for Future Work.....	109
9.1 Conclusion.....	109
9.2 Suggestions for Future Work.....	114
Appendix.....	118
A.1 Mesh Method.....	118
A.2 Computational Time.....	119
A.3 MATLAB Codes.....	120
A.4 Photos of the Experimental Setup at The Polytechnic University.....	124
References.....	128

List of Figures

Figure 3.1 A rectangular plate with elastic boundary supports along the edges (for simplicity and clarity, only the supports along the left edge are shown)	20
Figure 3.2 A rectangular plate mounted on an infinite rigid baffle	20
Figure 3.3 A rectangular plate element.....	24
Figure 3.4 The plate system used in the modal testing: (a) Schematic diagram of the baffled plate system; (c) Picture of the baffled plate system (front view)	27
Figure 3.5 Locations of accelerometer and impact points on the panel	28
Figure 3.6 Solutions for \bar{k}_{tb} and \bar{k}_{rb} that satisfy the characteristic equation of Panel 1	30
Figure 3.7 Solutions for \bar{k}_{tb} and \bar{k}_{rb} that satisfy the characteristic equation of Panel 2	30
Figure 4.1 A baffled rectangular plate subjected to transient forces (or transient incidence waves)	35
Figure 4.2 Schematic diagram of the experimental setup for measuring the TVSR of a baffled plate system.....	40
Figure 4.3 Locations of the impact force and the accelerometer	41
Figure 4.4 Comparison of the predicted results and experimental data: (a) Impact force time history; (b) Acceleration time history; (c) Pressure time history of “Mic 1”; (d) Pressure time history of “Mic 2”	44
Figure 4.5 A transient sound pulse (a triangular wave): (a) Pressure time history; (b) Pressure frequency spectrum	46
Figure 4.6 Acceleration responses at the center of the window	47
Figure 4.7 Radiated sound pressure at point “P”. Point “P” is on the axis of symmetry a distance of 0.1 m away from the window	48
Figure 4.8 The maximum values of the acceleration level and radiated sound pressure level as a function of rotational stiffness: (a) Maximum acceleration level;	

(b) Maximum radiated sound pressure level.....	50
Figure 5.1 A rectangular stiffened plate with elastic boundary supports along the edges (for simplicity and clarity, only the supports along the left edge are shown).....	54
Figure 5.2 A baffled rectangular plate subjected to incident plane waves	55
Figure 5.3 The stiffened plate element. A local (x' , y') axis is set along the tangent to the stiffener at the integration point P making an angle θ with the global (x , y) axis	58
Figure 5.4 Schematic diagram of the assembly of the stiffened plate system used in the experiments: (a) Before assembly; (b) After assembly	60
Figure 5.5 Schematic diagram of the experimental setup for measuring the STL of a baffled stiffened plate system.....	62
Figure 5.6 Comparison of the predicted and measured results: (a) Stiffened plate; (b) Unstiffened plate	64
Figure 5.7 Schematic diagram of the stiffened window.....	66
Figure 5.8 STL values for the stiffened window with respect to θ : (a) STL curves from 1 Hz to 300 Hz; (b) Overall STL values (25 Hz~100 Hz)	68
Figure 6.1 A baffled rectangular stiffened plate subjected to transient forces (or transient incidence waves)	72
Figure 6.2 Schematic diagram of the experimental setup for measuring the transient sound radiation of a baffled stiffened plate system.....	74
Figure 6.3 Locations of the stiffener and the impact force	74
Figure 6.4 Comparison of the predicted results and experimental data: (a) Pressure time history; (b) Pressure frequency spectrum. Note that predicted radiated pressure of the unstiffened plate is also included.....	76
Figure 6.5 Impact force: (a) Time history; (b) Frequency spectrum.....	77
Figure 6.6 Schematic diagram of the stiffened window.....	79
Figure 6.7 A transient sound pulse (a half-sine wave): (a) Pressure time history; (b) Pressure frequency spectrum	80

Figure 6.8 Acceleration responses at the center of the window: (a) Acceleration time history; (b) Acceleration frequency spectrum.....	80
Figure 6.9 Radiated sound pressure at point “P”: (a) Pressure time history; (b) Pressure frequency spectrum. Point “P” is on the axis of symmetry a distance of 0.1 m away from the window.....	81
Figure 6.10 The maximum values of the acceleration level and radiated sound pressure level as a function of θ : (a) Maximum acceleration level; (b) Maximum radiated sound pressure level	83
Figure 7.1 Elastic boundary supports along the edges (for simplicity and clarity, only the supports along the right edge are shown).....	90
Figure 7.2 A sketch of the concentrically stiffened plate	91
Figure 7.3 A sketch of the eccentrically stiffened plate	92
Figure 7.4 Schematic diagram of the stiffened window.....	94
Figure 7.5 STL plotted as a function of frequency for different values of r_s	95
Figure 7.6 Overall STL values (25Hz~100 Hz) as a function of r_s	96
Figure 8.1 A simply supported stiffened plate. Point B is at the center of the left half panel.....	101
Figure 8.2 Time history of deflection at point “B” of the stiffened plate. Point “B” is shown in Fig. 8.1	101
Figure 8.3 Schematic diagram of the stiffened window.....	102
Figure 8.4 Acceleration responses at the center of the window: (a) Acceleration time history; (b) Acceleration frequency spectrum.....	104
Figure 8.5 Radiated sound pressure at point “P”: (a) Pressure time history; (b) Pressure frequency spectrum. Point “P” is on the axis of symmetry a distance of 0.1 m away from the window.....	105
Figure 8.6 The maximum values of the acceleration level and radiated sound pressure level as a function of r_s : (a) Maximum acceleration level; (b) Maximum radiated sound pressure level	107
Figure A.1 Flow chart for the decision of mesh size.....	118

Figure A.2 The hole of the common wall between the two chambers. The yellow stuff is the acoustic absorptive material in the inside chamber.....	124
Figure A.3 Installation of the plate system.....	125
Figure A.4 A view of one of the two chambers after plate installation.....	125
Figure A.5 A loudspeaker box as a plane wave source	126
Figure A.6 A hammer as an impact source.....	126
Figure A.7 Microphones setup in the receiving chamber for measuring the radiated (transmitted) sound field.	127

List of Tables

Table 3.1 Measured and predicted natural frequencies (Hz) of Panel 1	28
Table 3.2 Measured and predicted natural frequencies (Hz) of Panel 2	28
Table 7.1 Natural frequencies of the clamped plate with a concentric stiffener.....	92
Table 7.2 Natural frequencies of the simply supported plate with an eccentric stiffener	93
Table A. 1 Computational Time & Hardware and Software.....	119

Chapter 1

Introduction

1.1 Background

Noise produced by vibrating structures is commonly caused by steady-state (or quasi-steady-state) sources such as compressors, pumps and fans, and transient sources such as impacts, construction work, road traffic noise, and the noise generated by the take-off and landing of airplanes. It is necessary to develop a method that is able to accurately predict noise radiated by vibrating structures due to different types of steady-state and transient sources.

Elastic plate-like structures (hereafter to be referred as “plate structures”) are widely used as primary structural components for variety of applications. The study of the plate structure can serve as a first step in understanding and assessing the dynamic and acoustic behavior of more complicated structures in real life, such as windows, walls, floor and ceiling of buildings, the outer hulls of ships and windows and shells of vehicles. In the analysis of plate structures, the classical plate theory (or called Kirchhoff thin-plate theory) is commonly used, in which the effects of rotatory inertia and shear are ignored. Such simplifications are widely recognized as valid

when the wavelength in the plate is not less than eight times the plate thickness [1-3].

It is well known that the properties of the boundary supports are important in the analysis of the dynamic and acoustic behavior of the structures [4-7]. Different boundary supports (also called “boundary conditions”) can lead to different vibroacoustic responses, especially in the low frequency domain. Another way to affect the vibroacoustic response is stiffening the structure with stiffeners [8-10]. Different types of stiffeners or different stiffeners’ locations can give rise to different vibroacoustic responses. Both the effects of the boundary supports and the stiffeners are of great interest to researchers, as they can be utilized to improve the structural performance. However, effective tools are still lacking for the vibroacoustic analysis of structures which have complex boundary conditions and stiffeners with complex shapes (or complex layout), and even for the transient vibration and sound radiation analysis.

Apart from a few analytically solvable cases, there is no general solution for the dynamic and acoustic analysis of complicated structures [7]. As computer resources become less expensive and more readily available, computational methods are becoming increasingly viable tools for solving these problems. In this situation,

approximate or numerical solution techniques at times are found to be useful tools especially for that of complex geometries and boundary conditions. Among the numerical models, the finite element method (FEM) is the most versatile and widely used method to predict the dynamic response of structures while the boundary element method (BEM) is proved to be an efficient analysis tool in examining the corresponding acoustic radiation problem.

1.2 Objectives of the Study

The principal objective of this research is to study numerically and experimentally the effects of different boundary supports and stiffeners on the vibroacoustic response of thin plate structures, and to develop the methods that can optimize the design of such structures.

The steps to help achieve the main objective are as follows:

1. To develop a method to identify the structural boundary condition of practical plate systems. The boundary conditions of the plate systems used in the experimental studies can then be identified by using this method.
2. To develop a prediction method that can effectively examine the effects of arbitrary elastic boundary conditions on the vibroacoustic response of plate structures, especially on the transient vibration and sound radiation (TVSR). In

this method, the elastic boundary conditions are modeled as a combination of translational and rotational springs.

3. To develop prediction methods that can effectively examine the effects of arbitrarily located stiffeners on the vibroacoustic response of plate structures, including the steady-state vibration and sound radiation (SVSR) and transient vibration and sound radiation (TVSR). In these methods, two different stiffener models are used to describe the stiffeners. For clarity, the first model is called “spring-type stiffener” model hereinafter, in which the stiffeners are represented as a combination of masses, translational and rotational springs. The other model is called “beam-type stiffener” model hereinafter, in which the stiffeners are represented as beam elements and the mass, axial force, bending moment, and torsional moment are considered in the beam element.
4. To conduct experimental studies on both the steady-state and transient vibroacoustic responses of unstiffened and stiffened plate systems to validate the developed methods.
5. To conduct parametric studies on unstiffened and stiffened window to check the possibility of using the proposed methods to optimize the window design.

1.3 Structure of the Thesis

The thesis is arranged in the following way. In Chapter 2, the past works related to

this study are reviewed and discussed.

Chapter 3 presents an identification method that can be used to identify the actual boundary condition of the plate structure. The method is developed based on a coupled FEM/BEM method. The procedure of the proposed method is illustrated through the identification of two practical plate systems.

Chapter 4 presents a method for predicting the TVSR of plate structures with arbitrary elastic boundary conditions, as well as the corresponding experimental validation. By using this method, the effects of various boundary conditions on the TVSR of a window are examined.

Based on the “spring-type stiffener” model, Chapter 5 presents a method for predicting the SVSR of stiffened plate structures with arbitrary elastic boundary conditions. The sound transmission loss (STL) of a stiffened plate system is measured to validate the proposed method. The effects of the stiffener on the sound transmission loss (STL) of a window are also studied in a parametric study.

Based on the “spring-type stiffener” model, Chapter 6 presents a method for predicting the TVSR of stiffened plate structures with arbitrary elastic boundary

conditions. The transient radiated sound pressure of a stiffened plate system is measured to validate the proposed method. Parametric studies are also carried out to examine the effects of the stiffener on the TVSR of a window.

Chapter 7 presents a method that is used for predicting the SVSR of stiffened plate structures. This method is similar to that mentioned in Chapter 5 but is based on the “beam-type stiffener” model. Numerical studies are conducted to analyze the natural frequencies of different types of stiffened plates and compared with earlier published results. The possibility of improving the sound insulation of a practical window by using stiffeners is also checked by the numerical simulations.

Chapter 8 presents a method for predicting the TVSR of stiffened plate structures. This method is similar to that mentioned in Chapter 6 but is based on the “beam-type stiffener” model. The performance of the proposed method is checked by analyzing the transient response of a stiffened plate and comparing the results with those of earlier published work. Parametric studies on the stiffened window by using the proposed method are also given.

The final chapter, Chapter 9 provides the conclusions to all the relevant methods and the findings in the thesis, as well as the suggestions for future work.

Chapter 2

Literature Review

It has been stated in Chapter 1 that the main purpose of this thesis is to study the effects of different boundary supports and stiffeners on the vibroacoustic response of thin plate structures. In this chapter, the previous works relevant to this study are reviewed and discussed.

2.1 Thin Plate Structures

Thin plate is an important structural element that is widely used as primary structural components for variety of applications; hence the characteristics of plate vibration, sound radiation and transmission have been extensively studied. A systematic summary of the history of the plate theory development was given by Ventsel et al. [11]. Another excellent review and survey of the topics of vibration of plates were compiled by Leissa [12], in which the major analytical and numerical results of a thin plate with various classical boundary conditions, such as free, simply supported, and clamped, were summarized.

Sound transmission (insulation) of thin plates has also been studied by numerous investigators [13-21]. Mass law is the simplest formula to determine the sound

transmission of thin plates below the coincidence frequency; it is obtained based on the infinite plate assumption. Novikov [20] provided a theoretical and experimental study on the sound transmission of a finite plate in a finite baffle at low frequencies and proposed a correction to the mass law. Several transmission loss equations for single or double plate structures have been summarized by Beranek [13]. In his book, the transmission of the single panel was divided into three well-known regions which were stiffness-controlled region, mass controlled region and wave-coincidence controlled region. In addition to dealing with the sound insulation problems of finite plates, a number of methods such as the statistical energy analysis [14], modal analysis [15, 17, 18] and numerical methods (like FEM/BEM) [21] have been developed. Moreover, the transmission of sound between two rooms coupled by a panel was studied by Mulholland et al. [16], in which they concluded that both the resonances of the panel and the room were important to the low-frequency insulation. A later study by Osipov et al. [19] considered a room-plate-room model, by which the effects of the parameters, such as the room's dimensions, the reverberation time and position of the source, on the sound transmission could be examined. The results again showed the sound transmission depends not only on the test plate but also the geometry of the rooms.

Since a large number of the actual excitations in daily life are transient in nature [22],

many prediction method and experiments have been developed to investigate the transient vibroacoustic response of the plate structures. The first investigation of sound radiation from impacted plates was probably done by Strasberg [23], who in 1948 calculated the radiated sound power from a diaphragm excited by periodic impacts. One of the earliest experimental studies of this subject was probably carried out by Tokia in 1961 [24], who conducted measurements of the vibration acceleration of a plate and the sound pressure near the plate surface. Discussions about the effects of the hammer momentum, plate's thickness, stiffness on the acceleration and the sound pressure were also given in his work. Since then many investigations [2, 3, 25-29] on the theoretical analysis of the mechanism of impact noise generation by plates have been carried out, some of which [2, 3, 25] were focused on the transient sound radiation from the plate excited by a collision force, while the others were focused on the analysis of sound radiation from plates excited by impulsive sound wave [26-29]. An extensive review of impact noise was completed by Akay [22]. Five mechanisms contributed to the impact noise generation were summarized, which were air ejection, rigid body radiation, radiation due to rapid surface deformations, pseudo-steady-state radiation and radiation from material fracture.

2.2 General Boundary Conditions

The properties of the boundary supports have significant effects on the vibroacoustic response of the plate structure. In the past two decades, numerical prediction methods [4, 6, 30, 31] have been developed to examine the effects of general boundary conditions. These methods were not only limited to the application to the classical boundary conditions but also to the non-classical boundary conditions. In these studies, a combination of translational and rotational springs without mass was commonly used in the modeling of the boundary supports; and arbitrary translational and rotational spring constants could be used to represent arbitrary elastic boundary conditions.

It is known that there exists no exact solution except for the special cases such as simply supported boundary conditions along at least one pair of opposite edges [7], and for other boundary conditions, however, the approximate methods need to be used. For instance, the Rayleigh-Ritz method was used by Berry et al. [4] to develop a general formulation for predicting the sound radiation from plates with general boundary conditions, and by Park et al. [31] to examine the influence of the plate boundary properties on the sound radiation. These studies provided good examples of how to derive analytically the vibroacoustic solutions of plates with general boundary conditions. However, it required that the admissible functions in

Rayleigh-Ritz method should permit the reconstruction of any possible deflection or rotation along the whole structure's contour, which at least brought their difficulties: (1) the requirement made the selection or choice of the admissible functions difficult; (2) even after these admissible functions were found, such as in references 4 and 32, a slow convergence of the solution when considering complex boundary condition would make the application difficult; and (3) the external loading (force) needed to be able to be expressed in the form of the chosen admissible functions, which would cause additional complexity in the analysis, especially when the forces were time-dependent distributed forces. Moreover, these studies did not show clearly how to solve a plate with arbitrary non-uniform elastic supports within edges (i.e. the boundary parameters were dependent on their location even within an edge), or how much additional complexity it would be when dealing with such cases.

As far as the transient vibroacoustic of plate structures is concerned, there are still few methods available to deal with the general boundary conditions. Fan [5] has considered the effects of general boundary supports in his model to investigate the transient vibroacoustic response of a rectangular plate. But in his model, different beam mode shape functions are required to calculate the modal loss factor and the final modal equations for different boundary conditions; consequently, a specific set of characteristic functions for each type of boundary condition is required. Moreover,

his model is not well suited for plates with arbitrary, non-uniform edge restraints.

Since boundary conditions are important to the performance of plate structures, we can see from the review that a more effective method is required for the study of the effects of arbitrary boundary conditions on the plate vibroacoustic response, especially on the transient vibroacoustic response.

2.3 Stiffened Plate Structures

Stiffeners are widely used in different types of structures [33-36]. The stiffened plate structure, one of these structures, has been widely used in various engineering areas and its applications can be found in buildings, aircraft, ships and many other industries.

As far as the vibroacoustic problem of stiffened plate structures was concerned, the model that considered the plate stiffened by periodic stiffeners was commonly used in the early studies [10, 37-39]. This type of stiffeners has been proven to significantly affect the vibroacoustic response of plate structures. For example, parameter studies, including of plate material, plate thickness, stiffener spacing, and stiffener size, have been conducted by Lee et al. [10] to guide a favorable design in order to improve the sound transmission loss.

In addition, non-periodic stiffened plates have also been studied [9, 40]. For this type of stiffened plates, an important phenomenon called “Anderson localization” has frequently been studied. It is the phenomenon of energy localization due to irregularities. Hodges et al. [40] have done a study on the “Anderson localization” effect and explained that this was an effect whereby the propagation of vibration in an irregular structure was impeded by its irregularities, leading on average to an exponential decay of the vibration level. Their work demonstrated that the “Anderson localization” phenomenon would occur for vibration in irregular plate structures. A subsequent study by Photiadis [9] further examined this phenomenon in an irregular fluid-loaded plate structure and suggested that a reduction of radiation efficiencies could be achieved by properly increasing the degree of irregularity.

Since the stiffeners as well as their locations have been proved to notably affect the vibroacoustic performance of the plate structures, several studies [41, 42] have appeared in succession in recent years on the optimization design of stiffeners (including their locations) for reducing the vibration and noise radiation of plate structures.

It is worth mentioning that there are few methods found in the literature that can be used to predict the vibroacoustic response of the stiffened plate by taking into

account of both the effects of arbitrary boundary conditions and the stiffeners. Berry et al. [43] have proposed a Ritz model to calculate the vibroacoustic response of a stiffened plate that incorporates the effects of the stiffeners and the boundary transverse stiffness. However, the rotational boundary constraint which could have a significant effect [6, 31] on the vibroacoustic response of a plate was neglected in their model. Also, the stiffeners were limited to be parallel to the plate edges in their model.

Moreover, most related studies simplified the vibroacoustic problem to a steady-state problem by assuming time-harmonic excitations. However, the corresponding transient prediction models are usually required when the stiffened plate structure is driven by excitations that are transient in nature. The analysis of the time histories of the vibration and sound radiation of the structures to such excitations is important for the estimation of the important parameters, such as the instantaneous displacement and acceleration, the instantaneous sound pressure and sound power, the peak (maximum) displacement and acceleration, and the peak (maximum) sound pressure.

Since the effects of boundary conditions and stiffeners (including their locations) are important to the performance of plate structures, we can see from the review that a more effective method is required for the study of the effects of arbitrary boundary

conditions and arbitrarily located stiffeners on the plate vibroacoustic response, especially on the transient vibroacoustic response.

2.4 Finite Element Method and Boundary Element Method

The finite element method (FEM) and the boundary element method (BEM) are widely used in the vibroacoustic analysis of structures [44-50]. The FEM is usually used in the vibration analysis of structures, while the BEM is usually used in the calculation of the resulting radiated sound field of the vibrating structures.

In the structural dynamic analysis, FEM has several advantages over most other numerical analysis methods [51], such as: (1) it has no geometric restriction; (2) boundary conditions and loading are not restricted; (3) material properties are not restricted; (4) different types of components can be combined; (5) the approximation can be easily improved by grading the mesh. Thus the FEM becomes a good choice in the dynamic analysis of the plate structures. Hrabok et.al [45] have conducted an extensive review of the FEM used in the analysis of plate structures, in which they cited about 150 FEM formulations that could be used to calculate the plate bending motion. A recent study by Chiello et al.[6] showed that the component mode synthesis (CMS) techniques could be easily built into the FEM to accurately predict

the effects of different boundary conditions on the analysis of plate structures. The FEM has also been widely applied in the dynamic analysis of stiffened plate structures [52-57]. In the recent years, various types of stiffened-plate elements have been developed to analyze plates with arbitrary shapes and disposition of stiffeners [58, 59].

Since the BEM satisfies the Sommerfeld radiation condition naturally, it is very suitable for evaluating the propagation of sound in both finite and infinite fluid media [44, 46, 60]. The most important advantage of the BEM is that the computational dimension of the problem can be reduced by one. To determine the radiation or scattering problems of plate structures, three-dimensional problems can be solved on the two-dimensional structural surfaces. One potential shortcoming of the BEM in acoustics is the non-uniqueness difficulty; however, numerical methods, such as the CHIEF method [61, 62], enhanced CHIEF methods [63, 64] and Burton and Miller method [65] can be used to overcome the non-uniqueness problems. Another difficulty in BEM is that the solution has singularity when the source point is very close to the integration element; however, there are also many mature methods that can be used to deal with this problem. A summary of these methods has been given by Koo et al. [66], while in this study a non-singular boundary integral equation was also developed.

Combining the advantages of the FEM and BEM, the coupling of these two methods are frequently used in the fluid-structure interaction problems [67-69]. Combining the FEM and a multi-domain BEM, Wu et al. [67] investigated the sound transmission through thin structures. Several numerical examples were given in their work to demonstrate the effectiveness of using the coupled FEM/BEM method in the analysis of multi-domain structure-fluid interaction problems and showed that, even for light fluids, the coupled method performed better than the uncoupled one. In a later study by Kopuz et al. [68], the integrated FEM/BEM method was employed to predict the interior acoustic radiation of an open ended box. In their work, the predictions were compared with the experimental measurements and the results showed the capability of the FEM/BEM method in the vibroacoustic analysis of complex structures

Chapter 3

Boundary Condition Identification of a Single Plate System

3.1 Introduction

In this chapter, a method was developed to determine the boundary condition of a practical single plate system (hereinafter the “BCI method”). The effects of boundary supports (also called “elastic boundary conditions”) on the vibroacoustic response of plate structures have been investigated for decades [12] and demonstrated to be significant on the vibration and sound radiation properties of plates (especially in the low frequency domain). Even plates with complex boundary conditions have been widely studied in recent years [5-7]; however, only numerical examples were reported in these studies. The lack of experimental implementation and validation studies reflects the difficulty of measuring accurately the boundary parameters of a specific plate system [6]. Therefore, the proposed method in this chapter can be a preliminary study or auxiliary tool for the analysis of plate structures with general boundary conditions, and is used in Chapters 4-8 where the numerical and experimental studies on the vibroacoustic response of plate structures with general boundary conditions are discussed.

A relationship between the natural frequencies and structural boundary conditions can be established by solving the characteristic equations. From this relationship, the boundary conditions can be identified using the measured natural frequencies. To derive the characteristic equations of the plate structure, a coupled finite element and boundary element method (FEM/BEM) was used, which allowed taking into account the fluid loading effects and was thus able to identify structural boundary conditions with higher accuracy and had the potential to be applied to a plate in contact with liquid.

The layout of this chapter is as follows. Section 3.2 describes the detail of the BCI method. An experimental setup developed to demonstrate the actual performance of the BCI method is present in Section 3.3, in which the identified results of two plate systems are also given. Finally, a summary is given in Section 3.4.

3.2 Boundary Condition Identification Method

3.2.1 Description of the Problem

Consider a thin rectangular plate with uniform elastic boundary supports along the four edges, as shown in Fig. 3.1. The plate is mounted on an infinite rigid baffled. This plate baffle system separates the fluid medium into section V^+ and section V^- (see Fig. 3.2). The plate is subject to a time-harmonic input force F . The

vibration of the plate induced by the input force then radiates sound waves into the fluid medium.

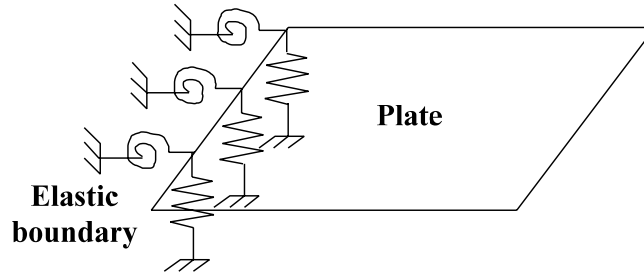


Figure 3.1 A rectangular plate with elastic boundary supports along the edges (for simplicity and clarity, only the supports along the left edge are shown)

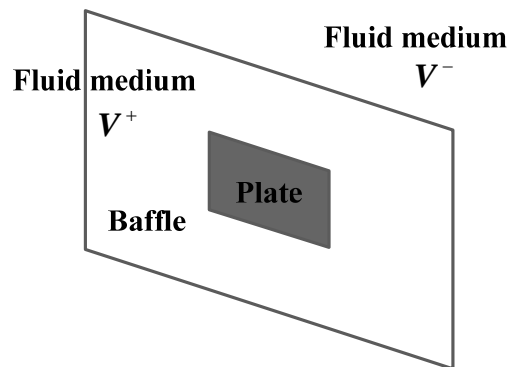


Figure 3.2 A rectangular plate mounted on an infinite rigid baffle

3.2.2 Characteristic Equation of the Plate System

The vibration response of the undamped plate system determined by the FEM is given as,

$$(-\omega^2 \{M\} + \{K\})\{U\} = \{F\} + \{\mathcal{S}\}(\{P^+\} - \{P^-\}), \quad (3.1)$$

where $\{M\}$, and $\{K\}$ are the global mass and stiffness matrices of the plate

system, $\{U\}$ is the global nodal displacement vector, $\{F\}$ is the external force applied on the plate, and the vectors $\{P^+\}$ and $\{P^-\}$ represent radiated sound pressures on the front (in section V^+) and back (in section V^-) plate surfaces (see Fig. 3.2), respectively. $\{\mathcal{S}\}$ is a global transformation matrix converting the fluid pressure to point forces that act on the nodes of the plate. The superscript T signifies the transpose matrix. The four-node rectangular Kirchoff plate element [51] is used in the FEM model. The mesh size of the element should be determined by considering both solution accuracy and computational cost. A suggestion proposed by Kim et al. [70] is a mesh size equal to one quarter of the wavelength of the highest frequency of interest.

The half-space boundary integral equation [71] is used to calculate the sound pressure on the plate surfaces. To solve the integral equation numerically, the discretization used in the BEM model is the same as in the FEM. The sound pressure on the plate surfaces can then be given as

$$\{P^\pm\} = \pm\{H\}\{w\}, \quad (3.2)$$

where $\{H\}$ is a square matrix [60] formed by the ‘‘collocation’’ procedure. $\{w\}$ is the transverse deflection vector which can be written as

$$\{w\} = \{\mathcal{R}\}\{U\}, \quad (3.3)$$

where $\{\mathcal{R}\}$ is a global transformation matrix converting the nodal displacement

vector to the transverse deflection vector. Combining Eqs. (3.1)~(3.3), the force-displacement relationship of the plate system can be given as

$$(-\omega^2 \{M\} + \{K\} - 2\{\mathcal{S}\}\{H\}\{\mathcal{D}\})\{U\} = \{F\}. \quad (3.4)$$

The characteristic equation of the plate system can then be given as

$$|-\omega^2 \{M\} + \{K\} - 2\{\mathcal{S}\}\{H\}\{\mathcal{D}\}| = 0. \quad (3.5)$$

3.2.3 Stiffness and Mass Matrices of the Plate System

To solve the characteristic equation Eq. (3.5), The global matrices $\{M\}$, and $\{K\}$ of the plate system are needed. The determination of these matrices is described in this subsection.

The stiffness matrix $\{K\}$ of the whole plate system is decomposed into plate and boundary supports, and can be expressed as

$$\{K\} = \{K_p\} + \{K_b\}, \quad (3.6)$$

where $\{K_p\}$ and $\{K_b\}$ are the stiffness matrices for the plate and boundary supports, respectively. In general, the mass properties of the boundary supports can be neglected [4, 6, 7, 31]. Therefore the mass matrix $\{M\}$ of the whole plate system only contains the mass matrix of the plate, and can be expressed as,

$$\{M\} = \{M_p\}. \quad (3.7)$$

The elastic supports, as in references 4, 6 and 7, are modeled as a combination of translational and rotational springs, with k_{tb} and k_{rb} being the translation stiffness

and rotational stiffness, respectively. The total strain energy Π_{be} of the plate element, as shown in Fig. 3.3, can now be given by

$$\Pi_e = \Pi_{pe} + \Pi_{be}, \quad (3.8)$$

where the strain energy of the plate element Π_{pe} and the strain energy of the boundary support in the plate element Π_{be} can be expressed by,

$$\Pi_{pe} = \frac{1}{2} \{U\}_e^T \{K_p\}_e \{U\}_e, \quad (3.9)$$

and

$$\Pi_{be} = \frac{1}{2} \{U\}_e^T \{K_b\}_e \{U\}_e. \quad (3.10)$$

$\{U\}_e$ is the nodal displacement vector of the element. $\{K_p\}_e$ and $\{K_b\}_e$ are the element stiffness matrices of $\{K_p\}$ and $\{K_b\}$, which can be expressed by,

$$\{K_p\}_e = \int \{B_p\}^T \{D_p\} \{B_p\} dx dy, \quad (3.11)$$

and

$$\{K_b\}_e = \int \left(k_{tb} \{N_w\}^T \{N_w\} + k_{rb} \left\{ \frac{\partial N_w}{\partial \bar{n}_b} \right\}^T \left\{ \frac{\partial N_w}{\partial \bar{n}_b} \right\} \right) d\Gamma_b, \quad (3.12)$$

where $\{B_p\}$ is the strain matrix of the plate, $\{D_p\}$ is the flexural rigidity matrix of the plate, $\{N_w\}$ is the shape function vector for the plate element and \bar{n}_b is the normal unit vector of the element boundary contour Γ_b . The total kinetic energy T_e of the plate element is given by

$$T_e = \frac{1}{2} \{\dot{U}\}_e^T \{M_p\}_e \{\dot{U}\}_e. \quad (3.13)$$

$\{M_p\}_e$ is the element mass matrices of $\{M_p\}$, given by,

$$\{M_p\}_e = \rho_p h \int \{N_w\}^T \{N_w\} dx dy, \quad (3.14)$$

where ρ_p and h is the density and thickness of the plate, respectively.

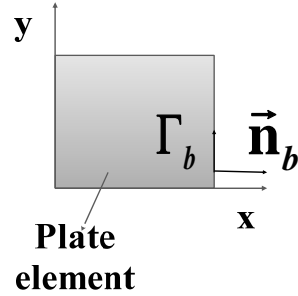


Figure 3.3 A rectangular plate element

Once the element matrices $\{K_p\}_e$, $\{K_b\}_e$ and $\{M_p\}_e$ are solved by Eqs. (3.11), (3.12) and (3.14), the global stiffness and mass matrix $\{K\}$, $\{M\}$ of the whole plate system in Eq. (3.5) can be obtained according to the finite element assembly procedure [51]. As mentioned in the subsection 3.2.1, the boundary conditions along the four edges of the plate are supposed to be uniform. The values of k_{tb} and k_{rb} in Eq.(3.1.2) are therefore the same for each element. With this assumption, only two unknown variables (k_{tb} and k_{rb}) are contained in the global stiffness matrix $\{K\}$. The procedure to identify these two variables is given in next subsection.

3.2.4 Identification Procedure

The essence of the BCI method is that a relationship between the natural frequencies and structural boundary conditions can be established by solving the characteristic equations. From this relationship, the boundary conditions can be identified using

the measured natural frequencies. The BCI method is similar to the identification method provided by Ahmadian et al. [72]. The main difference between the two methods is the process of establishing the characteristic equations. The main advantage of the BCI method is that it allows taking into account the fluid loading effects on the structural natural frequencies, and can thus be used when the structure is in contact with liquid. Even in the air, this method can give more accurate results since the effects of fluid loading have been proved to be more significant in near-resonance frequency regions [67].

Once the characteristic equation is formed, the procedures to identify the boundary parameters are the same as in reference 72. They can be briefly described as the following two steps: (i) A set of solutions for the boundary parameters is obtained by solving Eq. (3.5) for each measured mode, and (ii) a unique solution is then obtained by selecting the one that satisfies Eq. (3.5) for all measured modes. Because of the inevitable measurement errors, there may be no unique solution that satisfies Eq. (3.5) for every mode. But the most likely solution can still be estimated based on the accuracy of each measured mode [72]. In the following section, the capability of the BCI method is verified by the identification of two actual plate systems.

3.3 Identification of Practical Plate systems

3.3.1 Experimental Setup

Fig. 3.4 schematically illustrates the experimental setup. The measurements were conducted in two connected chambers at The Hong Kong Polytechnic University. The two chambers shared a common wall. The common wall had a square port at its center sized 26 cm × 26 cm, which was designed to hold the tested panel. A single aluminum (Al) panel was mounted in this port using two identical steel frames that screwed directly into the port. Each frame was 34 cm by 34 cm square and 3 mm thick, with a 24 cm by 24 cm square opening cut out of the middle (i.e., the actual calculation area of the Al panel was 24 cm by 24 cm). The Al panel was cut to 25.6 cm by 25.6 cm square to allow 8 mm of each edge to be clamped between these two steel frames. A modal test was conducted on the plate system, as described in the following subsections.

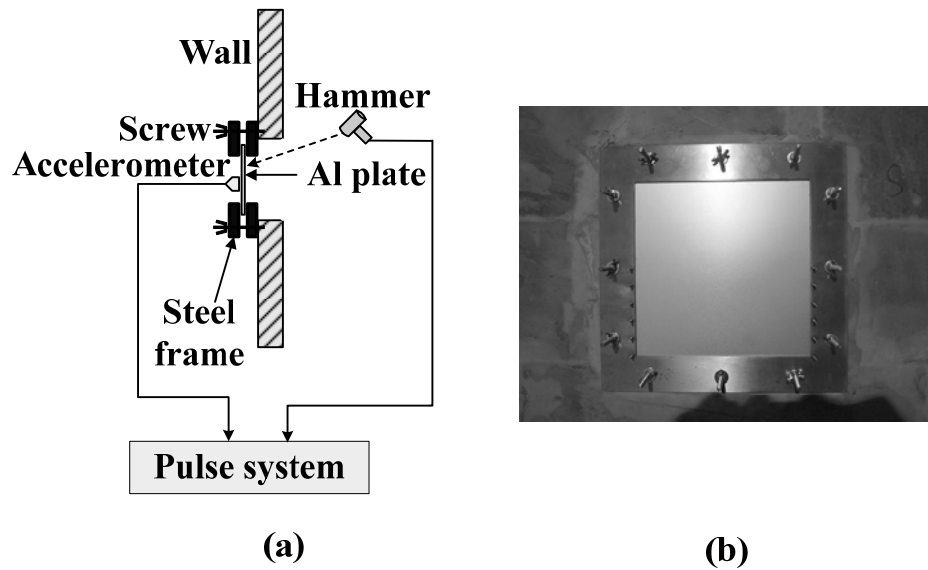


Figure 3.4 The plate system used in the modal testing: (a) Schematic diagram of the baffled plate system; (c) Picture of the baffled plate system (front view)

3.3.2 Modal Testing

To determine the natural frequencies, a modal test was conducted on the plate system using impact excitation. In the test, the method of “multi-point excitation and one-point pick-up” was used; i.e., an accelerometer (B&K: 4394) was located at a fixed point on the plate while seven different impact points were chosen, as shown in Fig. 3.5. The measured data were collected directly by PULSE and the MATLAB software was used for the data processing. The process can be summarized as follows: (1) Excite the Al panel with an impact hammer (Kistler: 9726A) at one impact point each time; (2) Collect the impact excitation signal and the corresponding acceleration response by PULSE (B&K: 3160-B-042); (3) Plot the frequency response function (FRF) curves and use the peak-picking method [73] to detect the natural frequencies; and (4) Obtain the estimated natural frequencies by

averaging the results in step 3.

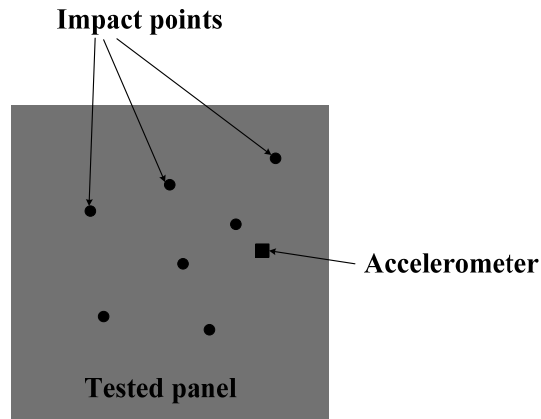


Figure 3.5 Locations of accelerometer and impact points on the panel

Two panels of different thickness were used in the measurements. One was 1 mm thick (referred as “Panel 1”) and the other was 1.5 mm thick (referred as “Panel 2”).

Tables 3.1 and 3.2 list the results of the natural frequencies.

Table 3.1 Measured and predicted natural frequencies (Hz) of Panel 1

Natural frequency	Panel 1 (1 mm thick)		
	Measured	Predicted	Error (%)
f_1	116.3	116.3	0
f_2	239.3	239.0	-0.13
f_3	239.3	239.0	-0.13
f_4	341.5	341.0	-0.14

Table 3.2 Measured and predicted natural frequencies (Hz) of Panel 2

Natural frequency	Panel 2 (1.5 mm thick)		
	Measured	Predicted	Error (%)
f_1	155.6	156.0	0.26
f_2	314.3	312.4	-0.60
f_3	314.3	312.4	-0.60
f_4	435.0	437.7	0.62

3.3.3 Identification Results and Discussion

The measured natural frequencies obtained from the modal test (listed in Tables 3.1 and 3.2) are used in the identification process mentioned in Sec. 3.2.4. The element number used in the BCI method was 64 (8×8). Figs. 3.6 and 3.7 show the acceptable solutions for each of the first four modes. The solutions that best satisfy all modes can be found in the figures, which are $\bar{k}_{tb} = 3201$ and $\bar{k}_{rb} = 13.28$ for Panel 1 and $\bar{k}_{tb} = 1162$ and $\bar{k}_{rb} = 7.69$ for Panel 2. Here, \bar{k}_{tb} and \bar{k}_{rb} are the dimensionless forms of k_{tb} and k_{rb} ($\bar{k}_{tb} = k_{tb}L_x^3/D$ and $\bar{k}_{rb} = k_{rb}L_x/D$, D is the flexural rigidity of the plate), which are the same as those used in references 4, 6, and 7.

Tables 3.1 and 3.2 also show the predicted natural frequencies for the identified boundary solutions. It can be seen from the tables that the predicted natural frequencies based on the identified boundary conditions agree very well with the measured values. The elastic boundary support parameters are more important in the lower modes than that in higher modes. For this reason the first four modes are chosen in the identification procedure and found to be enough for the identification of the tested plate systems.

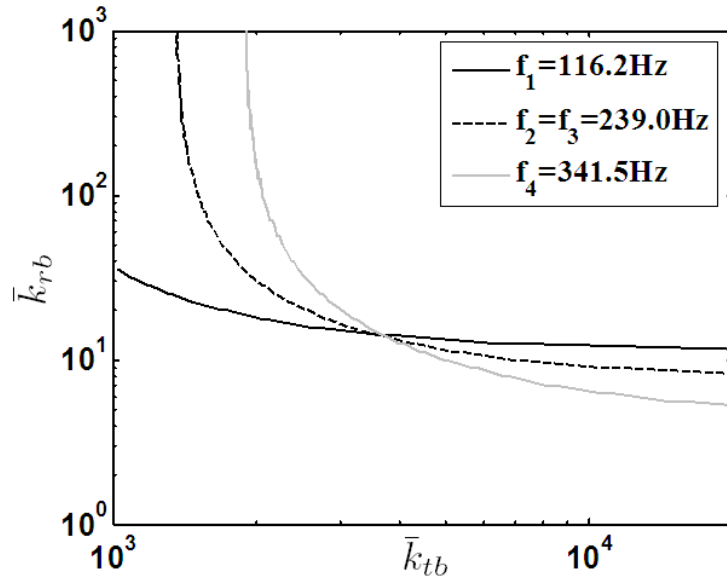


Figure 3.6 Solutions for \bar{k}_{tb} and \bar{k}_{rb} that satisfy the characteristic equation of
Panel 1

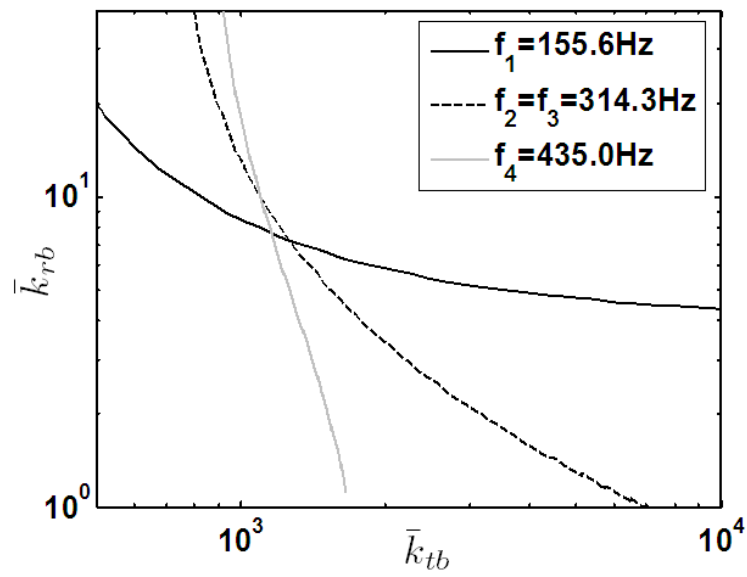


Figure 3.7 Solutions for \bar{k}_{tb} and \bar{k}_{rb} that satisfy the characteristic equation of
Panel 2

3.4 Summary

In this chapter, a method (BCI method) has been proposed to identify the boundary conditions of practical plate structures, which was based on a coupled finite element and boundary element method (FEM/BEM) that allowed taking into account the fluid loading effects and thus was able to obtain more accurate results. The essence of the BCI method was that a relationship between the natural frequencies and structural boundary conditions could be established by solving the characteristic equations. From this relationship, the boundary conditions could be identified using the measured natural frequencies.

An experimental setup was developed to examine the practical performance of the BCI method. Two Al panels of different thicknesses were used and modal tests were conducted on them. The approximate boundary conditions of the two plate systems were identified by using the measured natural frequencies. The effectiveness of the BCI method was thereby demonstrated and the results showed that only a few low-order natural frequencies were needed when using this method.

The two Al plate systems mentioned in this chapter are also used in other experiments (see Chapters 4-6) for different research purposes. The identified boundary conditions are directly used there and found to be accurate and efficient for

all the purposes.

Chapter 4

A Study of the Effects of Elastic Supports on the Transient Vibroacoustic Response of a Single Plate

4.1 Introduction

In Chapter 3, an identification method was developed to determine the boundary conditions of a practical plate structure. In order to further investigate the effects of different boundary conditions on the vibroacoustic response, especially on the transient vibration and sound radiation (TVSR) of plate structures, a time-domain prediction method and the corresponding experimental studies were developed in this chapter.

The boundary supports have been found to have significant effects not only on the steady-state response [7] but also on the transient response of the plate structures [74]. Apart from the studies of the steady state problems, other research has been focused on the analysis of the transient response of plate structures [2, 3, 25, 28, 29, 74-76]. However, most previous studies were limited to a plate with classical boundary conditions, such as free, simply supported, clamped, or their combinations.

A more systematic study of the effects of arbitrary boundary conditions on the TVSR of these structures is required.

In this chapter, a time-domain prediction method was used. It allowed the plate to have arbitrary elastic boundary conditions. The method was based on the time-domain finite element method (TDFEM) and time domain boundary element method (TDBEM). The elastic supports were modeled as a combination of translational and rotational springs, as treated in Chapter 3. Also, the Al plate system (Panel 1) described in Chapter 3 was used again in the experimental studies in this chapter. The TVSR of the plate system was measured and compared with the predictions. The prediction method was subsequently applied to evaluate the effects of elastic boundary supports on the TVSR of a window to check the possibility of using appropriate boundary supports to improve the transient vibration and noise isolation performance of a practical window.

The layout of this chapter is as follows. Section 4.2 describes the detail of the proposed method. Experimental validation studies are reported in Sec. 4.3. In Sec. 4.4, parametric studies on a practical window are present. Finally, Sec. 4.5 gives the summary.

4.2 Theoretical Framework

4.2.1 Description of the Problem

Consider a thin rectangular plate of length L_x , width L_y , thickness h with arbitrary elastic boundary supports along the four edges. The plate is mounted on an infinite rigid baffle and the whole baffled plate is immersed in an infinite light fluid medium (air). The effect of fluid loading on the plate's vibration is neglected. The plate is subject to a transient force $F(t)$ (or a transient incidence wave $p_0(t)$), as shown in Fig. 4.1. The vibration of the plate induced by the transient input excitations then radiates sound waves into the fluid medium.

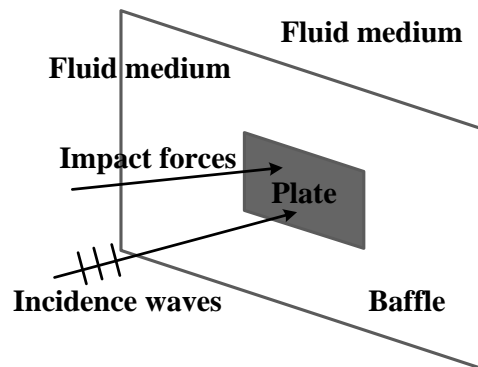


Figure 4.1 A baffled rectangular plate subjected to transient forces (or transient incidence waves)

4.2.2 Time-domain Finite Element Method (TDFEM)

The time-domain finite element method used to determine the vibration response of the plate due to a transient loading $F(t)$ (or a transient incidence wave $p_0(t)$) can be given as

$$\{M\}\{\ddot{U}\} + \{D\}\{\dot{U}\} + \{K\}\{U\} = \{F(t)\} + \{\mathcal{T}\}\{p_0(t)\} \quad (4.1)$$

where $\{M\}$, $\{D\}$, and $\{K\}$ are the mass, damping, and stiffness matrices of the plate system, respectively; $\{U\}$, $\{\dot{U}\}$, and $\{\ddot{U}\}$ are the global nodal displacement, velocity, and acceleration vectors (respectively). $\{\mathcal{T}\}$ is a transformation matrix converting the incidence sound pressure to point forces that act on the nodes of the plate. The damping matrix $\{D\}$ [73] is assumed to be proportional to the stiffness matrix $\{K\}$ and is written as $\{D\} = \beta\{K\}$, where $\beta = \frac{2\eta}{\omega_0}$, η is the damping factor, and ω_0 is the fundamental natural frequency of the plate system. The elastic supports are modeled as a combination of translational (k_{tb}) and rotational (k_{rb}) springs, as treated in Chapter 3.2.3. The mass matrix $\{M\}$ and stiffness matrix $\{K\}$ in Eqs. (3.6) and (3.7) can be directly used here. What is worth mentioning is that the elastic parameters along the plate boundary can be arbitrarily varied to reproduce simply supported ($k_{tb} = \infty$ and $k_{rb} = 0$), clamped ($k_{tb} = \infty$ and $k_{rb} = \infty$), free ($k_{tb} = 0$ and $k_{rb} = 0$), and guided ($k_{tb} = 0$ and $k_{rb} = \infty$) edges, or any intermediate situation (i.e., general elastic boundary conditions). Unless stated otherwise, in the numerical calculations through the whole thesis, the infinite large value is represented by a very large number, 1×10^{10} . Moreover, these parameters can vary spatially along each edge to represent arbitrary non-uniform elastic restraint, or in other words, the values of k_{tb} and k_{rb} can change from one element to another or even within an element.

The four-node rectangle Kirchoff plate element used in Chapter 3.2.2 is again used in the TDFEM model. A suggestion of the mesh size has been mentioned in Chapter 3.2.3. Or another simple mesh method can be: (1) to give an initial element number that is reasonable and economic; and (2) to increase this number until converged results are obtained. The latter mesh method is used in the calculations in this chapter.

The Newmark integration scheme [51] is used to integrate the finite element equation (Eq. 4.1) step-by-step in the time domain. The main assumptions of the Newmark method can be expressed as

$$\{\dot{U}(t + \Delta t)\} = \{\dot{U}(t)\} + [(1 - \gamma)\{\ddot{U}(t)\} + \gamma\{\ddot{U}(t + \Delta t)\}]\Delta t \quad (4.2)$$

$$\{U(t + \Delta t)\} = \{U(t)\} + \{\dot{U}(t)\}\Delta t + [(\frac{1}{2} - \alpha)\{\ddot{U}(t)\} + \alpha\{\ddot{U}(t + \Delta t)\}](\Delta t)^2 \quad (4.3)$$

where t represents time, Δt is the time step. α and γ are the standard Newmark parameters, which are set to 0.25 and 0.5 (respectively) in the following numerical calculations. The time step can be decided according the sampling theorem (or in other words, the sampling frequency should be at least larger than the highest frequency of interest). The time steps used in the calculations though the whole thesis meet this criterion.

4.2.3 Time-domain Boundary Element Method (TDBEM)

The time-domain boundary integral equation used to describe the radiated sound

field of a plate is given as

$$C(\xi)p(\xi, t) = \int_S \int_0^t \sigma^*(x, t; \xi, \tau) p(x, \tau) d\tau dS - \int_S \int_0^t \sigma(x, t; \xi, \tau) \frac{\partial p(x, \tau)}{\partial \bar{n}} d\tau dS, \quad (4.4)$$

where σ and σ^* are the fundamental pressure and fundamental flux, which can be expressed as

$$\sigma(x, t; \xi, \tau) = \frac{1}{4\pi r} \delta\left(t - \frac{r}{c} - \tau\right), \quad (4.5)$$

$$\sigma^*(x, t; \xi, \tau) = \frac{\partial \sigma(x, t; \xi, \tau)}{\partial \bar{n}} = -\frac{1}{4\pi r^2} \left[\delta\left(t - \frac{r}{c} - \tau\right) + \frac{r}{c} \dot{\delta}\left(t - \frac{r}{c} - \tau\right) \right] \frac{\partial r}{\partial \bar{n}}, \quad (4.6)$$

where p is acoustic pressure, δ is the Dirac delta function, the coordinates x and ξ are the source and receiver points respectively, the distance function $r = |\xi - x|$, the coefficient $C(\xi)$ represents the solid angle at ξ , c is the sound propagation speed, t represents time, \bar{n} is the unit normal direction on S , and S is the integration area, which includes both the baffle area S_b and the plate area S_p . The flux function $\frac{\partial p}{\partial \bar{n}}$ in Eq. (4.4) can be obtained using the boundary condition on the fluid-structure interface, which is

$$\frac{\partial p}{\partial \bar{n}} = -\rho_0 \ddot{w}, \quad (4.7)$$

where ρ_0 is the fluid density, and \ddot{w} is the normal acceleration of the plate.

If the plate is mounted on an infinite rigid baffle, as shown in Fig. 4.1, the image method can be used to construct the half-space fundamental pressure function σ_H and fundamental flux function σ_H^* . The process corresponds to the construction of the half-space Green's function [71] but in the time domain. Note that the whole

plate is flat and lies on the half-space plane; σ_H , σ_H^* and $C(\xi)$ can be determined as $\sigma_H = 2\sigma$, $\sigma_H^* = 0$ and $C(\xi) = 1$. Therefore, Eq. (4.4) finally reduces to the well-known Rayleigh integral equation,

$$p(\xi, t) = \int_{S_p} \int_0^t \rho_0 \sigma_H(x, t; \xi, \tau) \ddot{w}(x, \tau) d\tau dS. \quad (4.8)$$

It is worth mentioning that Eq. (4.8) is valid for p either in the acoustic domain or on the surface S .

The numerical implementation method in reference 60 is used to solve Eq. (4.8). The plate surface S_p is discretized into a number of boundary elements. The time-marching scheme is employed to obtain the numerical solution for the unknown $p(\xi, t)$ at each discrete time step, and each step uses the linear time interpolation function. Note that the discretization of the space and time variables is the same as that used in the TDFEM. Therefore the acceleration results of Eq. (4.1) can be directly used in Eq. (4.8) to calculate the corresponding radiated sound.

4.3 Experimental Validation

4.3.1 Experimental Setup

Fig. 4.2 schematically illustrates the experimental setup. The measurements were conducted in two connected chambers at The Hong Kong Polytechnic University. The net volumes of these two chambers were 200 m^3 and 70 m^3 , respectively. The

larger chamber was used as the receiving room and the smaller chamber as the source room. The two chambers shared a common wall and the wall had a square port at its center. A 1 mm thick aluminum (Al) panel was mounted in this port using two identical steel frames that screwed directly into the port. The wall and the steel frames were regarded as an infinite baffle. The same experimental setup has been used in Chapter 3.3.1 for the modal testing and the detailed dimension information of each component can be found there. It is worth mentioning that acoustic absorptive materials were added to the surface of the walls of these two chambers (except for the common wall) to reduce as much as possible the reflected sound (i.e. to make the chamber semi-anechoic).

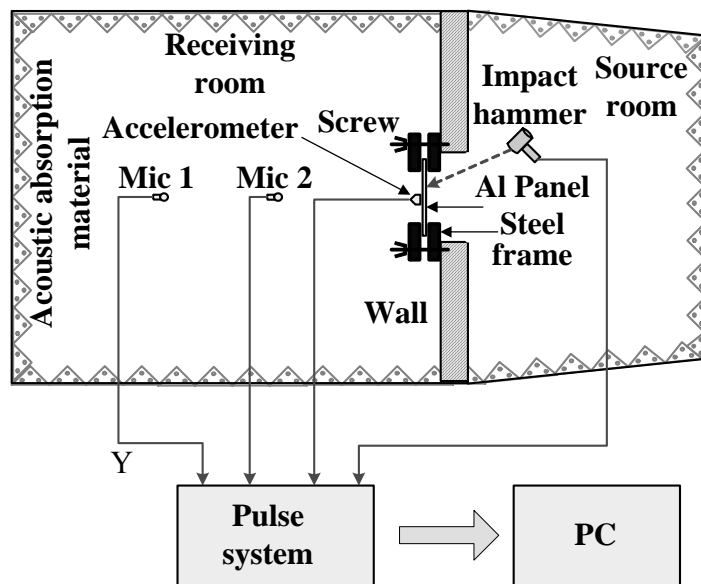


Figure 4.2 Schematic diagram of the experimental setup for measuring the TVSR of a baffled plate system

A Kistler 9726A impact hammer was used to produce a transient impact force acting on the Al panel in the source room, while at the same time two B&K4935 microphones were put in the receiving room to measure the radiated sound, and a B&K 4394 accelerometer was attached to the Al panel to measure the acceleration. The two microphones, referred as “Mic 1” and “Mic 2”, were located at the center line of the Al panel with 0.155 m and 1.112 m, respectively, away from the panel. The locations of the accelerometer and impact point were shown in Fig. 4.3. All data were collected by PULSE (Type B&K 3160-B-042) at a sampling rate of about 8.2 kHz (0.12 ms) for a record length of 1 second.

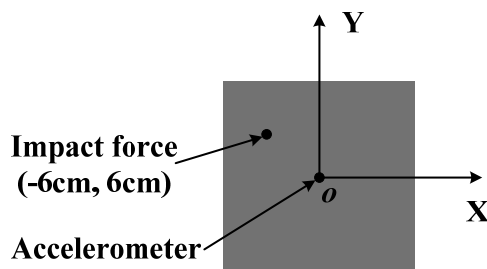
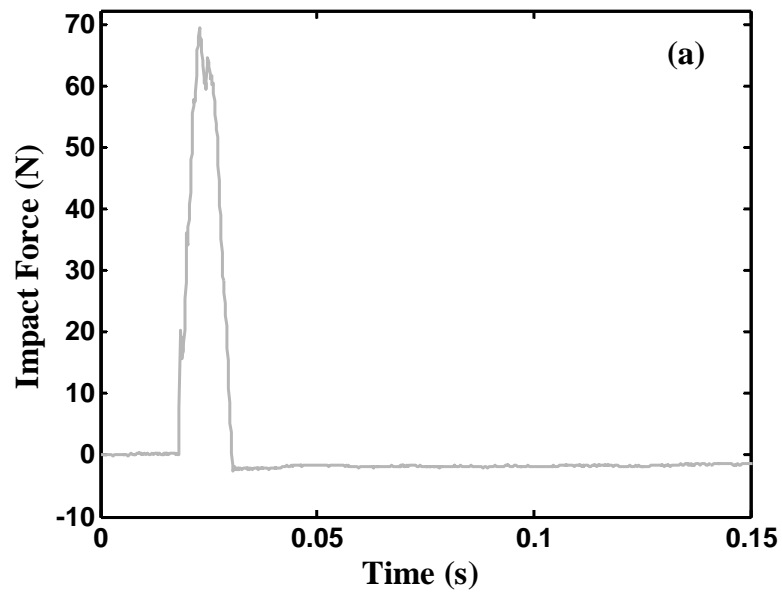


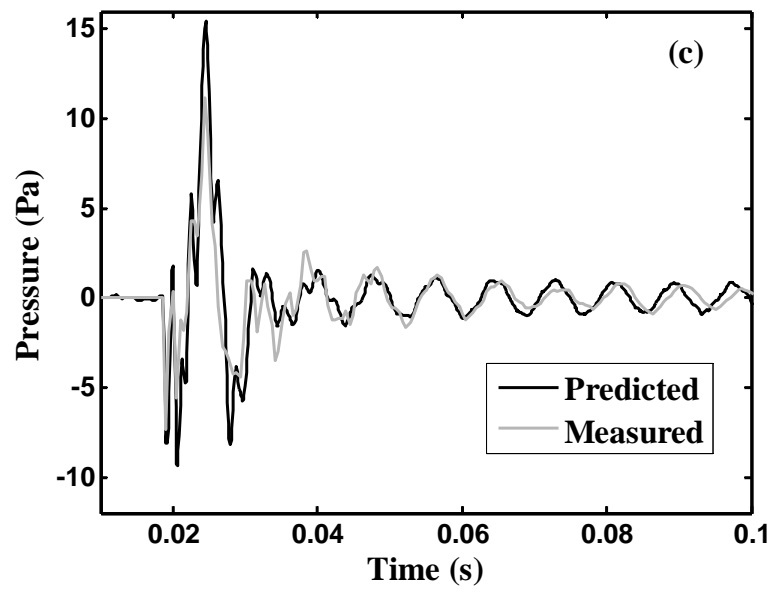
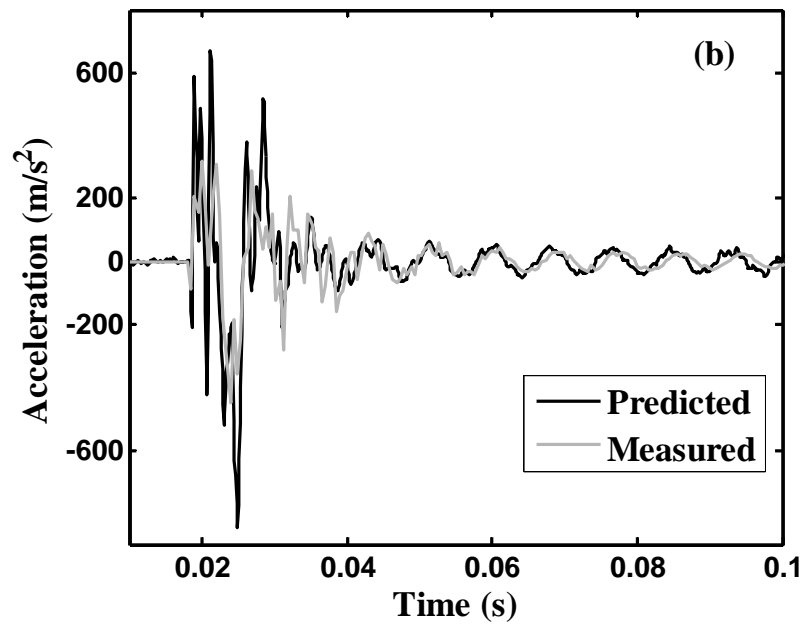
Figure 4.3 Locations of the impact force and the accelerometer

4.3.2 Experimental Results and Discussion

The time histories of the three measured parameters were the impact force, the acceleration of the panel, and the sound pressure in the receiving room. Fig. 4.4 shows the measured results, denoted as (a) impact force, (b) acceleration, (c) sound pressure of “Mic 1”, and (d) sound pressure of “Mic 2”. The impact force shown in

Fig. 4.4 (a) was used as the input to the numerical model. For comparison, the predicted results were also included in Fig. 4.4 (b)-(d). In the numerical calculations, the element number was 64 (8×8); the boundary parameters were $\bar{k}_{tb} = 3201$ and $\bar{k}_{rb} = 13.28$, which were obtained by using the BCI method in Chapter 3.3.3; and the damping factor was $\eta = 0.0115$, which was estimated by using a peak-picking method [73] based on the modal test in Chapter 3.3.2. Note that \bar{k}_{tb} and \bar{k}_{rb} were the dimensionless forms of k_{tb} and k_{rb} , as already mentioned in Chapter 3.3.3.





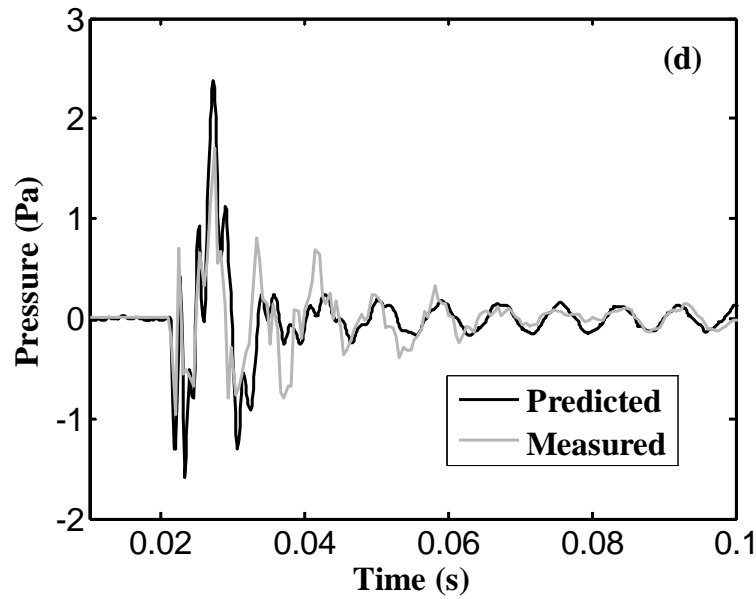


Figure 4.4 Comparison of the predicted results and experimental data: (a) Impact force time history; (b) Acceleration time history; (c) Pressure time history of “Mic 1”; (d) Pressure time history of “Mic 2”

As Fig. 4.4 shows, the predicted vibration (acceleration) and sound radiation (sound pressure) results are in good agreement with the experimental data. The discernible discrepancies can be attributed to a number of factors, such as the uneven panel thickness, the non-uniform boundary conditions along the four edges, approximate damping, and the added mass caused by the accelerometer. In addition, only a rough location of the impact point was available when striking a hammer by hand. Also, the predicted sound pressure of “Mic 1” agrees better with the experimental data than the predicted results of “Mic 2”; this is because of the imperfect sound absorption at the boundaries of the receiving room, since the location of “Mic 2” was much further from the tested panel and nearer to other walls of the room.

4.4 Parametric Studies

Parametric studies were carried out on a single-pane glass window to examine the effects of different boundary conditions on the transient vibration and sound radiation (TVSR). The window was 80 cm long, 80 cm wide and 5 mm thick, with the Young's modulus 65GPa, density 2500 kg/m³, Poisson's ratio 0.25, and damping factor 0.01. The window was assumed to be with uniform boundary supports along the four edges and impacted by a transient sound pulse (a triangular wave), as shown in Fig. 4.5. In the numerical calculations, the element number and time interval Δt were 64 (8×8) and 0.5 ms, respectively. Since the key concern in this study was the effect of the boundary supports rather than that of the wave incidence angle, in the following simulations the incidence sound wave was assumed to be at normal incidence for simplify. However, it should be noted that for a realistic sound wave any incidence angle is possible, and the actual incidence angle needs to be well estimated (or measured) since it can influence the final response [77].

Fig. 4.6 shows the acceleration responses of the window with all edges clamped and with all edges simply supported, while Fig. 4.7 shows the corresponding sound radiation. To make more comprehensive comparisons between these responses, a fast Fourier transform (FFT) was used to convert the responses into frequency spectrum data.

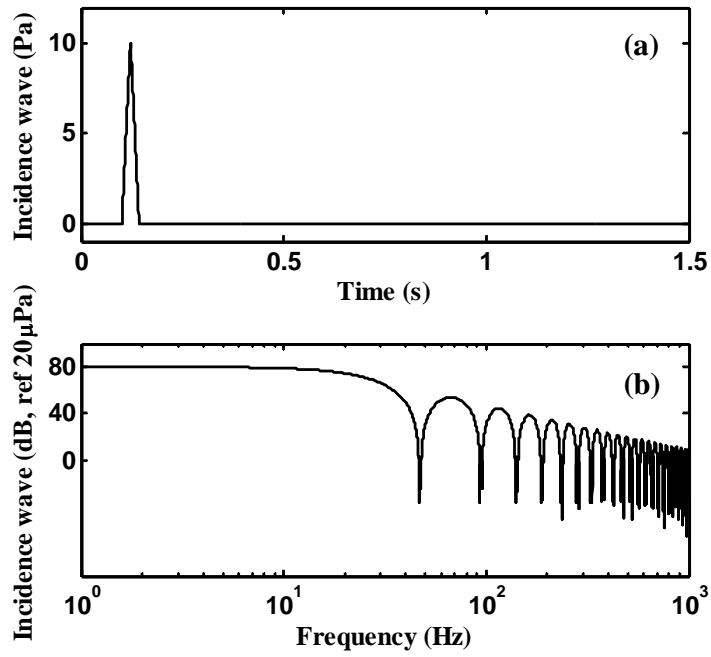
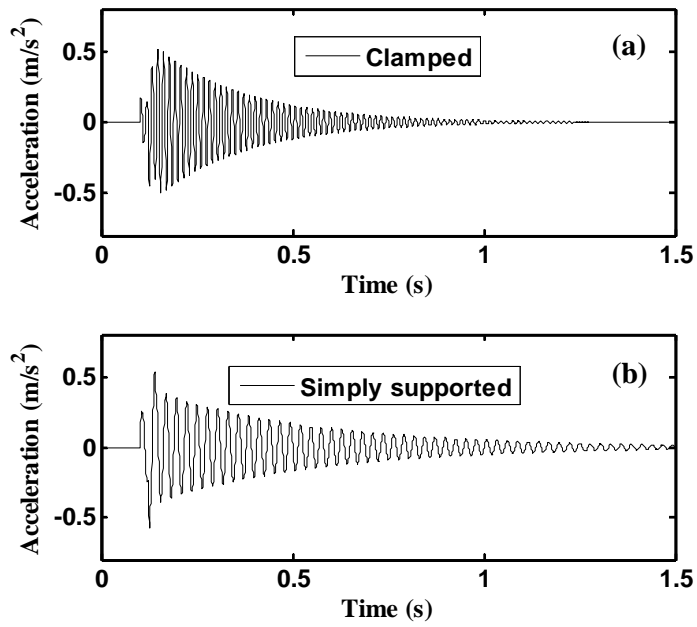


Figure 4.5 A transient sound pulse (a triangular wave): (a) Pressure time history; (b) Pressure frequency spectrum



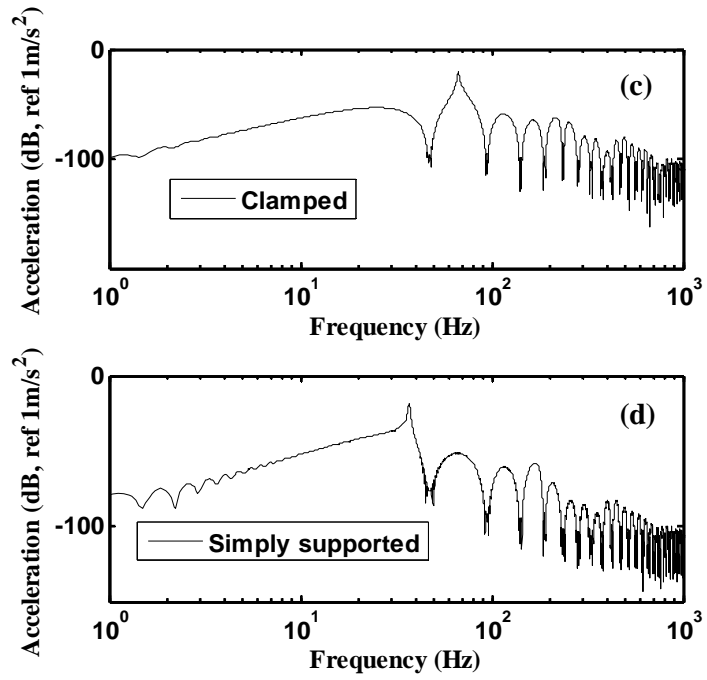
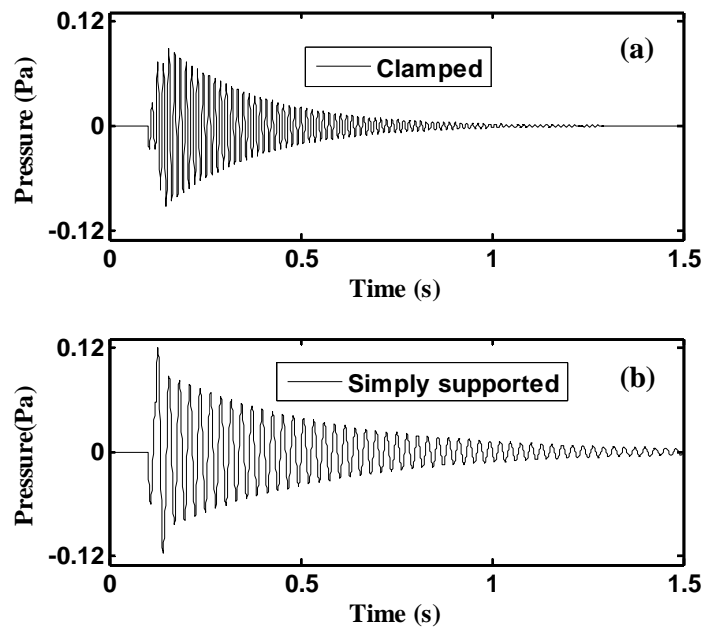


Figure 4.6 Acceleration responses at the center of the window



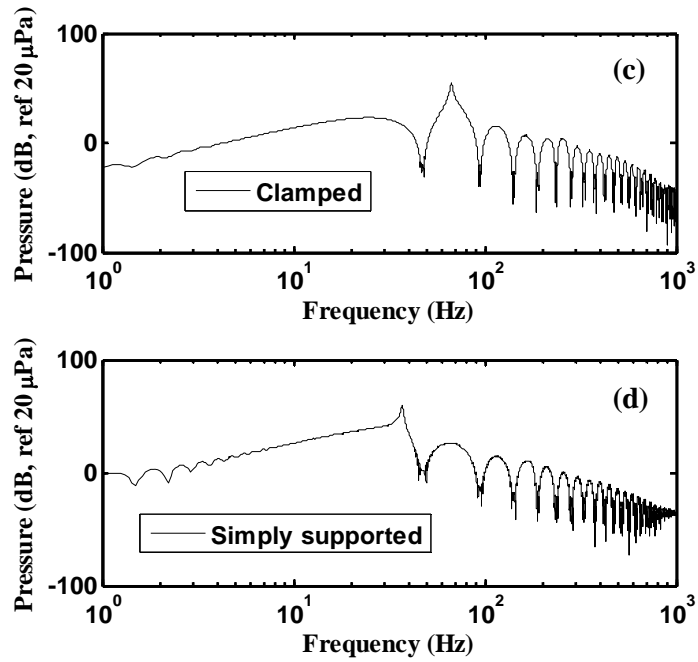


Figure 4.7 Radiated sound pressure at point “P”. Point “P” is on the axis of symmetry a distance of 0.1 m away from the window

It can be seen from Figs. 4.6 and 4.7 that the time histories of TVSR of the clamped window changed more quickly and decayed more quickly than those of the simply supported window. This is because the TVSR responses of the clamped window contained more high-frequency components and fewer low-frequency components compared with those of the simply supported window.

The window with more general boundary conditions, such as the ones varying between simply supported and clamped edges (i.e. $k_{tb} = \infty$ and $k_{rb} = 0 \sim \infty$), was also calculated in order to gain a further understanding of the effects of the boundary conditions. As noted by the authors in references 78 and 79, these types of boundary

conditions are common for practical windows in buildings. To better evaluate the window's transient performance, the maximum values of the acceleration level

$$A_{\max} = \max \left[20 \lg \left(\frac{|\ddot{w}(t)|}{\ddot{w}_{ref}} \right) \right] \quad \text{and} \quad \text{radiated sound pressure level}$$

$$SPL_{\max} = \max \left[20 \lg \left(\frac{|p(t)|}{p_{ref}} \right) \right]$$

were obtained from the TVSR responses and are shown in Fig. 4.8 as a function of \bar{k}_{rb} . It can be seen from the figure that the elastic boundary supports have a notable effect on the TVSR of the window. In this case, there exists an optimum value (around $\bar{k}_{rb} = 5$) at which A_{\max} and SPL_{\max} are minimized for this particular transient excitation. Reductions of about 7.4 dB and 8.2 dB can be obtained in A_{\max} and SPL_{\max} , respectively, in comparison with their maximum possible values. One major effect of different boundary conditions is that they can notably influence the resonance frequencies of the structure (window). By shifting the resonance frequencies (especially the fundamental resonance frequency) away from the unwanted range, an appropriate boundary condition can significantly improve the transient vibration and noise isolation performance of the structure (window).

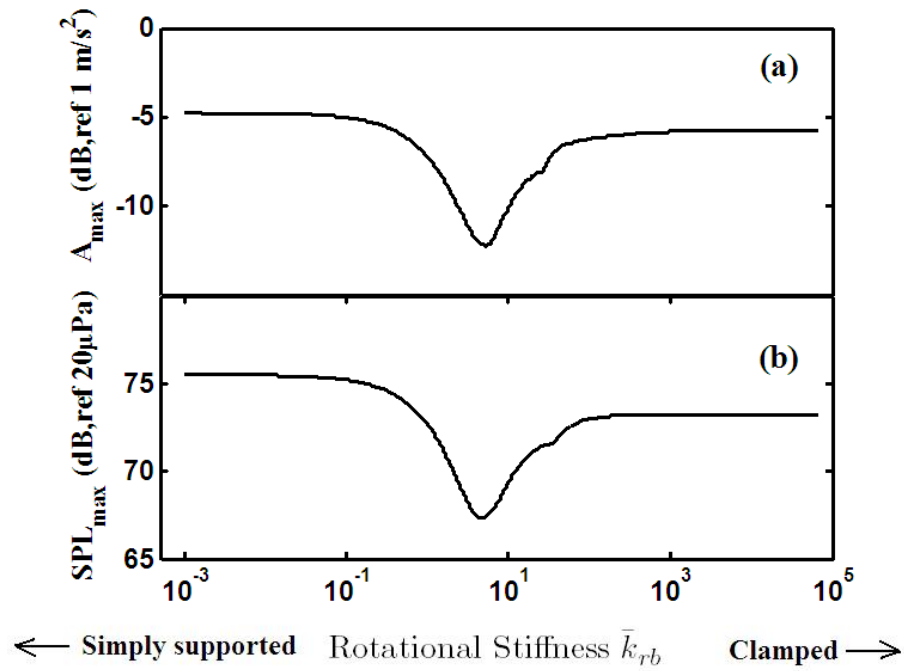


Figure 4.8 The maximum values of the acceleration level and radiated sound pressure level as a function of rotational stiffness: (a) Maximum acceleration level; (b) Maximum radiated sound pressure level

4.5 Summary

In this chapter, a time-domain prediction method has been developed to examine the effects of elastic boundary supports on the transient vibration and sound radiation (TVSR) of plate-like structures. The approach was based on the TDFEM and TDBEM, which allowed the plate to have arbitrary elastic boundary conditions.

An experimental setup was developed to validate the proposed model. In the experiment, the TVSR of a single Al panel with a non-classical boundary condition in two connected semi-anechoic chambers was measured. The actual boundary

condition of this plate system was obtained by using the BCI method in Chapter 3 and treated as an input of the proposed prediction model. The predictions agreed well with the experimental data.

Parametric studies were conducted to examine the effects of different boundary conditions on the TVSR of a single-pane glass window. The results showed a significant effect of the elastic boundary supports on the window's TVSR. The maximum values of the acceleration and radiated sound pressure could be effectively reduced by using appropriate boundary conditions. The results also demonstrated the feasibility and effectiveness of the proposed model as a design tool. Although the numerical examples were focused on the boundary conditions that vary between simply supported and clamped edges, the proposed method could be applied to solve the transient vibroacoustic problems of any arbitrary uniform or non-uniform elastic edge supports.

The development of the prediction method in this chapter can be a preliminary study for the following chapters (especially for Chapters 6 and 8) where the prediction method is extended to deal with the vibroacoustic problems of stiffened plate structures with general boundary conditions.

Chapter 5

A Study of the Effects of Spring-type Stiffeners on the Sound Transmission Loss of a Single Plate with General Elastic Boundary Conditions

5.1 Introduction

As mentioned in Chapter 1, two models were used to describe the effects of the stiffeners on a plate structure; these were the “spring-type stiffener” model and “beam-type stiffener” model. In this chapter, stiffened plate structures were investigated by using the “spring-type stiffener” model. The steady-state vibration and sound radiation (SVSR) of a stiffened plate is the focus of this chapter, while the transient vibration and sound radiation (TVSR) is studied in the next chapter. The study and application of the other stiffener model, the “beam-type stiffener” model, is introduced and studied in Chapters 7 and 8.

It is known that adding the stiffeners to a structure can influence structure dynamic characteristics and hence numerous models and theories have been constantly developed to investigate the effects of stiffeners. One of these studies by Lee et al.

[10] (who also used the “spring-type stiffener” model) revealed that the stiffener’s position and stiffness had notable effects on the sound transmission loss (STL) of the plate and could be possibly utilized to improve sound insulation performance in the frequency range of interest. Also, from the previous chapters, it could be seen that the boundary conditions had important effects and could not be neglected in the analysis of the vibroacoustic response of practical plate structures. Therefore, in order to systemically study the stiffened plate structure, a prediction method that can handle both the boundary conditions and the stiffeners is needed.

In this chapter, based on the “spring-type stiffener” model, a prediction method was developed that allowed the plate to have arbitrary elastic boundary conditions and arbitrarily located stiffeners. This method could be regarded as an extension of the method in Chapter 1 and was also based on the coupled finite element and boundary element method (FEM/BEM). A stiffened plate system was designed and used in the experiments to validate the proposed method. The STL values of this system were measured and compared with the predictions. The prediction method was subsequently applied to parametric studies that examine the effects of the stiffener on the STL of a window.

The layout of this chapter is as follows. Section 5.2 describes the basic principle of

the proposed method. Experimental validation studies are reported in Sec. 5.3. In Sec. 5.4, parametric studies on a practical stiffened window are present. Finally, a summary is given in Sec. 5.5.

5.2 Theoretical Framework

5.2.1 Description of the Problem

Consider a thin rectangular plate (length L_x , width L_y , thickness h) stiffened by a stiffener (or stiffeners) at arbitrary position on the plate, as shown in Fig. 5.1. The plate is considered to have arbitrary elastic boundary supports along the edges and be mounted on an infinite rigid baffle, as shown in Fig. 5.2. This plate baffle system separates the fluid medium into source section V^+ and receiver section V^- . A plane wave varying harmonically in source section V^+ is normally incident to the plate. The vibration of the plate induced by the incidence wave then radiates sound waves into the receiver section V^- .

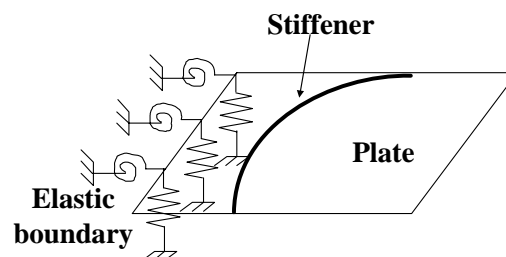


Figure 5.1 A rectangular stiffened plate with elastic boundary supports along the edges (for simplicity and clarity, only the supports along the left edge are shown)

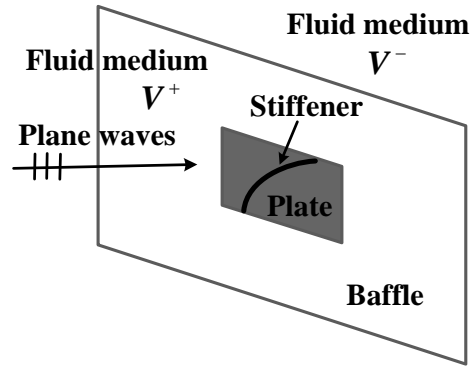


Figure 5.2 A baffled rectangular plate subjected to incident plane waves

5.2.2 The Coupled Vibroacoustic Model (Coupled FEM/BEM)

The vibration response of the stiffened plate system of Fig. 5.2 calculated by the FEM is given as,

$$(-\omega^2 \{M\} - j\omega \{D\} + \{K\})\{U\} = \{\mathcal{F}\}(\{P^+\} - \{P^-\}), \quad (5.1)$$

while the sound pressure on the plate surfaces calculated by the BEM are given as,

$$\{P^+\} = \{P_0\} + \{H\}\{w\}, \quad (5.2)$$

$$\{P^-\} = -\{H\}\{w\}, \quad (5.3)$$

The notations are the same as in Chapter 3.2.2, and are not described here again.

Some items worth mentioning are: $\{P_0\}$ is the vector representing the pressure of the incidence plane wave; $\{M\}$ and $\{K\}$ here are the global mass and stiffness matrices of the whole stiffened plate system, which are derived in the next subsection; the same relationship between $\{D\}$ and $\{K\}$ used in Chapter 4.2.2 is used here. Combining Eqs. (5.1)~(5.3), the unknown displacement $\{U\}$ can be

determined as

$$\{U\} = \left[-\omega^2 \{M\} - j\omega \{D\} + \{K\} - 2\{\mathcal{T}\}\{H\}\{\mathcal{R}\} \right]^{-1} \{\mathcal{T}\}\{P_0\}. \quad (5.4)$$

Once $\{U\}$ is obtained, the deflection $\{w\}$ and the sound pressures $\{P^+\}$ and $\{P^-\}$ can then be solved by Eqs. (3.3), (5.2) and (5.3). Since the fluid loading effect is taken into account (see Eq. (5.4)), this coupled vibroacoustic model can give more accurate results and have the potential to be applied to a plate in contact with liquid.

5.2.3 Stiffness and Mass Matrices of the Whole Stiffened Plate System

The stiffness matrix $\{K\}$, in Eq. (5.1), of the stiffened plate system is decomposed into plate, boundary supports and stiffeners contributions, and can be expressed as

$$\{K\} = \{K_p\} + \{K_b\} + \{K_s\}, \quad (5.5)$$

where $\{K_p\}$, $\{K_b\}$, $\{K_s\}$ are the stiffness matrices for the plate, boundary supports and stiffeners, respectively. The mass matrix $\{M\}$, in Eq. (5.1), of the whole plate system is decomposed into plate and stiffeners contributions, and can be

$$\{M\} = \{M_p\} + \{M_s\}, \quad (5.6)$$

expressed as where $\{M_p\}$ and $\{M_s\}$ are the mass matrices for the plate and stiffeners, respectively. Since $\{K_p\}$, $\{K_b\}$ and $\{M_p\}$ have been derived in Chapter 3.3.2 (see Eqs. (3.6) and (3.7)), the following is focused on the determination of the matrices $\{K_s\}$ and $\{M_s\}$.

As in reference 10, the stiffeners can be represented as a combination of masses,

translational (k_{ts}), and rotational (k_{rs}) springs. The kinetic (T_{se}) and strain (Π_{se}) energy of the stiffener in the plate element (as shown in Fig. 5.3) can be expressed as

$$T_{se} = \int \frac{1}{2} \sigma_s \left(\frac{\partial w}{\partial t} \right)^2 dl_{se}, \quad (5.7)$$

$$\Pi_{se} = \int \left(\frac{1}{2} k_{ts} w^2 + \frac{1}{2} k_{rs} \left(\frac{\partial w}{\partial \bar{n}_s} \right)^2 \right) dl_{se}, \quad (5.8)$$

where σ_s is the line density function describing the added-mass effect caused by the stiffener, and \bar{n}_s is the normal unit vector of the stiffener axis l_{se} (see Fig. 5.3).

The transverse displacement can be represented by the element nodal displacement vector $\{U\}_e$ as $w = \{N_w\} \{U\}_e$. Eqs. (5.7) and (5.8) can then be rewritten as

$$T_{se} = \frac{1}{2} \{\dot{U}\}_e^T \{M_s\}_e \{\dot{U}\}_e, \quad (5.9)$$

$$\Pi_{se} = \frac{1}{2} \{U\}_e^T \{K_s\}_e \{U\}_e, \quad (5.10)$$

where

$$\{M_s\}_e = \int \left(\sigma_s \{N_w\}^T \{N_w\} \right) dl_{se}, \quad (5.11)$$

$$\{K_s\}_e = \int \left(\begin{array}{l} k_{ts} \left(\{N_w\}^T \{N_w\} \right) + k_{rs} \sin^2 \theta \left(\{N_x\}^T \{N_x\} \right) \\ -k_{rs} \sin 2\theta \left(\{N_x\}^T \{N_y\} \right) + k_{rs} \cos^2 \theta \left(\{N_y\}^T \{N_y\} \right) \end{array} \right) dl_{se}, \quad (5.12)$$

where σ_s is the line density function describing the added-mass effect caused by the stiffener, l_s is taken along the stiffener axis, $\{N_x\}$ and $\{N_y\}$ stand for

$\frac{\partial \{N_w\}}{\partial x}$ and $\frac{\partial \{N_w\}}{\partial y}$ (respectively), and θ is the angle between the global axis

and the local axis of the stiffener. If the stiffener is curved with its direction changing from point to point, θ is not a constant but a function of the x coordinate, as shown

in Fig. 5.3. It can be seen from Eqs. (5.11) and (5.12) that the position of the stiffener inside the plate element is not restricted. This model can use straight-line stiffeners that are not parallel to the plate edges or even curved stiffeners.

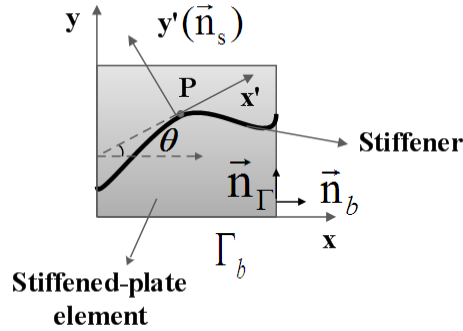


Figure 5.3 The stiffened plate element. A local (x', y') axis is set along the tangent to the stiffener at the integration point P making an angle θ with the global (x, y) axis

Once the matrices $\{M_s\}_e$ and $\{K_s\}_e$ are solved, the matrices $\{K_s\}$ and $\{M_s\}$ in Eqs. (5.5) and (5.6) can be easily obtained according to the finite element assembly procedure [51].

5.2.4 Sound Transmission Loss (STL)

The sound transmission loss (STL) of the plate can be defined as [80]

$$\text{STL} = 10 \log_{10} \left(\frac{W^+}{W^-} \right), \quad (5.13)$$

where W^+ and W^- are the sound power at the front plate surface (in the source section V^+) and the radiated sound power at the back plate surface (in the receiver section V^-) (see Fig. 5.2). They can be expressed as

$$W^{\pm} = \frac{1}{2}(j\omega\Delta S) \times \text{Re} \left[\left\{ P^{\pm} \right\}^T \left(\left\{ w^{\pm} \right\}^* \right) \right], \quad (5.14)$$

where ΔS is the area of the plate element, $\{w^+\} = -\{w^-\} = \{w\}$, and the superscript asterisk denotes the complex conjugate.

The overall STL in a given frequency range is defined as

$$\text{STL}_{\text{overall}} = 10 \log_{10} \left(\frac{\sum_{f=f_1}^{f_2} W^+}{\sum_{f=f_1}^{f_2} W^-} \right), \quad (5.15)$$

where f_1 and f_2 are, respectively, the lower and upper frequencies of the given frequency range.

5.3 Experimental Validation

5.3.1 Experimental Setup

The stiffened plate system used in the experiments consisted of a 1mm-thick aluminum (Al) panel, two identical steel beams and two identical steel frames. Fig. 5.4 shows the assembly of these components. The same Al panel (“Panel 1”) and steel frames have been used in Chapter 3.3.1 for the modal testing and their dimension information can be found there. The Al panel was installed in the two steel frames. Screws #1 on the steel frames were used to fix the frames to the wall, while screws #2 were used to fix the steel beam. The two steel beams, with 23mm depth and 5mm width for each, could then be placed on the Al panel on both sides (parallel to the bottom line of the plate). Note that the two beams worked together to

represent a single stiffener, and the length of the stiffener was 24 cm. The position of the stiffener is shown in Fig. 5.4 (b).

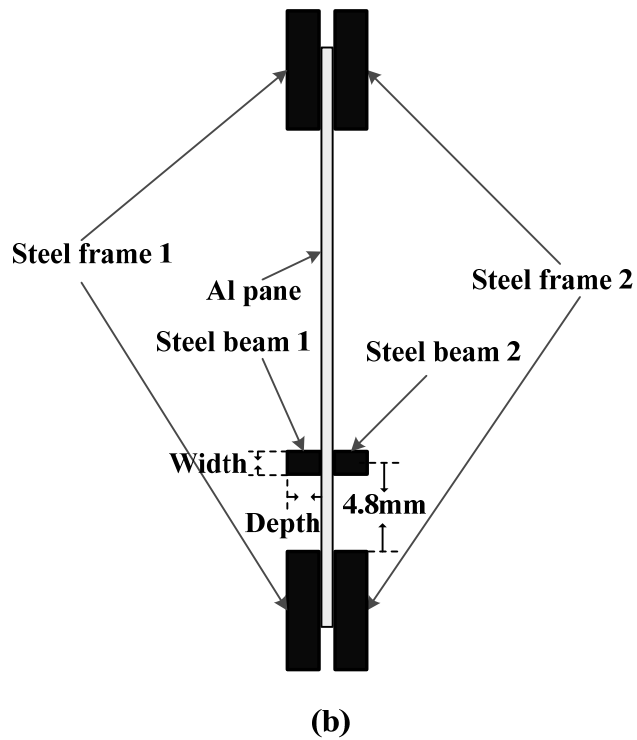
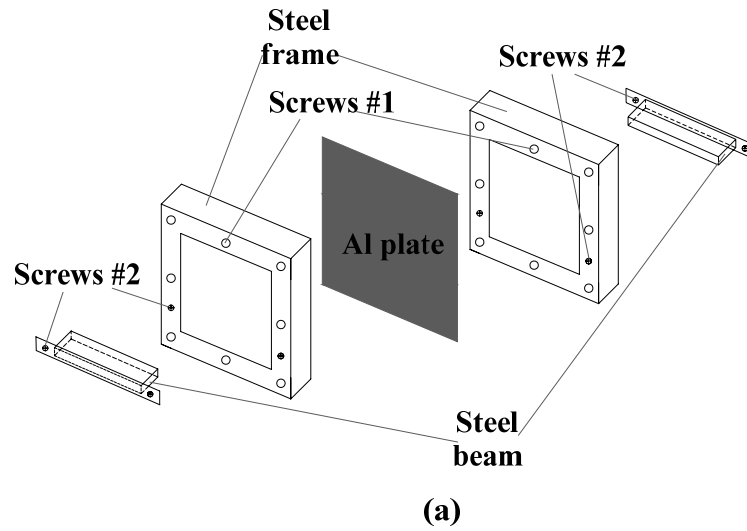


Figure 5.4 Schematic diagram of the assembly of the stiffened plate system used in the experiments: (a) Before assembly; (b) After assembly

The feature of this design was that stiffeners (like beams) could easily be set on different positions of the panel or taken away from the panel. The parametric studies in next section show that the stiffener laid in different position leads to different STL curve. Hence, this system could be a good example for the stiffened window design in buildings. Even when a window has already been mounted on the wall, the stiffeners can conveniently be added to the window (in the proper positions) to improve the sound insulation performance or removed from the window to avoid the visual obstruction.

The measurements were conducted in two connected chambers at The Hong Kong Polytechnic University. The same spot has been used in the experimental studies in Chapter 4.3.1 and details can be found there. As shown in Fig. 5.5, a loudspeaker (diameter 25 cm) was located in the smaller chamber with a distance of 40 cm from the Al panel to provide an approximation of a normally incident plane wave. A broadband white noise signal (0-800Hz) was used to drive the speaker. Two microphones (B&K: 4935) were located respectively on the incident side and the radiated side at the same distance (20 cm) from the Al panel at the center line to measure the sound pressure on both sides. The microphone on the radiated side was placed normal to the Al panel to give a representative sound pressure level of the whole radiated field [80]. All measured data were collected by PULSE (B&K:

3160-B-042). The STL of the plate system could then be determined using these data, as in reference 80.

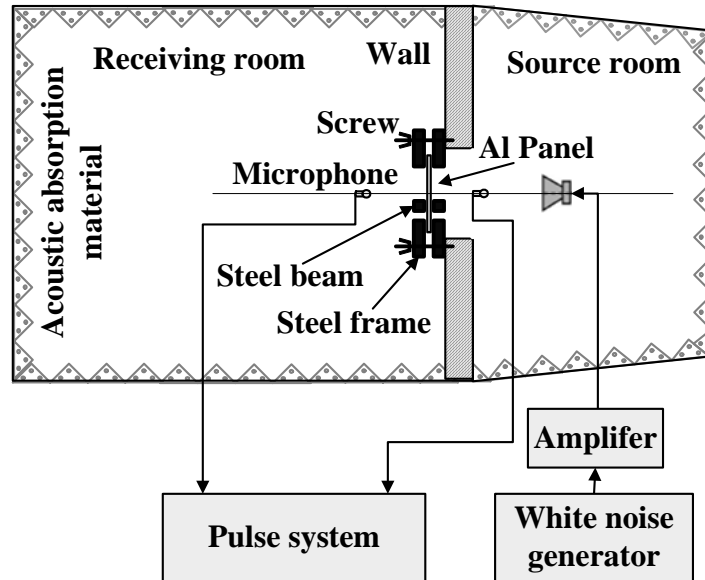


Figure 5.5 Schematic diagram of the experimental setup for measuring the STL of a baffled stiffened plate system

5.3.2 Parameters of the Boundary Supports and the Stiffener

The actual parameters of the boundary supports and the stiffener used in the experiments need to be determined before comparing the predictions and experimental measurements.

The boundary condition of the plate system was virtually identical before and after the stiffener was installed in the experimental installation (Fig. 5.4). Therefore, the boundary parameters of the same plate system (without the stiffener) identified in

Chapter 3.3.3 were directly used here, which were $\bar{k}_{tb} = 3201$ and $\bar{k}_{rb} = 13.28$.

For the stiffener, the translational spring constant k_{ts} was supposed to be infinitely large. The reasons were: (1) the steel beam was much stiffer than the Al panel; (2) the beam depth was far greater than the panel thickness; and (3) both the steel beams were hard pressed on the panel. The exact actual added mass and rotational stiffness to the plate system due to the stiffener were not easy to assess. Fortunately they were found to have almost no effect on the system's vibration or sound radiation when k_{ts} was very large (such as $k_{ts} = 10^{10}$). Lee and colleagues [10] have also noted this phenomenon. Therefore, in the prediction model the stiffener parameters were set to be $k_{ts} = \infty$, $k_{rs} = 0$ and $\sigma_s = 0$ for simplicity.

5.3.3 Experimental Results and Discussion

Fig. 5.6 (a) shows a comparison of the predicted and experimental STL values of the stiffened plate system as a function of frequency (50-800Hz). The element number and damping factor in the numerical calculations were the same as used in Chapter 4.3.2. The STL of the same plate system but without the stiffener was also measured and shown in Fig. 5.6 (b) for comparison. STL values below 50Hz do not exist, since this was the frequency range where the output of the loudspeaker was too poor to obtain a sufficient signal-to-noise ratio.

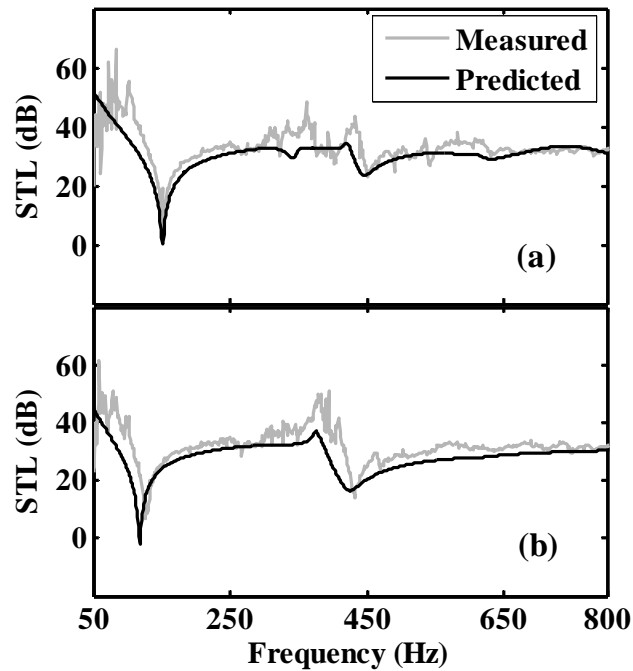


Figure 5.6 Comparison of the predicted and measured results: (a) Stiffened plate; (b) Unstiffened plate

Fig. 5.6 (a) shows that the predicted STL results agree well with those from the experiment. The discernible discrepancies can be attributed to a number of factors, such as the unavoidable flanking transmission paths, non-uniform boundary conditions along the plate edges, and imperfect stiffener (beam) installation.

The results of Fig. 5.6 (a) and (b) clearly demonstrate the significant influence of stiffener on the STL of a plate system. Owing to the additional stiffness, the first resonance frequency of the stiffened system was about 40Hz higher than that of the unstiffened case. The main effect of the stiffener is to shift the locations of the

resonance frequencies, especially the fundamental resonance frequency. Therefore, the stiffening treatment could be a potential means to improve the sound insulation property by shifting the fundamental resonance frequency away from the unwanted range. It is also worth mentioning that by the stiffening treatment, the dips of the system's STL curve can be moved but not removed. In this case, the fundamental resonance frequency has been shifted to about 160 Hz; therefore, if the external excitation has a high energy closed to this frequency, the stiffening treatment shown in Fig. 5.4 would cause even poorer sound insulation. The parametric studies in next sub-section show that different stiffener location leads to different system resonance frequencies. When facing to a specific plate system, the proposed prediction method can therefore be an effective tool to decide whether or not to add the stiffening treatment and where to add.

5.4 Parametric Studies

Parametric studies were carried out on a stiffened glass window by using the present model. The window was 0.8m long, 0.8m wide, and 4mm thick. Young's modulus, density, Poisson's ratio, and damping factor were 65 GPa, 2500 kg/m³, 0.25, and 0.01, respectively. A single stiffener of 0.8 m length was used to stiffen the window. The dimensionless boundary parameters (\bar{k}_{tb} and \bar{k}_{rb}), the stiffener stiffness parameters (k_{ts} and k_{rs}), and the element number used in this section were the

same as in Sec. 5.3.

The effects of different locations of the stiffener on the window's STL were our focus. Unlike most of the existing studies that assumed the stiffener to be parallel to the plate edges, the stiffener was unparallel to the edges. The location of the stiffener was dependent only on the angle θ , as shown in Fig. 5.7. The angle θ was the only variable in this parametric study.

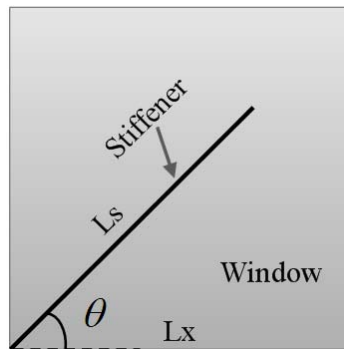
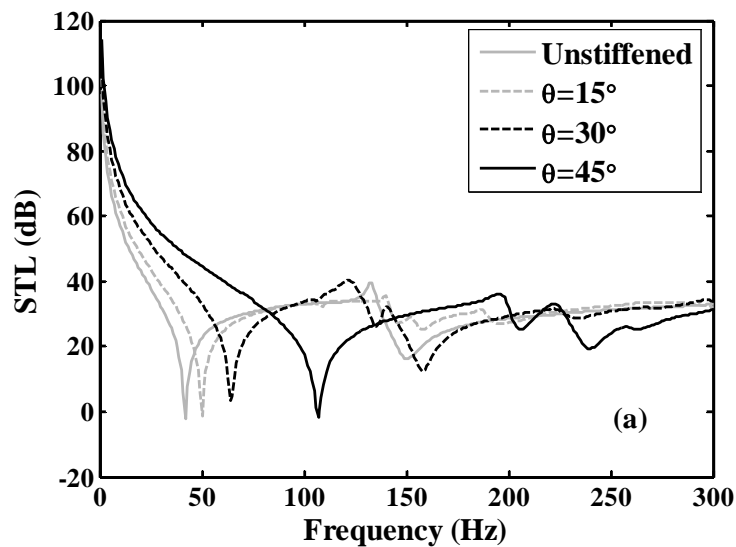


Figure 5.7 Schematic diagram of the stiffened window

Fig. 5.8 shows the effect of the stiffener location on the STL, and for comparison the STL curve of the same window but without stiffeners is included. It can be seen from the Fig. 5.8 (a) that due to the additional stiffness the stiffened window has higher resonance frequency than the unstiffened window. The resonance frequency increases as θ ($0 < \theta < 45$) increases. Fig. 5.8 (b) shows the overall STL values for different θ . The overall STL values were calculated in the band between 25 and 100Hz (i.e. only applicable to the band between 25 and 100Hz). The reason to choose this frequency range was because this was the frequency range where the

noise could be more annoying to human, as shown in Tokita and Nakamura's threshold [81] for the perception of low-frequency noise. It can be seen from Fig. 5.8 (b) that the stiffener location (or θ) has a notable effect on the overall STL of the window. In this case, the window with the stiffener at the angle of 45° has the largest overall STL which is about 13 dB higher than that of the unstiffened window. This is because, as shown in Fig. 5.8 (a), the fundamental resonance frequency of $\theta = 45^\circ$ is beyond the frequency range (25~100Hz). Fig. 5.8 (b) also shows that the window with the stiffener at angles 5° , 20° , 25° , and 30° has even lower overall STL than the unstiffened window, indicating that stiffening the window at the proper locations is also important.



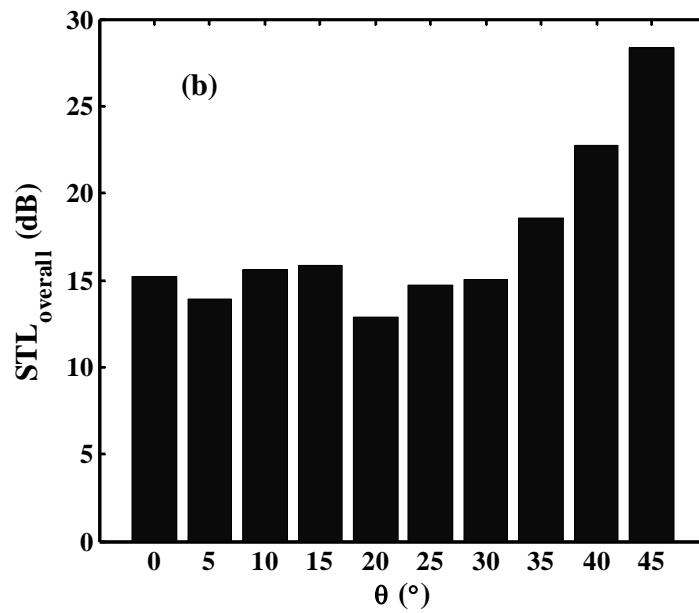


Figure 5.8 STL values for the stiffened window with respect to θ : (a) STL curves from 1 Hz to 300 Hz; (b) Overall STL values (25 Hz~100 Hz)

The simulations in this parametric study have shown that even a single stiffener has significant effect on the STL of a window. The resonance frequencies are notably influenced by the stiffener location. Stiffening the window at a proper position could be a potential means to improve the sound insulation property in the frequency range of interest.

5.5 Summary

In this chapter, a method has been developed to examine the steady-state vibration and sound radiation (SVSR) of a stiffened plate. The approach was based on a coupled FEM/BEM method, which allowed the plate to have arbitrary elastic boundary conditions and arbitrarily located stiffeners. The “spring-type stiffener”

model was used in the modeling of the stiffeners. The fluid loading effect was taken into account, making the model more realistic.

An experimental setup was developed to validate the proposed model. In the experiment, the sound transmission loss (STL) of a stiffened aluminum (Al) plate system with a non-classical boundary condition in two connected semi-anechoic chambers was measured. The actual boundary parameters of this plate system were obtained by using the BCI method in Chapter 3 and the stiffener parameters were estimated according to the experimental setup. The predictions agreed well with the experimental data.

Parametric studies were conducted to examine the effects of the stiffener on the STL of a single-pane glass window. The results showed a significant effect of the stiffener on the window's STL. The resonance frequencies were notably influenced by the stiffener location. The overall STL in the frequency range of interest could be effectively increased by stiffening the window at proper positions. The results also demonstrated the feasibility and effectiveness of the proposed model as a design tool. Although the effects of stiffeners were the focus of these studies, the proposed method could also be applied to examine the effects of boundary supports on the SVSR of a stiffened window.

Chapter 6

A Study of the Effects of Spring-type Stiffeners on the Transient Vibroacoustic Response of a Single Plate with General Elastic Boundary Conditions

6.1 Introduction

The steady-state vibration and sound radiation (SVSR) of a stiffened plate with general elastic boundary conditions have been studied in Chapter 5. The sound transmission loss was predicted by using the method in Chapter 5. However, since a large portion of the actual excitations in daily life are transient in nature, the SVSR model is sometimes not so efficient for solving the transient vibroacoustic response to such excitations. In this chapter, a time-domain prediction method was developed, as well as the corresponding experimental studies, to examine the transient vibration and sound radiation (TVSR) of the stiffened plate with general boundary conditions.

The time-domain finite element method (TDFEM) and time domain boundary element method (TDBEM) in Chapter 4 and the “spring-type stiffener” model in

Chapter 5 were utilized in the development of the present method. This allowed the method to be more efficient for solving the transient vibroacoustic response of plate structures with arbitrary elastic boundary conditions and arbitrarily located stiffeners. Also, in order to validate the proposed method, a similar experimental setup as in Chapter 5 was used in this chapter for the measurement of the transient sound radiation of the stiffened plate system. The prediction method was subsequently applied to parametric studies that examine the effects of the stiffener on the TVSR of a window.

The layout of this chapter is as follows. Section 6.2 describes the basic ideas of the proposed method. Experimental validation studies are reported in Sec. 6.3. In Sec. 6.4, parametric studies on a practical stiffened window are present. Finally, Sec. 6.5 gives the summary.

6.2 Theoretical Framework

6.2.1 Description of the Problem

Consider a thin rectangular plate (length L_x , width L_y , thickness h) stiffened by a stiffener (or stiffeners) at arbitrary position on the plate. The plate is considered to have arbitrary elastic boundary supports along the edges and is mounted on an infinite rigid baffle. The whole baffled plate is immersed in an infinite light fluid

medium (air). The effect of fluid loading on the plate's vibration is neglected. The plate is subject to a transient force $F(t)$ (or a transient incidence wave $p_0(t)$), as shown in Fig. 6.1. The vibration of the plate induced by the transient input excitations then radiates sound waves into the fluid medium.

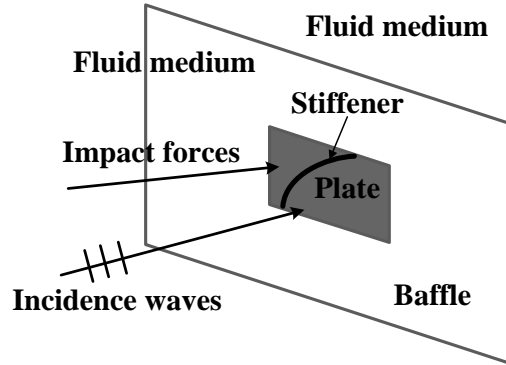


Figure 6.1 A baffled rectangular stiffened plate subjected to transient forces (or transient incidence waves)

6.2.2 Time-domain Vibroacoustic Model

Based on the TDFEM and TDBEM, the expressions for the vibration responses of the plate system (see Fig. 6.1) to transient excitations and the corresponding radiated sound field have already been derived in Chapter 4.2, which are given by

$$\{M\}\{\ddot{U}\} + \{D\}\{\dot{U}\} + \{K\}\{U\} = \{F(t)\} + \{\mathcal{S}\}\{p_0(t)\}, \quad (6.1)$$

and

$$p(\xi, t) = \int_{S_p} \int_0^t \rho_0 \sigma_H(x, t; \xi, \tau) \dot{w}(x, \tau) d\tau dS. \quad (6.2)$$

The element, mesh method and numerical implementation method used in the

TDFEM and TDBEM are the same as in Chapter 4.2, and are not described here again. What is worth mentioning is that $\{M\}$ and $\{K\}$ in Eq. (6.1) are the global mass and stiffness matrices (respectively) of the whole stiffened plate system, which need to include the mass and stiffness matrices of the stiffeners. The “spring-type stiffener” model is used to determine the matrices for the stiffeners, in which the stiffeners are represented as a combination of masses, translational, and rotational springs. The determination of the global mass and stiffness matrices $\{M\}$ and $\{K\}$ have been described in detail in Chapter 5.2.3 and can be found there.

6.3 Experimental Validation

6.3.1 Experimental Setup

The stiffened plate system used in the experiments was a 1.5 mm aluminum (Al) panel (“panel 2” in Chapter 3.3.2), two identical steel beams, and two identical steel frames. The assembly of these components was the same as in Chapter 5.3.1 (see Fig. 5.4 (a)). The measurements were conducted in two connected chambers at The Hong Kong Polytechnic University. The same spot have been used in the experimental studies in Chapter 4.3.1 and details can be found there. As shown in Fig. 6.2, A Kistler 9726A impact hammer was used to produce a transient impact force acting on the Al panel, and a B&K4935 microphone was located at the center line of the Al panel (20 cm away from the panel) to measure the radiated sound. The locations of

the stiffener and the impact point are shown in Fig. 6.3. All data were collected by PULSE (Type B&K 3160-B-042) at a sampling rate of about 8.2 kHz (0.12 ms) for a recorded length of 1 second.

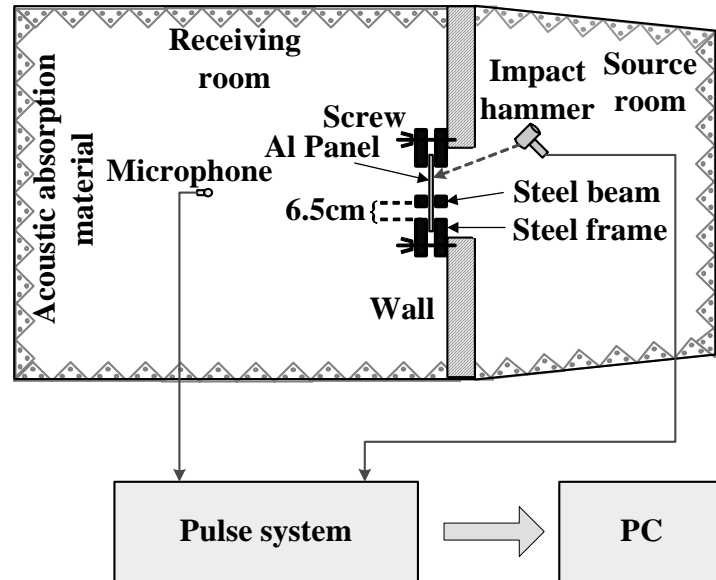


Figure 6.2 Schematic diagram of the experimental setup for measuring the transient sound radiation of a baffled stiffened plate system

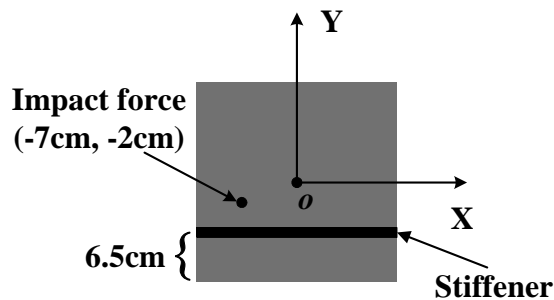


Figure 6.3 Locations of the stiffener and the impact force

6.3.2 Experimental Results and Discussion

Fig. 6.4 compares the predicted and measured radiated sound. To make more comprehensive comparisons between these responses, a fast Fourier transform (FFT)

was used to convert the responses into frequency spectrum data. The measured impact force shown in Fig. 6.5 was used as the input to the prediction model. In the numerical calculations, the element number was 64 (8×8); the boundary parameters were $\bar{k}_{tb} = 1162$ and $\bar{k}_{rb} = 7.69$, which were obtained by using the BCI method in Chapter 3.3.3; the damping factor was $\eta = 0.04$, which was estimated by using a peak-picking method [73]; and the stiffener parameters were $k_{ts} = \infty$, $k_{rs} = 0$ and $\sigma_s = 0$, which have been explained in Chapter 5.3.2. The predicted radiation pressure of the unstiffened plate to the same force was also included in Fig. 6.4 for comparison. For the unstiffened plate, all the parameters remained the same except for those related to the stiffener, whose values were simply set to zero.

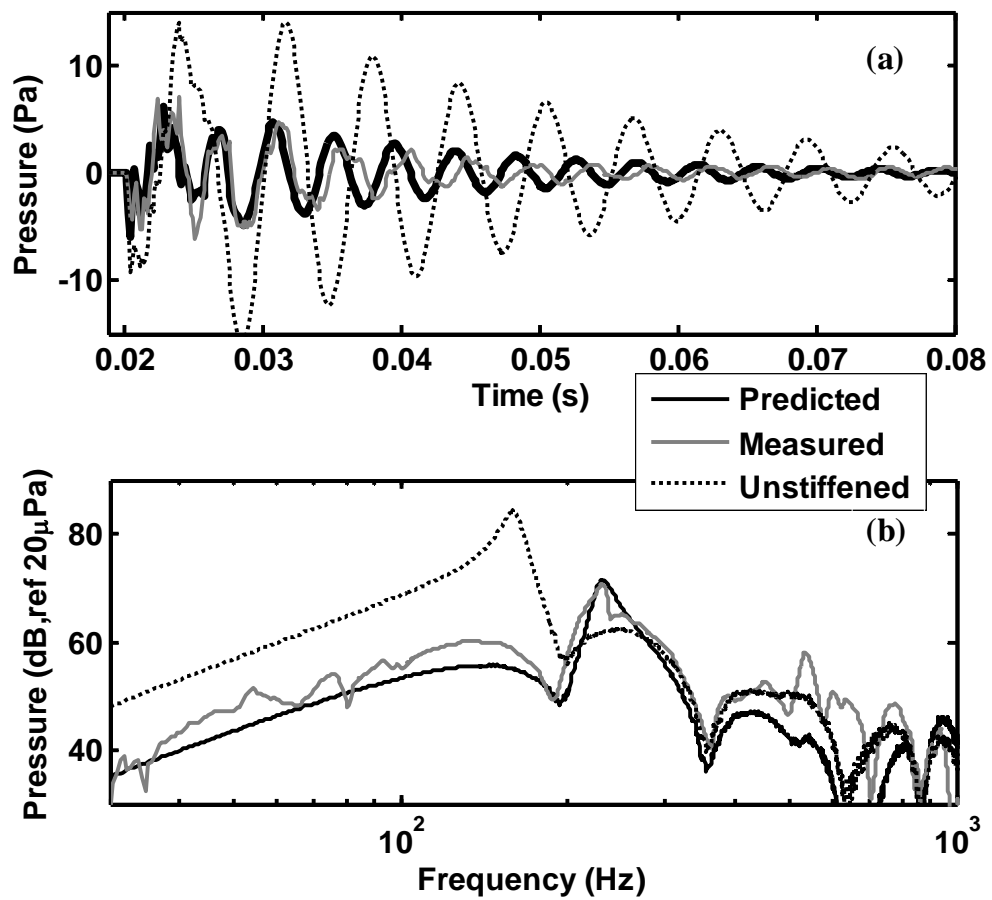


Figure 6.4 Comparison of the predicted results and experimental data: (a) Pressure time history; (b) Pressure frequency spectrum. Note that predicted radiated pressure of the unstiffened plate is also included

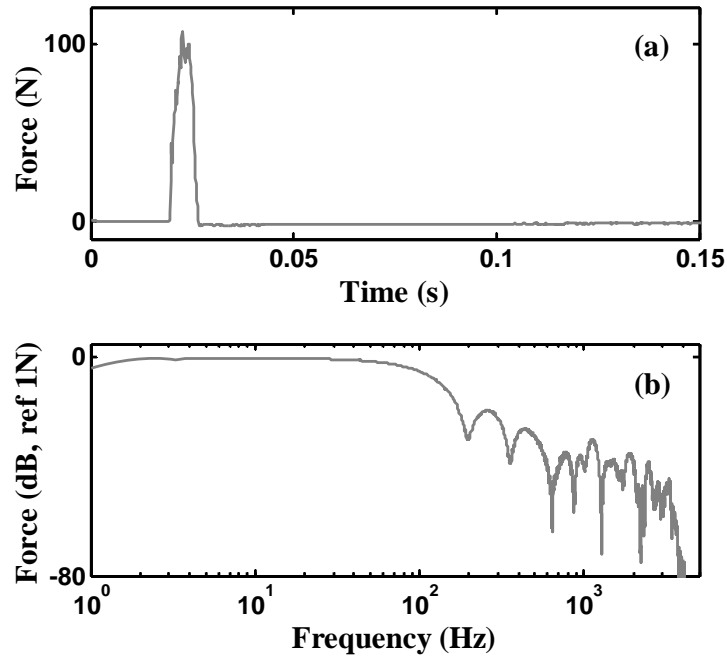


Figure 6.5 Impact force: (a) Time history; (b) Frequency spectrum

As Fig. 6.4 shows, the predicted transient sound radiation results are in good agreement with the experimental data. The discernible discrepancies can be attributed to a number of factors, such as the unavoidable flanking transmission paths, non-uniform boundary conditions along the plate edges, and imperfect stiffener (beams) installation. In addition, there was only a rough estimate of the location of the impact point when the hammer was struck by hand.

Fig. 6.4 also clearly demonstrates the significant influence of a stiffener on the transient radiation of the plate system. The radiation pressure of the stiffened plate was much lower than that of the unstiffened plate, which could be explained as

follows: (1) the excitation energy generally decreased as the frequency increased, especially above 100 Hz (see Fig. 6.5); and (2) the fundamental modes of the stiffened and unstiffened plates were around 160 Hz and 230 Hz (respectively), which indicated that the fundamental mode of the stiffened plate was farther away from the higher energy range of the source (excitation) spectrum.

6.4 Parametric Studies

Parametric studies were carried out on a stiffened glass window by using the present model. The window was 70cm long, 70cm wide and 5mm thick, with the Young's modulus 65GPa, density 2500 kg/m³ and Poisson's ratio 0.25. A single stiffener of 0.4 m length was used to stiffen the window. The location of the stiffener was dependent only on the angle θ , as shown in Fig. 6.6. The angle θ was the only variable in this parametric study. The dimensionless boundary parameters (\bar{k}_{tb} and \bar{k}_{rb}), the stiffener stiffness parameters (k_{ts} and k_{rs}), the damping factor and the element number used in this section were the same as in Sec. 6.3.

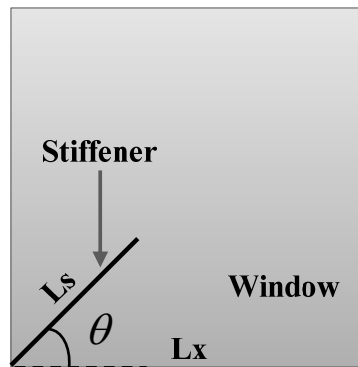


Figure 6.6 Schematic diagram of the stiffened window

The stiffened window was impacted at normal incidence by a transient sound pulse (a half-sine wave), as shown in Fig. 6.7. Fig. 6.8 shows the resulting acceleration response at the center of the window while Fig. 6.9 shows the resulting sound radiation at point “P”. Point “P” is on the axis of symmetry a distance of 0.1 m away from the window. For comparison, the predictions of the same window without stiffeners are also included in the figures. To make more comprehensive comparisons between these responses, a fast Fourier transform (FFT) was used to convert the responses into frequency spectrum data. The time interval Δt used in the numerical calculation was 0.5 ms.

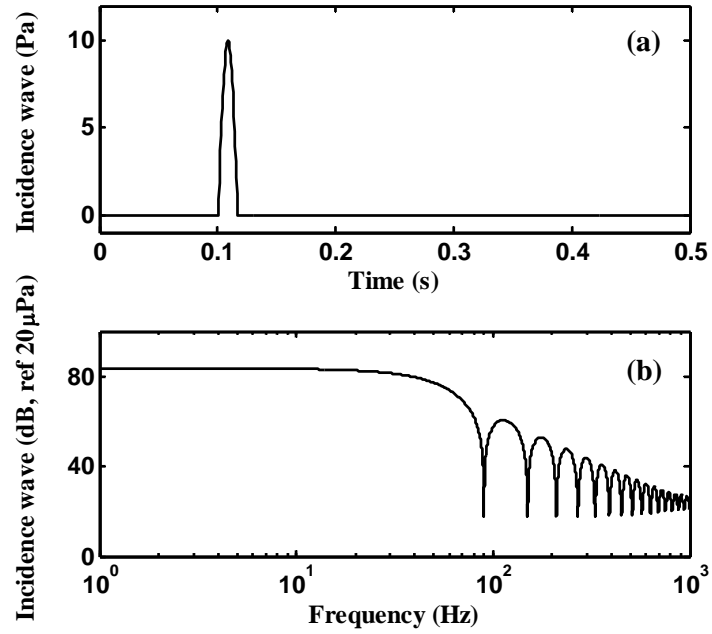


Figure 6.7 A transient sound pulse (a half-sine wave): (a) Pressure time history; (b) Pressure frequency spectrum

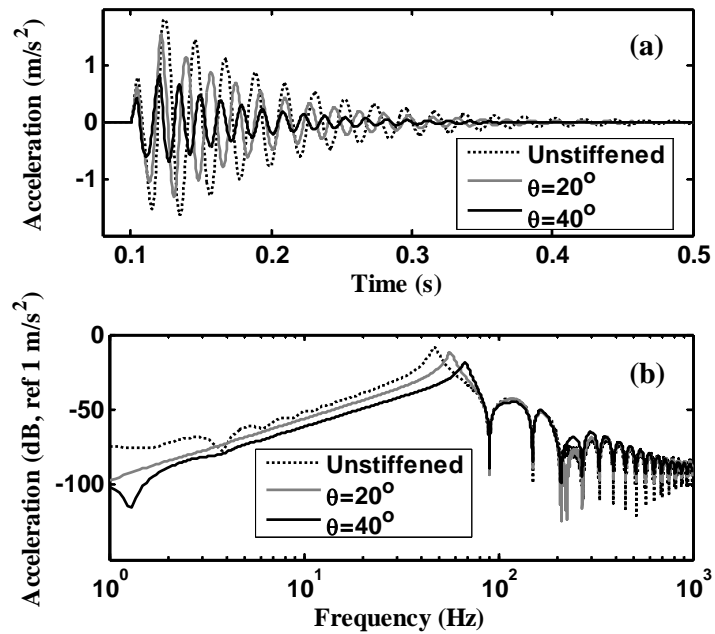


Figure 6.8 Acceleration responses at the center of the window: (a) Acceleration time history; (b) Acceleration frequency spectrum

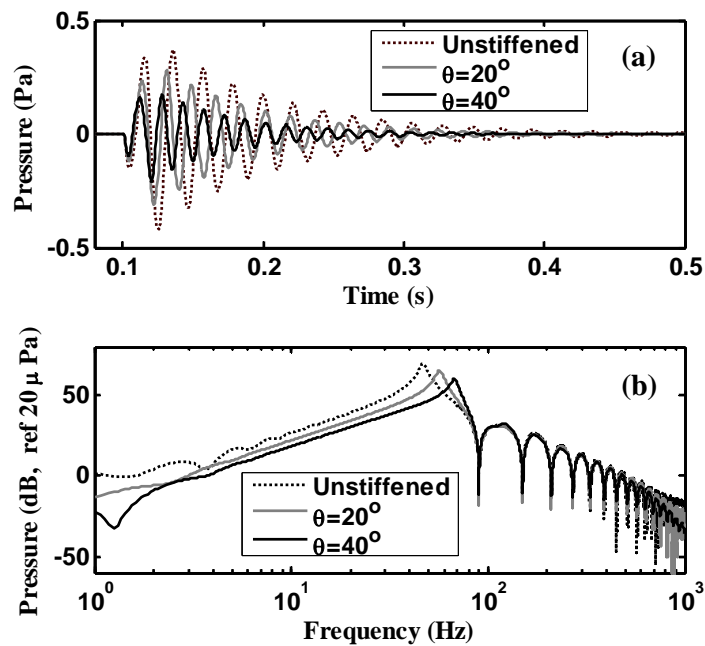


Figure 6.9 Radiated sound pressure at point “P”: (a) Pressure time history; (b) Pressure frequency spectrum. Point “P” is on the axis of symmetry a distance of 0.1 m away from the window

It can be seen clearly from Figs. 6.8 and 6.9 that the TVSR responses of the stiffened window are different from those of the unstiffened window. Also, different stiffener locations (or θ) lead to different TVSR responses. One major effect of the stiffeners (and their locations) is that they can influence the resonance frequencies of the structure (window). Stiffening the window at proper locations can shift the resonance frequencies to higher values, and the TVSR responses of the window can therefore be reduced when impacted by the transient loads having higher energy in low-frequency range. This type of loads (noise) commonly exists in the daily life and is of particular concern because of its efficient propagation and reduced efficacy of

many building structures in attenuating low-frequency noise compared with other noise [82].

The maximum values of the acceleration level $A_{\max} = \max \left[20 \lg \left(\frac{|\ddot{w}(t)|}{\ddot{w}_{ref}} \right) \right]$ and radiated sound pressure level $SPL_{\max} = \max \left[20 \lg \left(\frac{|p(t)|}{p_{ref}} \right) \right]$ can be easily obtained from the TVSR responses and are shown in Fig. 6.10 as a function of θ , where $\ddot{w}(t)$ is the nodal accelerations of the whole plate and $p(t)$ is the sound pressure at point “P”. It can be seen from the figure that the stiffener location (or θ) has a notable effect on A_{\max} and SPL_{\max} of the window. In this case, there exists an optimum value ($\theta = 45^\circ$) at which A_{\max} and SPL_{\max} are minimized. Reductions of about 5 dB and 6 dB can be obtained in A_{\max} and SPL_{\max} , respectively, in comparison with those of the unstiffened window.

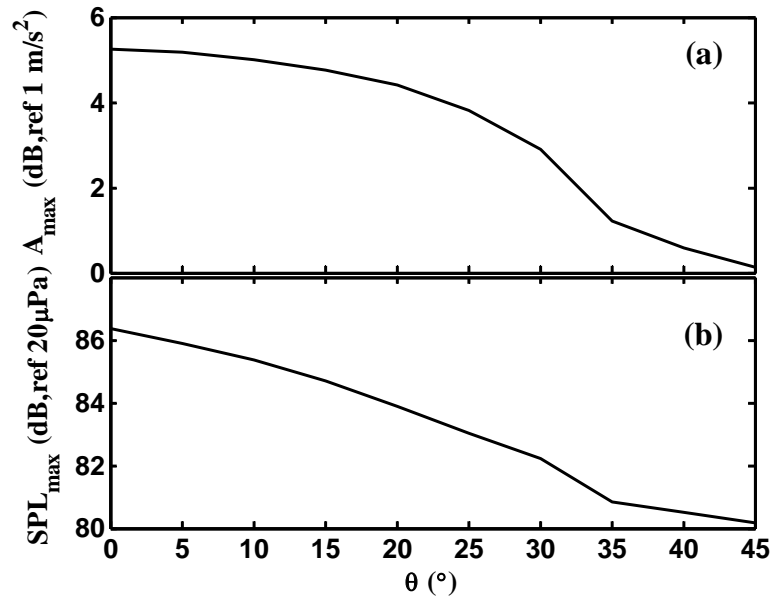


Figure 6.10 The maximum values of the acceleration level and radiated sound pressure level as a function of θ : (a) Maximum acceleration level; (b) Maximum radiated sound pressure level

6.5 Summary

In this chapter, a time-domain prediction method has been developed to examine the transient vibration and sound radiation (TVSR) of a stiffened plate. The approach was based on the TDFEM and TDBEM, which allowed the plate to have arbitrary elastic boundary conditions and arbitrarily located stiffeners. The “spring-type stiffener” model was used in the modeling of the stiffeners.

A similar experimental setup as in Chapter 5 was used to validate the proposed model. In the experiment, the transient sound radiation of a stiffened aluminum (Al) plate system with a non-classical boundary condition in two connected

semi-anechoic chambers was measured. The actual boundary parameters of this plate system were obtained by using the BCI method in Chapter 3 and the stiffener parameters were estimated according to the experimental setup. The predictions agree well with the experimental data.

Parametric studies were conducted to examine the effects of the stiffener on the TVSR of a single-pane glass window. The maximum values of the acceleration and radiated sound pressure could be effectively reduced by using appropriate stiffeners. Moreover, although the effects of stiffeners were the focus of these studies, the proposed method could also be applied to examine the effects of boundary supports on the TVSR of a stiffened window. The proposed model can be used as a design tool to improve the transient noise insulation performance of a window.

Chapter 7

A Study of the Effects of Beam-type Stiffeners on the Sound Transmission Loss of a Single Plate with General Elastic Boundary Conditions

7.1 Introduction

The effects of the stiffeners on a single plate with general elastic boundary conditions have been studied in Chapters 5 and 6 by using the “spring-type stiffener” model. The results clearly showed the significant effects of the stiffeners on both the steady-state and transient response of plate structures. As mentioned in Chapter 1, there is another model, “beam-type stiffener” model that is also commonly used in the modeling of the stiffened plate structures. A large number of the practical structures, such as aircraft, ships, bridges and buildings, were modeled and analyzed by using this model [58, 59, 83]. In this chapter, stiffened plate structures were investigated by using the “beam-type stiffener” model. The steady-state vibration and sound radiation (SVSR) of a stiffened plate is the focus of this chapter, while the transient vibration and sound radiation (TVSR) is studied in the next chapter.

Most earlier work dealing with the vibroacoustic problems of stiffened plate structures by using the “beam-type stiffener” model were limited to periodically stiffened plates [10, 39, 84, 85], or else to cases where stiffeners were parallel to the plate edges [86]. Moreover, the clamped or simply supported boundary condition (or their combinations) were usually assumed in these studies. These requirements limit their practical applications. In addition, the in-plane displacement of the plate should be considered, especially when eccentric stiffeners are used, because the eccentricity gives rise to the in-plane deformation of the plate in addition to a bending deformation [43, 87].

In this chapter, based on the “beam-type stiffener” model, a method was developed for estimating the SVSR of the stiffened plate structure. The coupled finite element and boundary element method (FEM/BEM) in Chapter 5 was used in the present model. The stiffened-plate element proposed by Barik et al. [59] was adopted to extend the method to allow the analysis of plates with arbitrary elastic boundary conditions and arbitrarily located stiffeners. Also, this element took into account of the plate in-plane deformation. It is known that the natural frequencies of a structure are important to both its vibration and its sound radiation performance. Numerical studies were therefore conducted to analyze the natural frequencies of concentrically/eccentrically stiffened plates with different boundary conditions and

the results were compared with existing published data to examine the performance of the proposed model. The proposed method was subsequently applied to parametric studies on an eccentrically stiffened window to check the possibility of using stiffeners to improve the sound insulation of a practical window.

The layout of this chapter is as follows. Section 7.2 provides a summary of the proposed method, while Sec. 7.3 reports the numerical studies. Finally, a summary is given in Sec. 7.4.

7.2 Theoretical Framework

The same problem as described in Chapter 5.2.1 is now investigated by using the “beam-type stiffener” model. The detail of the model is described in this subsection. Based on the coupled FEM/BEM method in Chapter 5.2.2, the expressions for the coupled vibroacoustic problem (see Fig. 5.2) can be given by

$$\{U\} = \left[-\omega^2 \{M\} - j\omega \{D\} + \{K\} - 2\{\mathcal{I}\}\{H\}\{\mathcal{R}\} \right]^{-1} \{\mathcal{I}\}\{P_0\}. \quad (7.1)$$

$$\{P^+\} = \{P_0\} + \{H\}\{\mathcal{R}\}\{U\}, \quad (7.2)$$

$$\{P^-\} = -\{H\}\{\mathcal{R}\}\{U\}, \quad (7.3)$$

$$\text{STL} = 10 \log_{10} \left(\frac{\text{Re} \left[\{P^+\}^T \left(\{\mathcal{R}\}\{U\} \right)^* \right]}{\text{Re} \left[\{P^-\}^T \left(-\{\mathcal{R}\}\{U\} \right)^* \right]} \right), \quad (7.4)$$

$$\text{STL}_{\text{overall}} = 10 \log_{10} \left(\frac{\sum_{f=f_1}^{f_2} \text{Re} \left[\{P^+\}^T (\{\mathcal{R}\} \{U\})^* \right]}{\sum_{f=f_1}^{f_2} \text{Re} \left[\{P^-\}^T (-\{\mathcal{R}\} \{U\})^* \right]} \right). \quad (7.5)$$

The meanings of the notations are the same as in Chapter 5.2.2. But since the in-plane deformation of the plate is taken into account, the matrices $\{M\}$ and $\{K\}$ need to be modified. To determine these matrices, the stiffened plate element provided by Barik et al. [59] is adopted, in which the displacement field contains the in-plane displacements (u and v), the transverse displacement (w) and the rotational displacements ($\frac{\partial w}{\partial x}$ and $\frac{\partial w}{\partial y}$). The advantages of this element are (1) the in-plane displacements are taken into account, and (2) the stiffeners can be of arbitrary shape and their positions inside the element are without restriction. The stiffness matrix and the mass matrix of this stiffened plate element are given as,

$$\{K_{ps}\}_e = \{K_p\}_e + \{K_s\}_e, \quad (7.6)$$

and

$$\{M_{ps}\}_e = \{M_p\}_e + \{M_s\}_e, \quad (7.7)$$

where $\{K_p\}_e$ and $\{K_s\}_e$ are the stiffness matrices of the plate element and the stiffener element, respectively, and $\{M_p\}_e$ and $\{M_s\}_e$ are the mass matrices of the plate element and the stiffener element, respectively, given as,

$$\{M_p\}_e = \rho_p h \iint \{N\}^T \{P\} \{N\} dx dy, \quad (7.8)$$

$$\{M_s\}_e = \rho_s \int \{N\}^T \{T_s'\}^T \{P_s\} \{T_s'\} \{N\} dl_{se}, \quad (7.9)$$

$$\{K_p\}_e = \iint \{B_p\}^T \{D_p\} \{B_p\} dx dy, \quad (7.10)$$

and

$$\{K_s\}_e = \int \left(\{T_s\} \{B_p\} \right)^T \{D_s\} \left(\{T_s\} \{B_p\} \right) dl_{se}. \quad (7.11)$$

The subscripts “ p ” and “ s ” represent the plate and the stiffener, respectively. ρ is the density, h is the plate’s thickness, $\{N\}$ is the shape function vectors for the displacements (including the transverse and in-plane displacements), l_{se} is taken along the stiffener axis, $\{P\}$ is a diagonal matrix (which is a function of h), $\{D\}$ is the rigidity matrix, $\{B\}$ is the strain matrix, and $\{T_s\}$ and $\{T_s'\}$ are the transformation matrices relating stiffener global and local axes (which are functions of θ). θ is the angle between the global axis and the local axis of the stiffener, as shown in Fig. 5.3). Details about these matrices can be found in reference 59.

The elastic boundary is idealized by combining elastic springs with k_{tb} , k_{rb} , k_{nb} , and k_{mb} denoting linear stiffnesses (spring constants) in the transverse direction, in the rotational directions, in the in-plane direction normal to the edge, and in the in-plane direction tangential to the edge, respectively (see Fig. 7.1). The strain energy Π_{be} of the elastic boundary in the plate element, as shown in Fig. 5.3, can be given by

$$\Pi_{be} = \int \left(\frac{1}{2} k_{tb} w^2 + \frac{1}{2} k_{rb} \left(\frac{\partial w}{\partial \bar{n}_b} \right)^2 + \frac{1}{2} k_{nb} \left[(u(\bar{x} \cdot \bar{n}_b))^2 + (v(\bar{y} \cdot \bar{n}_b))^2 \right] \right) d\Gamma_b, \quad (7.12)$$

$$\left(+ \frac{1}{2} k_{mb} \left[(u(\bar{x} \cdot \bar{n}_\Gamma))^2 + (v(\bar{y} \cdot \bar{n}_\Gamma))^2 \right] \right)$$

where the superscript arrow indicates the unit vector, \bar{n}_b , \bar{n}_Γ are the unit normal vector and the unit tangent vector of the element boundary contour Γ_b (see Fig.

5.3). Eq. (7.12) can be written as

$$\Pi_{be} = \frac{1}{2} \{U\}_e^T \{K_b\}_e \{U\}_e, \quad (7.13)$$

where $\{U\}_e$ is the nodal displacement vector of the element (including the in-plane displacements). $\{K_b\}_e$ can be expressed by,

$$\{K_b\}_e = \int \left(\begin{array}{l} \frac{1}{2} k_{tb} \{N_w\}^T \{N_w\} + \frac{1}{2} k_{rb} \left\{ \frac{\partial N_w}{\partial \bar{n}_b} \right\}^T \left\{ \frac{\partial N_w}{\partial \bar{n}_b} \right\} \\ + \frac{1}{2} k_{nb} \left[\{N_u\}^T \{N_u\} (\bar{x} \cdot \bar{n}_b)^2 + \{N_v\}^T \{N_v\} (\bar{y} \cdot \bar{n}_b)^2 \right] \\ + \frac{1}{2} k_{mb} \left[\{N_u\}^T \{N_u\} (\bar{x} \cdot \bar{n}_\Gamma)^2 + \{N_v\}^T \{N_v\} (\bar{y} \cdot \bar{n}_\Gamma)^2 \right] \end{array} \right) d\Gamma_b, \quad (7.14)$$

where $\{N_w\}$, $\{N_u\}$ and $\{N_v\}$ are the shape functions [59].

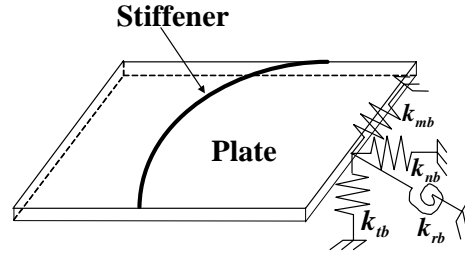


Figure 7.1 Elastic boundary supports along the edges (for simplicity and clarity, only the supports along the right edge are shown)

Once the mass matrix $\{M_{ps}\}_e$ and the stiffness matrices $\{K_{ps}\}_e$ and $\{K_b\}_e$ are solved by Eqs. (7.6), (7.7) and (7.14), the contributions of the elastic boundary supports and the stiffeners to the global mass matrix $\{M\}$ and global stiffness

matrix $\{K\}$ of the whole stiffened plate system in Eq. (7.1) can be obtained according to the finite element assembly procedure [51].

7.3 Numerical Results and Discussion

7.3.1 Concentrically Stiffened Plate

A square plate clamped in all edges having a centrally placed concentric stiffener has been analyzed by Nair and Rao [88] and several other investigators [59, 89], as shown in Fig. 7.2. The plate was 0.6 m long, 0.6 m wide, and 1 mm thick, with a central stiffener (3.11 mm \times 20.25 mm) lying in the width direction. The plate and the stiffener were made of the same material, with Young's modulus 68.7 GPa, density 2780 kg/m³, and Poisson's ratio 0.34. The first six natural frequencies of this stiffened plate were calculated using the present method, with k_{tb} , k_{rb} , k_{nb} , and k_{mb} set to ∞ to represent the clamped boundary condition. Table 7.1 shows the calculation results compared with those of the previous investigators; good agreement can be seen among these results.

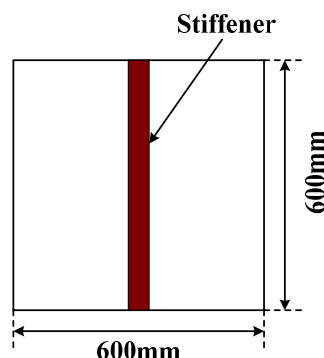


Figure 7.2 A sketch of the concentrically stiffened plate

Table 7.1 Natural frequencies of the clamped plate with a concentric stiffener

Method	Mesh size	Natural frequency (Hz)					
		1	2	3	4	5	6
Present	16×16	50.13	63.41	74.08	84.25	111.93	118.37
Barik et al. [59]	16×16	50.15	63.41	74.13	84.24	111.99	118.34
Nair et al. [88]		50.45	63.71	75.16	85.50	113.69	120.89
Sheikh et al. [89]	10×8	50.43	63.72	75.07	85.46	113.96	120.82

7.3.2 Eccentrically Stiffened Plate

A square plate clamped in all edges having a centrally placed eccentric stiffener has been analyzed by Aksu [90] and several other investigators [57, 91, 92]. The plate was 0.41 m long, 0.60 m wide, and 6.33 mm thick, with a central stiffener (12.7 mm × 22.2 mm) lying in the width direction. The plate and the stiffener were made of the same material, with Young's modulus 211 GPa, density 7830 kg/m³, and Poisson's ratio 0.3. The first three natural frequencies of this stiffened plate were calculated using the present method, with k_{tb} , k_{rb} , k_{nb} and k_{rb} set to set to ∞ and k_{rb} set to 0, to represent the simply supported boundary condition. Table 7.2 shows the calculation results compared with those of the previous investigators; again, good agreement can be seen among these results.

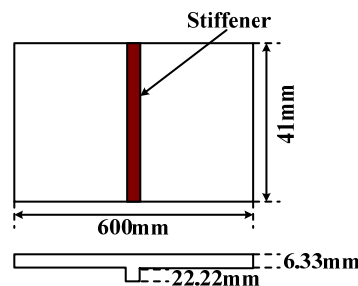


Figure 7.3 A sketch of the eccentrically stiffened plate

Table 7.2 Natural frequencies of the simply supported plate with an eccentric stiffener

Method	Mesh size	Natural frequency (Hz)		
		1	2	3
Present	8×12	254.57	273.89	521.52
Mukherjee et al. [91]		257.05	272.10	524.70
Aksu [90]	8×12	254.94	269.46	511.64
Harik et al. [92]		253.59	282.02	513.50

7.3.3 Stiffened Window Simulation

As reported in this subsection, parametric studies were next carried out on a stiffened glass window to examine the effects of stiffeners on the window's STL. The window's Young's modulus, density, Poisson's ratio, and damping factor were 65 GPa, 2500 kg/m³, 0.25, and 0.003, respectively. Since the boundary condition of a practical window in a building is usually neither simply supported nor clamped but lies in between [78, 79], the boundary parameters k_{tb} , k_{rb} and k_{nb} were set to ∞ while \bar{k}_{rb} was set to 10, in this parametric study. In real applications, one can use the boundary condition identification (BCI) method in Chapter 3 to determine the approximate boundary condition of a practical window. Considering the window's transparency, the stiffeners were made of the same material as the window. Also, curved stiffeners were used in this study. They were seldom reported in the available literature but could have potential applications to window design (e.g., design from an aesthetic point of view). Fig. 7.2 shows the schematic diagram of the stiffened window, which was 65 cm long, 65 cm wide, and 5 mm thick. Four identical

quarter-circle-shaped eccentric stiffeners with a radius of r_s were located at each corner of the window. The cross-section dimensions of the stiffener cross section had a width of 5 mm and a thickness of 20 mm. As shown in the figure, the location of the stiffeners now was dependent only on radius r_s . In the following analysis, the effects of different locations of the stiffeners were examined by changing the value of r_s . The element number used here was 64 (8×8).

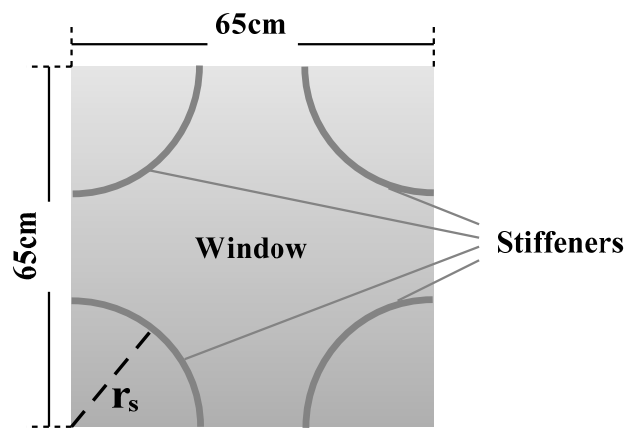


Figure 7.4 Schematic diagram of the stiffened window

Fig. 7.3 shows the effect of the stiffener location on the STL of the window; for comparison, the STL curve of the same window but without stiffeners is included. Because of its additional stiffness, the stiffened window has a higher fundamental natural frequency than the unstiffened window. The window's resonance frequencies change with the location of the stiffeners (or r_s). Fig. 7.4 shows the overall STL values in the frequency range 25Hz~100Hz for different r_s . The reason to choose this range has been explained in Chapter 5.4. It can be seen from Fig. 7.4 that the

stiffener location (or r_s) has a notable effect on the overall STL of the window. In this case, the window with the stiffeners of $r_s = 40$ cm has the largest overall STL, which is about 27 dB higher than that of the unstiffened window. This is because, as shown in Fig. 7.3, the fundamental resonance frequency of $r_s = 40$ cm is beyond the frequency range (25Hz~100Hz). Fig. 7.4 also shows that the window with the stiffener of $r_s = 10$ cm or 20 cm has an even lower overall STL than the unstiffened window, indicating that stiffening the window at the proper locations is also important.

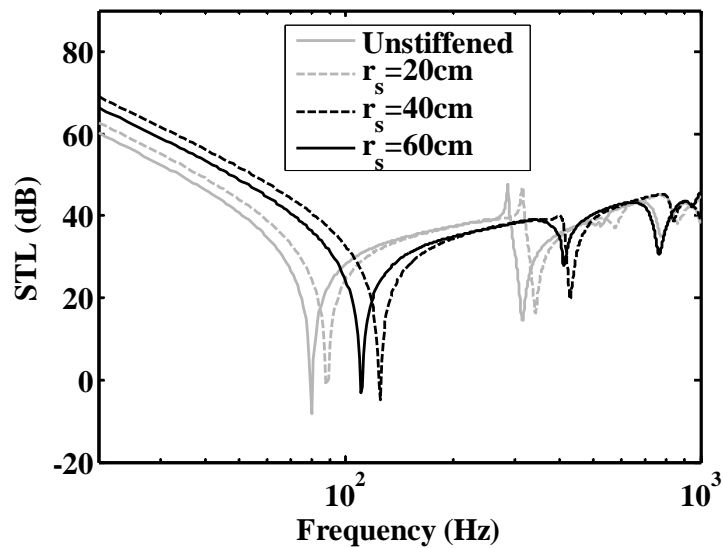


Figure 7.5 STL plotted as a function of frequency for different values of r_s

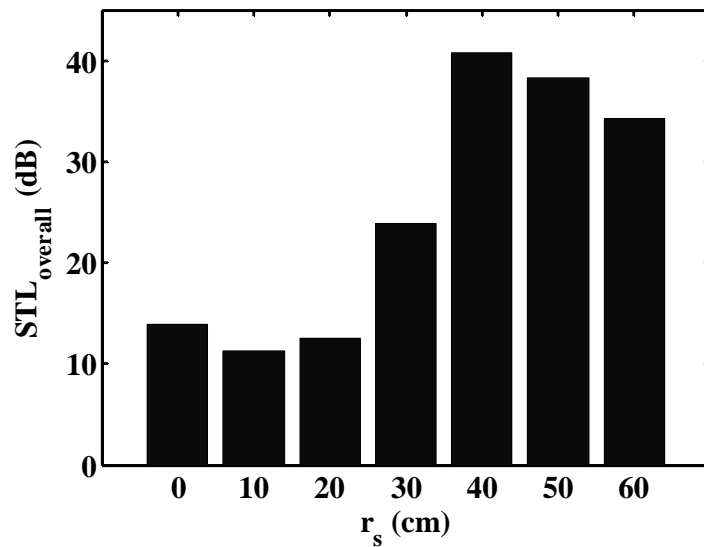


Figure 7.6 Overall STL values (25Hz~100 Hz) as a function of r_s

The simulations in this parametric study have shown that stiffeners have a significant effect on the STL of a window. Resonance frequencies are notably influenced by stiffeners (or their locations). Stiffening the window at proper positions could thus be a potential way to improve its sound insulation in the frequency range of interest.

7.4 Summary

In this chapter, a method was used to examine the steady-state vibration and sound radiation (SVSR) of stiffened plate structures. Similar to Chapter 5, this approach was developed based on the coupled FEM/BEM method, allowing the plate to have arbitrary elastic boundary conditions and arbitrarily located stiffeners, and taking into account the fluid loading effect. The difference was that the “beam-type

stiffener” model was used instead of the “spring-type stiffener” model. Moreover, the in-plane deformation of the plate was taken into account that can improve the model accuracy (especially for eccentrically stiffened plates).

Numerical studies were conducted to analyze the natural frequencies of concentrically/eccentrically stiffened plates with different boundary conditions and the results showed good agreement with earlier published results. Parametric studies were carried out on a glass window stiffened by curved stiffeners. Similar to Chapter 5, the results also showed that the stiffeners had a significant effect on the window’s STL and the overall STL in the frequency range of interest could be effectively increased by stiffening the window at proper positions.

Chapter 8

A Study of the Effects of Beam-type Stiffeners on the Transient Vibroacoustic Response of a Single Plate with General Elastic Boundary Conditions

8.1 Introduction

In Chapter 7, the “beam-type stiffener” model has been adopted in a frequency-domain FEM/BEM model to examine the effects of stiffeners on the steady-state vibration and sound radiation (SVSR) of stiffened plate structures. In order to systematically study the stiffened plate-like structures, a time-domain prediction model was developed in this chapter based on the “beam-type stiffener” model that was more efficient to solve the transient vibroacoustic problems. The time-domain finite element method (TDFEM) and time domain boundary element method (TDBEM) in Chapter 4 were used in the model. Similar to the model developed in Chapter 7, this approach allowed the plate to have arbitrary elastic boundary conditions and arbitrarily located stiffeners. This approach took into account of the plate in-plane deformation. To validate the proposed method, numerical studies were conducted to analyze the transient vibration of a stiffened

plate and the results were compared with existing published data. The proposed method was subsequently applied to parametric studies on an eccentrically stiffened window to check the possibility of improving the TVSR insulation properties of a practical window by using stiffeners.

The layout of this chapter is as follows. Section 8.2 provides an outline of the proposed method, while Sec. 8.3 reports the numerical studies. Finally, Sec. 8.4 presents the summary.

8.2 Theoretical Framework

The same problem as described in Chapter 6.2.1 is now investigated by using the “beam-type stiffener” model. Based on the TDFEM and TDBEM in Chapter 4.2, the expressions for the vibration responses of the plate system (see Fig. 6.1) to transient excitations and the corresponding radiated sound field can be given by

$$\{M\}\{\ddot{U}\} + \{D\}\{\dot{U}\} + \{K\}\{U\} = \{F(t)\} + \{\mathcal{S}\}\{p_0(t)\}, \quad (8.1)$$

and

$$p(\xi, t) = \int_{S_p} \int_0^t \rho_0 \sigma_H(x, t; \xi, \tau) \ddot{w}(x, \tau) d\tau dS. \quad (8.2)$$

The element, mesh method and numerical implementation method used in the TDFEM and TDBEM are the same as in Chapter 4.2. It is worth mentioning that $\{M\}$ and $\{K\}$ in Eq. (8.1) are the global mass and stiffness matrices (respectively)

of the whole stiffened plate system that need to include the mass and stiffness matrices of the stiffeners. The “beam-type stiffener” model is used to determine the matrices for the stiffeners, in which the stiffened plate element provided by Barik et al. [59] is adopted. The determination of the global mass and stiffness matrices $\{M\}$ and $\{K\}$ have been described in detail in Chapter 7.2 and can be found there.

8.3 Numerical Results and Discussion

8.3.1 Comparisons with Existing Published Results

The transient deflection response of a simply supported plate (Fig. 8.1) subjected by a suddenly applied uniform pressure of 0.3 MPa over the entire plate surface has been studied by the proposed method. The plate was 0.203 m long, 0.203 m wide, and 1.37 mm thick with a central eccentric stiffener (6.35 mm \times 11.33 mm). The plate and the stiffener were made of the same material with Young’s modulus 68.9 GPa, density 2670 kg/m³, and Poisson’s ratio 0.3. The boundary parameters $k_{tb} = \infty$, $k_{nb} = \infty$, $k_{mb} = \infty$ and $k_{rb} = 0$ were used to represent the simply supported boundary condition. The element number was 256 (16 \times 16) and the time step was 0.05 ms. The time history of deflection at point “B” obtained by the proposed method is presented with those of Jiang and Olson [93] and Sheikh and Mukhopadhyay [94] in Fig. 8.2. A good agreement can be seen among these results. The location of point “B” is shown in the figure.

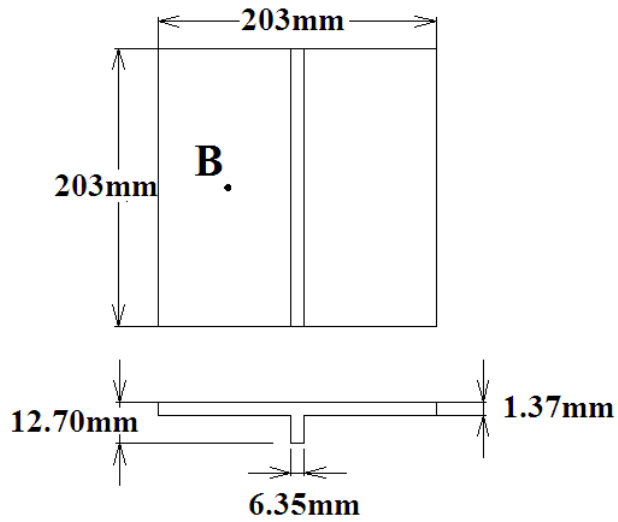


Figure 8.1 A simply supported stiffened plate. Point B is at the center of the left half panel

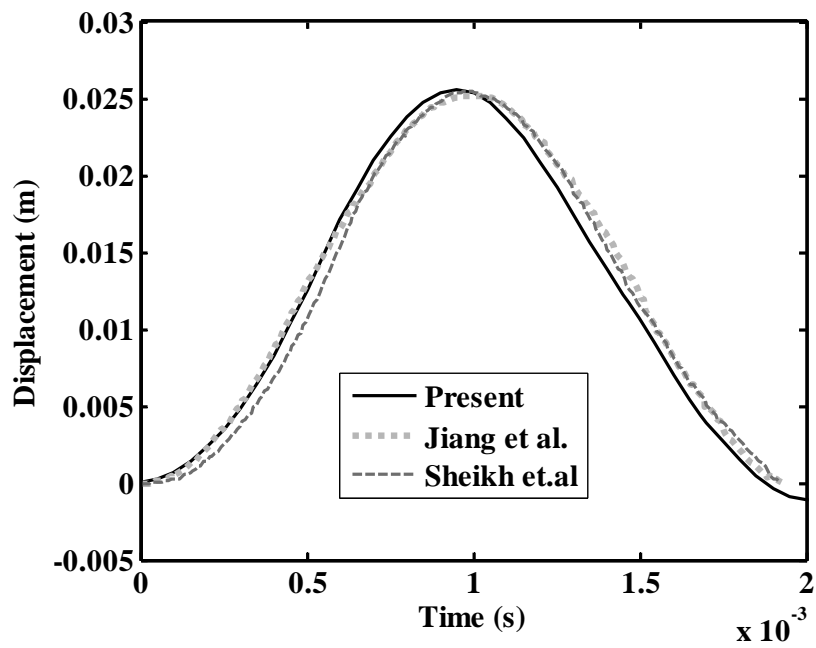


Figure 8.2 Time history of deflection at point "B" of the stiffened plate. Point "B" is shown in Fig. 8.1

8.3.2 Parametric Studies

Parametric studies were carried out on an eccentrically stiffened glass window to examine the effects of the stiffeners on the transient vibration and sound radiation (TVSR). The window was 70 cm long, 70 cm wide and 5 mm thick, with the Young's modulus 65GPa, density 2500 kg/m³, Poisson's ratio 0.25, and damping factor 0.01. The boundary parameters k_{tb} , k_{rb} and k_{nb} were set to ∞ while \bar{k}_{rb} was set to 10. Curve stiffeners were used in this parametric study. As shown in Fig. 8.3, four identical quarter-circular shape eccentric stiffeners with a radius of r_s were located at each corner of the window. Considering the window's transparency, the stiffeners were made of the same material as the window. The cross-section dimensions of the stiffener cross section are 5 mm in width and 20 mm in thickness. It can be seen from the figure that the location of the stiffeners was only dependent on the radius r_s . The effects of different locations of the stiffeners on the TVSR were examined by changing the value of r_s .

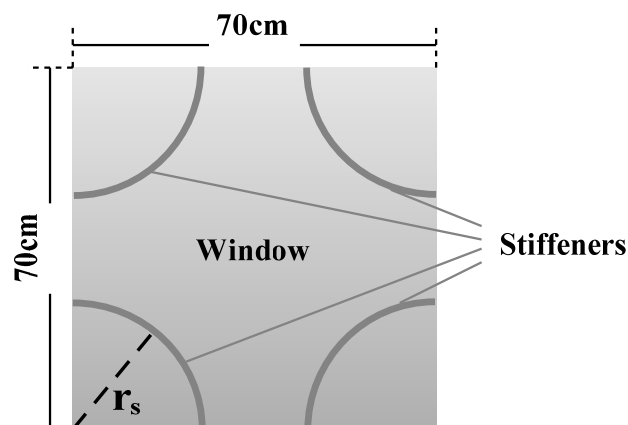
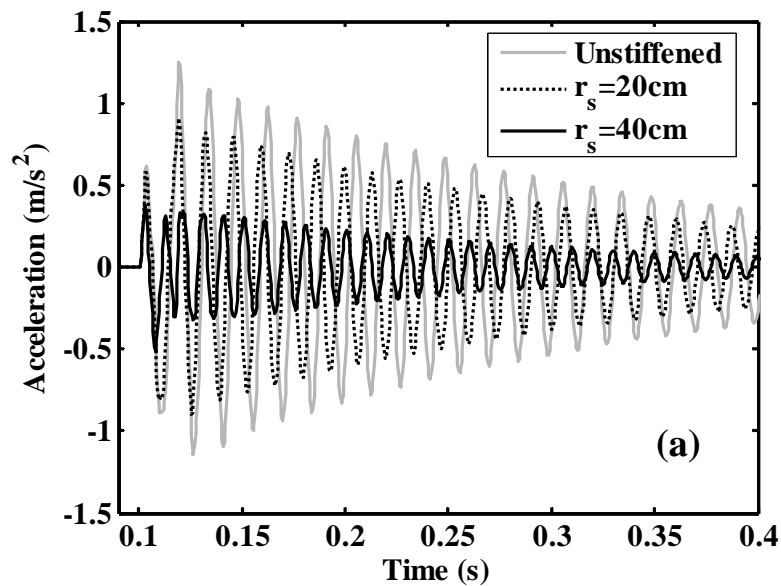


Figure 8.3 Schematic diagram of the stiffened window

The same transient sound pulse as in Chapter 6.4 (see Fig. 6.7) was used as the impact source. Fig. 8.4 shows the resulting acceleration response at the center of the window while Fig. 8.5 shows the resulting radiated sound pressure at point “P”. Point “P” is on the axis of symmetry a distance of 0.1 m away from the window. For comparison, the predictions of the same window without stiffeners are also included in the figures. To make more comprehensive comparisons between these responses, a fast Fourier transform (FFT) was used to convert the responses into frequency spectrum data. The element number and time interval Δt used in the numerical calculation were 64 (8×8) and 0.5 ms, respectively.



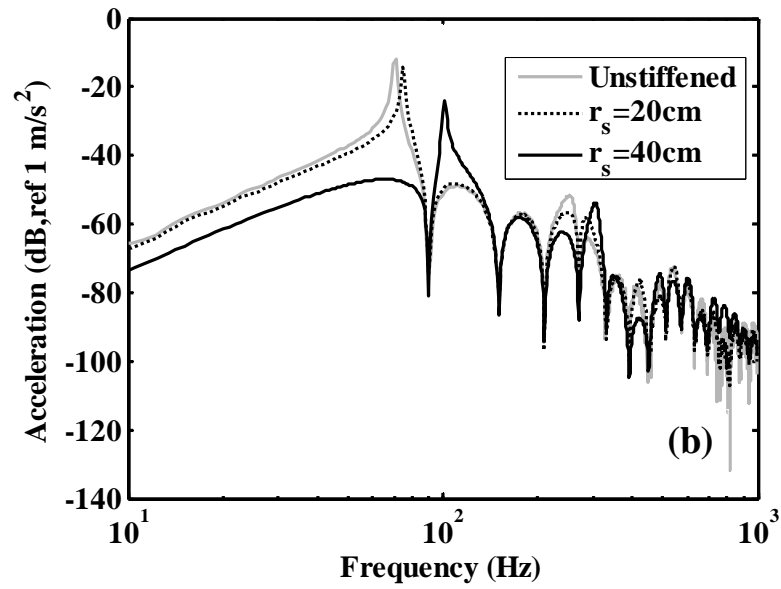
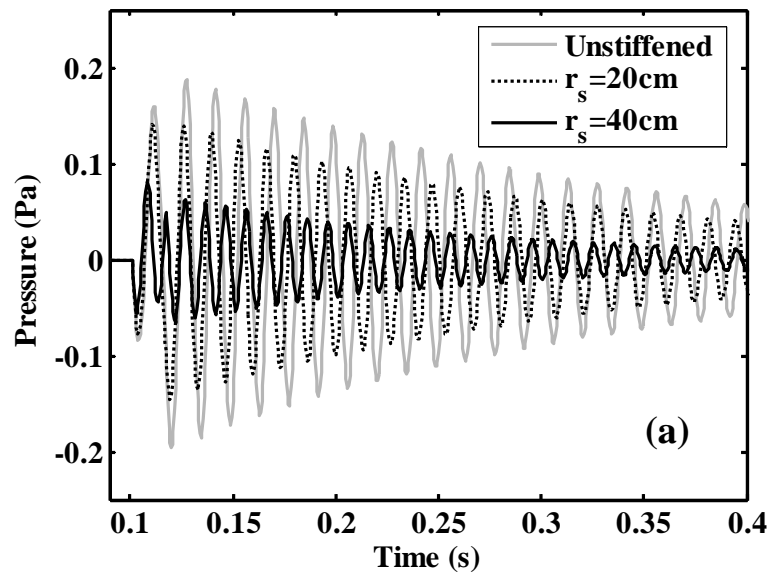


Figure 8.4 Acceleration responses at the center of the window: (a) Acceleration time history; (b) Acceleration frequency spectrum



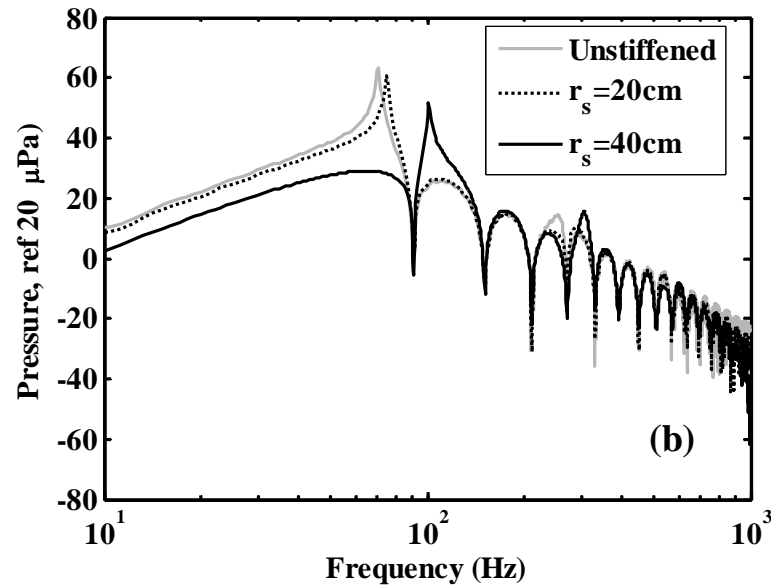
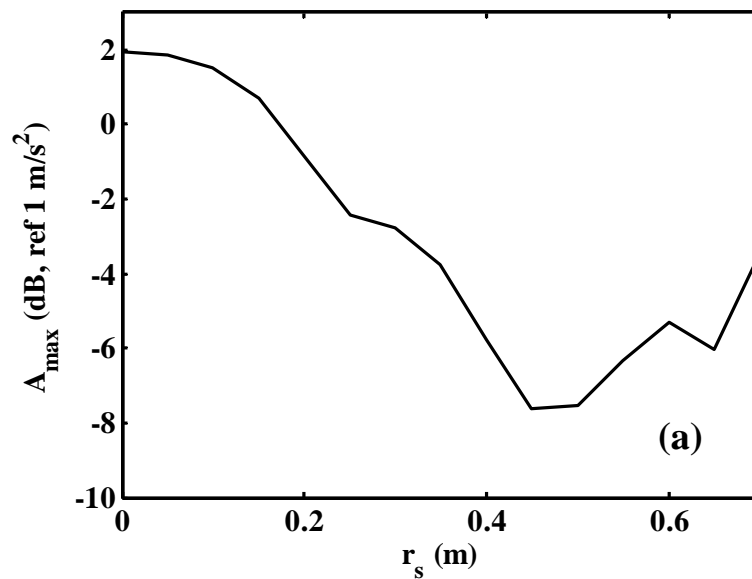


Figure 8.5 Radiated sound pressure at point “P”: (a) Pressure time history; (b) Pressure frequency spectrum. Point “P” is on the axis of symmetry a distance of **0.1 m** away from the window

It can be seen clearly from Figs. 8.4 and 8.5 that the TVSR responses of the stiffened window are different from those of the unstiffened window. Also, different stiffener locations (or r_s) lead to different TVSR responses. This is because the addition of the stiffeners or the change of the stiffener locations can notably influence the resonance frequencies of the structure (window). By shifting the resonance frequencies to higher values, the final TVSR responses of the structure (window) can be reduced when impacted by loadings having higher energy in low-frequency range (like the impact sound source used in this case).

The maximum values of the acceleration level and radiated sound pressure level

obtained from the TVSR responses are shown in Fig. 8.6 as a function of r_s . The calculation equations for these values can be found in Chapter 6.4. It can be seen from the figure that the stiffener location (or r_s) has a notable effect on A_{\max} and SPL_{\max} of the window. In this case, there exists an optimum value (around $r_s = 45$ cm) at which A_{\max} and SPL_{\max} are minimized. Reductions of about 10 dB and 8 dB can be obtained in A_{\max} and SPL_{\max} , respectively, in comparison with those of the unstiffened window.



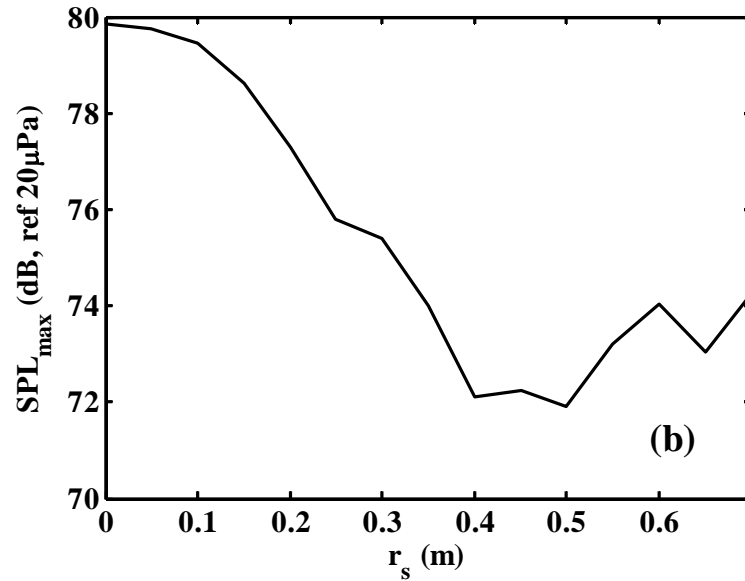


Figure 8.6 The maximum values of the acceleration level and radiated sound pressure level as a function of r_s : (a) Maximum acceleration level; (b) Maximum radiated sound pressure level

8.4 Summary

In this chapter, a time-domain prediction method has been developed to examine the transient vibration and sound radiation (TVSR) of a stiffened plate. Similar to Chapter 6, this approach was developed based on the TDFEM and TDBEM, allowing the plate to have arbitrary elastic boundary conditions and arbitrarily located stiffeners. The difference was that the “beam-type stiffener” model was used instead of the “spring-type stiffener” model and the in-plane deformation of the plate was also taken into account.

The performance of the proposed method was checked by analyzing the transient

response of a stiffened plate and comparing the results with those of earlier published work; a good agreement could be seen among these results. Parametric studies were carried out on a glass window stiffened by curved stiffeners. Similar to Chapter 6, the results also showed that the stiffeners had a significant effect on the window's TVSR and the maximum values of the acceleration and radiated sound pressure could be effectively reduced by using appropriate stiffeners.

Chapter 9

Conclusions and Suggestions for Future Work

9.1 Conclusion

Several efficient prediction methods have been proposed in this study to examine the effects of the elastic boundary supports (i.e., boundary conditions) and the stiffeners on the vibroacoustic performance of plate structures so as to optimize the design and installation of such structures for sound insulation (or vibration isolation). Experiments have been carried out at The Hong Kong Polytechnic University to validate the proposed methods. The predictions agreed well with the experimental data. A window is a typical plate structure that forms a major noise transmission path in residential buildings. The vibroacoustic performance of the window has therefore been examined in the parametric studies by each of the proposed methods.

The first proposed method was an identification method which could be used to identify the actual boundary condition of the plate structures. The method was developed based on a couple finite element method and boundary element method (FEM/BEM) and took into account of the fluid loading effects. This method was able

to identify structural boundary conditions with a higher accuracy and had the potential to be applied to structures in contact with liquid. The boundary conditions along the four edges of the plate were supposed to be uniform when using this identification method and The procedure could be summarized as follows: (1) measure several low-order natural frequencies of the plate system; (2) establish the relationship curves between the measured natural frequencies and the system's boundary conditions; and (3) find a most possible boundary condition by using these curves. The capability of the proposed method was verified by the identifications of two Aluminum (Al) plate systems. The results showed the effectiveness of the proposed method. The proposed method could be a useful auxiliary tool for the analysis of plate structures since the boundary condition is important but difficult to be directly measured.

The second proposed method was developed to examine the effects of elastic boundary conditions on the transient vibration and sound radiation (TVSR) of plate-like structures. The method was based on the time-domain finite element method (TDFEM) and time-domain boundary element method (TDBEM); this allowed the plate to have arbitrary elastic boundary conditions. The TVSR of an Al plate system with a non-classical boundary condition in two connected semi-anechoic chambers was measured. The actual boundary condition of the plate

system was determined by using the first proposed method and treated as an input of the proposed method. The predicted results agreed well with the experimental data. In the subsequent parametric studies, the TVSR of a single-pane glass window with general boundary conditions were investigated and the results showed a significant effect of the boundary supports on the window's TVSR. The maximum values of the acceleration and radiated sound pressure were found to be effectively reduced by using appropriate boundary conditions. The possibility of improving the transient vibration and noise isolation performance by selecting appropriate boundary conditions was thereby demonstrated.

The third proposed method, based on a "spring-type stiffener" model, was developed for predicting the steady-state vibration and sound radiation (SVSR) of stiffened plate structures with general boundary conditions. In the proposed method, a coupled frequency-domain finite element and boundary element method (FEM/BEM) was used and the stiffeners were idealized as a combination of masses, translational and rotational springs. The model allowed the plate to have arbitrary elastic boundary conditions and arbitrarily located stiffeners. The sound transmission loss (STL) of a stiffened Al plate system was measured. The experimental data were compared with the prediction results and showed a good agreement. The plate system designed for the experiment had the attraction of simplicity and flexibility and could be a good

example for the design of a stiffened window. The prediction method was subsequently applied to a parametric study that examined the effects of the stiffener on the sound transmission loss (STL) of a window. The possibility of improving sound insulation performance of a practical window by using the stiffener was thereby demonstrated.

The fourth proposed method for estimating the TVSR of the stiffened plate-like structures was developed. The method could be regarded as an extension of the second and third proposed models, in which the TDFEM and TDBEM in the second proposed model and the “spring-type stiffener” model in the third proposed model were utilized. This made the proposed method efficient for solving the transient vibroacoustic response of plate structures with arbitrary elastic boundary conditions and arbitrarily located stiffeners. Experimental measurements with a stiffened Al plate system were carried out to validate the proposed method. The predicted results agreed well with the experimental data. Parametric studies of the effects of various stiffening treatments on the TVSR of the window were also carried out and the results demonstrated the important transient parameters, such as the maximum acceleration and maximum sound radiation, could be effectively reduced by using appropriate stiffeners.

The fifth proposed method was developed with the same attempt as the third proposed method, but based on a “beam-type stiffener” model, to examine the effects of stiffeners on the SVSR of the plate structures. The coupled FEM/BEM was again used in the present model, in which, however, an efficient stiffened-plate element was developed to allow for the analysis of plate structures having arbitrary elastic boundary conditions and arbitrarily located stiffeners that takes into account the plate in-plane deformation. Numerical studies were conducted to analyze the natural frequencies of different types of stiffened plates and the results showed a good agreement with earlier published results. Parametric studies were subsequently carried out on a glass window stiffened by curve-shape stiffeners. The results showed the stiffeners had a significant effect on the window’s STL and the overall STL in the frequency range of interest could be effectively increased by stiffening the window at proper positions.

The sixth proposed method was an extension of the second and fifth proposed methods. The analysis of the TVSR of stiffened plate structures was the purpose of the proposed method which was the same as that of the fourth proposed method. The difference was that the “beam-type stiffener” model was used instead of the “spring-type stiffener” model and the in-plane deformation of the plate was also taken into account. The performance of the proposed method was checked by

analyzing the transient response of a stiffened plate and comparing the results with those of earlier published work; a good agreement could be seen among these results. Parametric studies were carried out on a glass window stiffened by curve-shape stiffeners and the results demonstrated the possibility of improving the transient vibration and noise isolation performance of a practical window by using appropriate stiffeners.

It is hoped that the proposed methods in this study could be useful auxiliary tools in noise and vibration control engineering, especially in the optimization of building structures. Parametric studies on various types of windows in this thesis have shown that (1) it is possible to improve the sound insulation (or vibration isolation) performance of a practical window by using appropriate boundary supports or stiffeners; and (2) the proposed methods can help develop design tools for this purpose.

9.2 Suggestions for Future Work

In order to develop more feasible and powerful prediction methods in practical applications, additional future work is required. Improvements of the theoretical model and experiments are recommended as follows:

Future work can be conducted to improve the proposed models:

1. The Rectangular-shape plate assumption was used in the proposed methods. Additional work is needed to extend the models so that they can be more effective in the analysis of structures with different shapes.
2. Thin-plate theory assumption was used in the proposed methods. Thick-plate theories, such as Timoshenko-Mindlin theory, can be used to improve the methods and make them suitable for analyzing the thick plate structures.
3. Free sound field assumption was used in the proposed methods; however, the practical surrounding environments can influence the radiated sound field of the structures. Environmental factors, such as the room parameters, need to be taken into account in the models when dealing with practical problems.
4. The proposed methods for the SVSR can be applied to very general elastic boundary supports and with fluid loading being accounted for; however, these methods have been applied in this thesis to only uniform boundary conditions and air as the fluid. In the future studies, the SVSR of the plate structure with more complex boundary conditions and in a heavy fluid (like water) should be studied.
5. The proposed methods for the TVSR can be applied to very general elastic boundary supports; however, these methods have been applied in this thesis to only uniform boundary conditions. The TVSR of the plate structure with more

complex boundary conditions should be studied. In addition, the fluid loading effect is not taking into account in the proposed methods. In the future studies, the method should be improved and extended for predicting the TVSR of the plate structure by taking into account the fluid loading effect.

Additional efforts can be sought to improve the experimental studies:

6. Only square plates were used in the parametric studies and the experiments. Non-square plates should be used in the future studies to examine the effects of the plate aspect ratios.
7. Different types of plate frames should be designed to produce different boundary conditions. The effects of the boundary conditions of the plate can then be systematically studied by the experiments. The optimized boundary conditions can then possibly be applied to practical plate systems such as windows.
8. In this thesis, the stiffener with large translational stiffness (k_{ts}) was used in the experimental studies and the mass effect of the stiffener was neglected since the mass was found to have almost no effect on system's response when k_{ts} has large value. In the future studies, the stiffener with smaller translational stiffness should be designed and used in the experiments to examine more systematically the effects of the stiffness and mass of the stiffeners.
9. In this thesis, only the straight-shape stiffener was used in the experimental

studies. Plate systems with curve-shape stiffeners should be designed and used in the future experimental studies to further validate the proposed methods. The optimized curve-shape stiffener layout can then possibly be applied to practical plate systems such as windows.

Appendix

A.1 Mesh Method

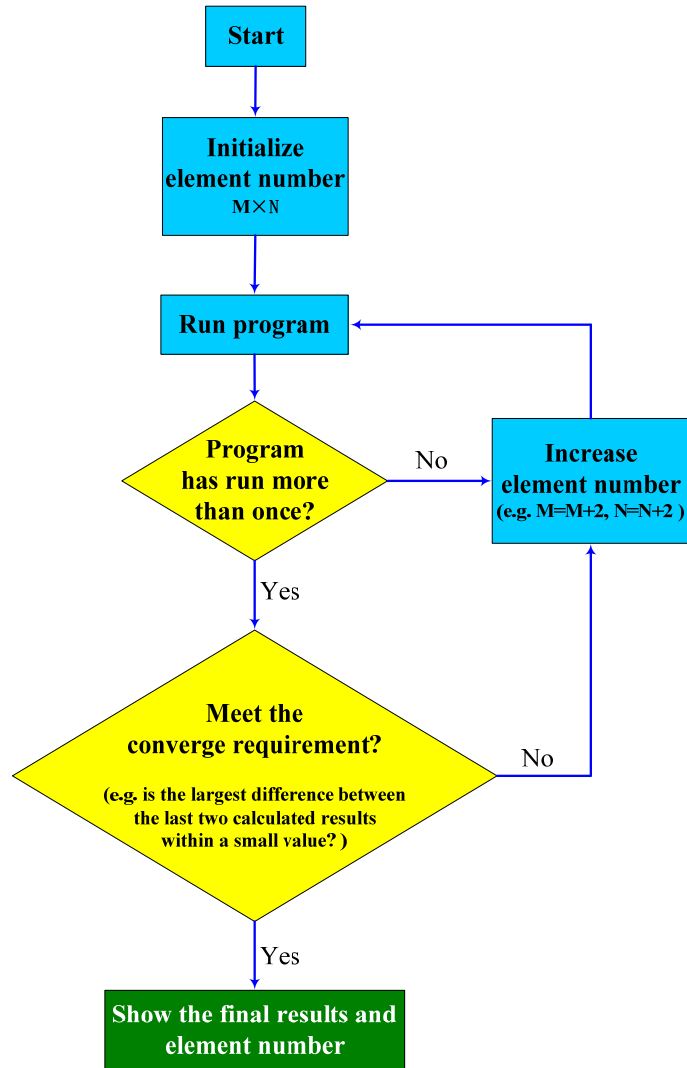


Figure A.1 Flow chart for the decision of mesh size

A.2 Computational Time

Table A. 1 Computational Time & Hardware and Software

	Element number	Computational time
SVSR	8×8 (64)	170ms per Hz (e.g. 1~1000Hz=170s)
TVSR	8×8 (64)	3.9ms per time-step (e.g. if Time-length=1s and Time-step=0.5ms, takes 7.8s)
Hardware and software		
Notebook PC (2009); Intel(R) Core(TM)2 CPU 2.26GHz; 3GB memory; Windows XP; MATLAB 7.0.4. Note: only one core is used when running the software		

A.3 MATLAB Codes

Part of the MATLAB Codes for solving the transient response of plate

```
%=====An example for examining a simply supported plate system=====
```

```
% Main Function
```

```
%=====
```

```
clc,clear
```

```
% Plate dimension
```

```
Lx = 0.80 ;           % Plate length
```

```
Ly = 0.80 ;           % Plate width
```

```
h = 0.005 ;           % Plate thickness
```

```
% Material definition
```

```
E = 65e9 ;           % Young's modulus
```

```
Poisson = 0.25 ;     % Poisson's ratio
```

```
ro= 2500;             % Dentensity of plate
```

```
BB=E*h^3/12/(1-Poisson^2);
```

```
damping_factor=0.01; % Plate damping ratio
```

```
% Fluid material definition
```

```
ro0=1.21;
```

```
c0=344;
```

```
% Element number defination
```

```
Nx = 8 ;
```

```
Ny = 8;
```

```
element_number=Nx*Ny;
```

```
% Create impact incidence wave
```

```
gDeltaT=5e-4;
```

```
tempt=0:gDeltaT:1.5;
```

```
gTimeEnd = max(tempt);
```

```
timestep_number = length(tempt);
```

```
%=====Triangular plane wave=====
```

```
rise_T=0.021;
```

```
temptt0=0:gDeltaT:0.1;
```

```
temptt1=0:gDeltaT:rise_T;
```

```
temptt2=rise_T:gDeltaT:2*rise_T;
```

```
amplitude_p0=10;
```

```

signal_t=[zeros(1,length(temptt0)),amplitude_p0*temptt1/rise_T,-amplitude_p0/rise
_T*temptt2+2*amplitude_p0];
Plane_Source_amp=zeros(1,length(tempt));
Plane_Source_amp(1:length(signal_t))=signal_t;
gload_f=fun_gload_f(Plane_Source_amp, Tp2f);
%Tp2f --- transformation matrix converting the incidence sound pressure to point
forces that act on the nodes of the plate
%=====

% calculating the proportional coefficient for the damping
Damp_K=fun_Damp_K(Lx,Ly,h,ro,BB);
%=====

% Calculation of the element stiffness matrix of
% the simply supported boundary support
Kbe=fun_Kbe(Nw, 1e10);
%=====

% Calculation of the matrices for the plate using finite element assembly procedure
[K, M, D]=Element_Synthesize(Kpe, Kbe, Mpe, Damp_K);
%Kpe --- stiffness matrix of the plate element without the boundary support
%Mpe --- mass matrix of the plate element without the boundary support
%=====

% Calculation of transient response of the plate
[gDisp, gVelo, gAcce] = SolveModel_Newmark(K, M, D, Nx, Ny, gDeltaT,
gTimeEnd, timestep_number, gload_f);
%=====

% Some important sub-functions

% function for converting the pressure to point forces that act on the plate nodes
function gload_f=fun_gload_f(Source, Tran_Matrix)
gload_f= Source*Tran_Matrix;
return
%=====

% function for calculating the proportional coefficient for the damping
function Damp_K=fun_Damp_K(Lx, Ly, h, ro, BB)
natural_omega0=fun_natural_omega0(Lx, Ly, h, ro, BB);

```

```

Damp_K=2*damping_factor/natural_omega0;
return
%=====

% function for calculating the fundamental natural frequency
% for a simply supported plate
function natural_omega0= fun_natural_omega0(Lx, Ly, h, ro, BB)
natural_omega0=sqrt(BB/ro/h)*((pi/Lx)^2+(pi/Ly)^2);
return
%=====

% function for calculating the stiffness matrix of the boundary supports
% of a simply supported plate
%=====
% N----Shape function vectors
% k-----Spring constant
function Kbe=fun_Kbe(N, k)
syms x y
x_y=[x, x, y, y];
for t=1:4
Kbe(:,t)=inv(k*(N(t,:).'*N(t:)), x_y(t), -1, 1);
end
return
%=====

%===== Newmark_method=====
function [gDisp, gVelo, gAcce] = SolveModel_Newmark(K, M, D, Nx, Ny, gDeltaT,
gTimeEnd, timestep_number, gload_f)
% gDisp, gVelo, gAcce --- displacement, velocity and acceleration of nodes
%=====
node_number=(Nx+1)*(Ny+1);
gama = 0.50;
beta = 0.25 ;
alpha0 = 1/beta/gDeltaT^2 ;
alpha1 = gama/beta/gDeltaT ;
alpha2 = 1/beta/gDeltaT ;
alpha3 = 1/2/beta - 1 ;
alpha4 = gama/beta - 1 ;
alpha5 = gDeltaT/2*(gama/beta-2) ;
alpha6 = gDeltaT*(1-gama) ;
alpha7 = gama*gDeltaT ;

```

```

K1 = K + alpha0*M + alpha1*D;
[KL,KU] = lu(K1) ;
for i=2:1:timestep_number+1
f1=gload_f(:,i-1)+M*(alpha0*gDisp(:,i-1)+alpha2*gVelo(:,i-1)+alpha3*gAcce(:,i-1)
)+D*(alpha1*gDisp(:,i-1)+alpha4*gVelo(:,i-1)+alpha5*gAcce(:,i-1));
y = KL\f1 ;
gDisp(:,i) = KU\y ;
gAcce(:,i) = alpha0*(gDisp(:,i)-gDisp(:,i-1)) - alpha2*gVelo(:,i-1) -
alpha3*gAcce(:,i-1) ;
gVelo(:,i) = gVelo(:,i-1) + alpha6*gAcce(:,i-1) + alpha7*gAcce(:,i) ;
end
return
%=====

```

A.4 Photos of the Experimental Setup at The Polytechnic University



Figure A.2 The hole of the common wall between the two chambers



Figure A.3 Installation of the plate system



Figure A.4 A view of one of the two chambers after plate installation



Figure A.5 A loudspeaker box as a plane wave source



Figure A.6 A hammer as an impact source



Figure A.7 Microphones setup in the receiving chamber for measuring the radiated (transmitted) sound field

References

- [1] R.D.Mindlin. Influence of rotatory inertia and shear on flexural motions of isotropic, elastic plates. *Journal of Applied Mechanics* 1951; **19**:31-38.
- [2] S.S.Mackertich and S.I.Hayek. Acoustic radiation from an impulsively excited elastic plate. *Journal of the Acoustical Society of America* 1981; **69**:1021-1028.
- [3] A.Akay and M.Latcha. Sound radiation from an impact-excited clamped circular plate in an infinite baffle. *Journal of the Acoustical Society of America* 1983; **74**:640-648.
- [4] A.Berry and J.L.Guyader and J.Nicolas. A general formulation for the sound radiation from rectangular, baffled plates with arbitrary boundary conditions. *Journal of the Acoustical Society of America* 1990; **88**:2792-2802.
- [5] Z.J.Fan. Transient vibration and sound radiation of a rectangular plate with viscoelastic boundary supports. *International Journal for Numerical Methods in Engineering* 2001; **51**:619-630.
- [6] O.Chiello, F.C.Sgard and N.Atalla. On the use of a component mode synthesis technique to investigate the effects of elastic boundary conditions on the transmission loss of baffled. *Computers & Structures* 2003; **81**:2645-2658.
- [7] W.L.Li. Vibration analysis of rectangular plates with general elastic boundary supports. *Journal of Sound and Vibration* 2004; **273**:619-635.
- [8] J.H.Ginsberg and J.G.McDaniel. An acoustic variational principle and component mode synthesis applied to the analysis of acoustic radiation from a concentrically stiffened plate. *Journal of Vibration and Acoustics* 1991; **113**:401-408.
- [9] D.M.Photiadis. Anderson localization of one-dimensional wave propagation on a fluid-loaded plate. *Journal of the Acoustical Society of America* 1992; **91**:771-781.
- [10] J.H.Lee and J.Kim. Analysis of sound transmission through periodically stiffened panels by space-harmonic expansion method. *Journal of Sound and Vibration* 2002; **251**:349-366.

- [11] E.Ventsel and T.Krauthammer. Thin plates and shells: theory analysis and applications. New York: Marcel Dekker; 2001.
- [12] A.W.Leissa. Vibration of plates. New York: Acoustical Society of America; 1993.
- [13] L.L.Beranek. Noise reduction. New York: McGraw-Hill; 1960.
- [14] M.J.Crocker and A.J.Price. Sound transmission using statistical energy analysis. *Journal of Sound and Vibration* 1969; **9**:469-486.
- [15] E.C.Sewell. Transmission of reverberant sound through a single-leaf partition surrounded by an infinite rigid baffle. *Journal of Sound and Vibration* 1970; **12**:21-32.
- [16] K.A.Mulholland and R.H.Lyon. Sound insulation at low-frequencies. *Journal of the Acoustical Society of America* 1973; **54**:867-878.
- [17] F.G.Leppington, K.H.Heron, K.H.Broadbent and S.M.Mead. Resonant and non-resonant acoustic properties of elastic panels. II. The transmission problem. *Proceedings of the Royal Society of London. Series A, Mathematical and Physical Sciences* 1987; **412**:309-337.
- [18] D.Takahashi. Effects of panel boundedness on sound transmission problems. *Journal of the Acoustical Society of America* 1995; **98**:2598-2606.
- [19] A.Osipov, P.Mees and G.Vermeir. Low-frequency airborne sound transmission through single partitions in buildings. *Applied Acoustics* 1997; **52**:273-288.
- [20] I.I.Novikov. Low-frequency sound insulation of thin plates. *Applied Acoustics* 1998; **54**:83-90.
- [21] T.Sakumat and T.Oshima. Numerical vibro-acoustic analysis of sound insulation performance of wall members based on a 3-D transmission model with a membrane/plate. *Acoustical Science and Technology* 2001; **22**:367-369.
- [22] A.Akay. A review of impact noise. *Journal of the Acoustical Society of America* 1978; **64**:977-987.
- [23] M.Strasberg. Radiation from a diaphragm struck periodically by a light mass. *Journal of the Acoustical Society of America* 1948; **20**:683-690.

- [24] Y.Tokita. Vibration of a plate and sound radiation generated by an impulsive force. *Journal of the Physical Society of Japan* 1961; **16**:1008-1019.
- [25] E.B.Magrab and W.T.Reader. Farfield radiation from an infinite elastic plate excited by a transient point loading. *Journal of the Acoustical Society of America* 1968; **44**:1623-1627.
- [26] I.Nakayama, A.Nakamura and R.Takeuchi. Insulation characteristics of a circular plate for a single sound pulse. *Japanese Journal of Applied Physics* 1977; **16**:2285-2286.
- [27] I.Nakayama. Sound insulation of a circular plate for a single sound pulse. *Acustica* 1980; **46**:330-340.
- [28] I.Nakayama, A.Nakamura and R.Takeuchi. Transient radiation field from an elastic circular plate excited by a sound pulse. *Acustica* 1980; **46**:276-282.
- [29] I.Nakayama and A.Nakamura. Mechanism of transient sound radiation from a circular plate for impulsive sound wave. *Journal of the Acoustical Society of Japan* 1981; **2**:151-159.
- [30] A.Berry and J.Nicolas. Structural acoustics and vibration behavior of complex panels. *Applied Acoustics* 1994; **43**:185-215.
- [31] J.Park, L.Mongeau and T.Siegmund. Influence of support properties on the sound radiated from the vibrations of rectangular plates. *Journal of Sound and Vibration* 2003; **264**:775-794.
- [32] A.Berry, J.L.Guyader and J.Nicolas. Reply to " Comments on 'A general formulation for the sound radiation from rectangular, baffled plates with arbitrary boundary conditions' ". *Journal of the Acoustical Society of America* 1992; **92**:2991-2992.
- [33] R.S.Langley. A dynamic stiffness technique for the vibration analysis of stiffened shell structures. *Journal of Sound and Vibration* 1992; **158**:521-540.
- [34] P.A.A.Laura and R.H.Gutierrez. A note on transverse vibrations of stiffened rectangular plates with edges elastically restrained against rotation. *Journal of Sound and Vibration* 1981; **78**:139-144.
- [35] Y.Yun and C.M.Mak. A study of coupled flexural-longitudinal wave motion in

a periodic dual-beam structure with transverse connection. *Journal of the Acoustical Society of America* 2009; **126**:114-121.

[36] J.R.Wu and W.H.Liu. Vibration of rectangular plates with edge restraints and intermediate stiffeners. *Journal of Sound and Vibration* 1988; **123**:103-113.

[37] D.J.Mead. Wave propagation and natural modes in periodic systems: I. Mono-coupled systems. *Journal of Sound and Vibration* 1975; **40**:1-18.

[38] B.R.Mace. Sound radiation from fluid loaded orthogonally stiffened plates. *Journal of Sound and Vibration* 1981; **79**:439-452.

[39] D.J.Mead. Plates with regular stiffening in acoustic media: Vibration and radiation. *Journal of the Acoustical Society of America* 1990; **88**:391-401.

[40] C.H.Hodges and J.Woodhouse. Vibration isolation from irregularity in a nearly periodic structure. *Journal of the Acoustical Society of America* 1983; **73**:894-905.

[41] P.Joshi, S.B.Mulani, S.P.Gurav and R.K.Kapania. Design Optimization for Minimum Sound Radiation from Point-Excited Curvilinearly Stiffened Panel. *Journal of Aircraft* 2010; **47**:1100-1110.

[42] K.Inoue, M.Yamanaka and M.Kihara. Optimum stiffener layout for the reduction of vibration and noise of gearbox housing. *Journal of Mechanical Design* 2002; **124**:518-523.

[43] A.Berry and C.Locqueteau. Vibration and sound radiation of fluid-loaded stiffened plates with consideration of in-plane deformation. *Journal of the Acoustical Society of America* 1996; **100**:312-319.

[44] C.A.Brebbia and S.Walker. Boundary element techniques in engineering. London: Newnes-Butterworths; 1980.

[45] M.M.Hrabok and T.M.Hrudey. A review and catalogue of plate bending finite elements. *Computers & Structures* 1984; **19**:479-495.

[46] R.D.Ciskowski and C.A.Brebbia. Boundary element methods in acoustics. Southampton,Boston: Computational Mechanics Publications; 1991.

[47] G.Bezine and B.Millet. A new plate finite element using integral representation interpolation. *Engineering Analysis with Boundary Elements* 1999; **23**:549-554.

- [48] G.A.Mohr. Finite element solutions for optimal square plates. *International Journal of Mechanical Sciences* 2000; **42**:2337-2345.
- [49] A.G.Razaqpur, M.Nofal and A.Vasilescu. An improved quadrilateral finite element for analysis of thin plates. *Finite Elements in Analysis and Design* 2003; **40**:1-23.
- [50] H.Nguyen Xuan, T.Rabczuk, S.Bordas and J.F.Debongnie. A smoothed finite element method for plate analysis. *Computer Methods in Applied Mechanics and Engineering* 2008; **197**:1184-1203.
- [51] D.C.Robert, S.M.David, E.P.Michael and J.W.Robert. Concepts and Applications of Finite Element Analysis, 4th ed. New York: Wiley; 2002.
- [52] A.B.Andreev, J.T.Maximov and M.R.Racheva. Two approaches to the finite element analysis of the stiffened plates. *Numerical Methods and Applications* 2003; **2542**:353-362.
- [53] M.Barik and M.Mukhopadhyay. Finite element free flexural vibration analysis of arbitrary plates. *Finite Elements in Analysis and Design* 1998; **29**:137-151.
- [54] B.Chattopadhyay, P.K.Sinha and M.Mukhopadhyay. Finite element free vibration analysis of eccentrically stiffened composite plates. *Journal of Reinforced Plastics and Composites* 1992; **11**:1003-1034.
- [55] A.Deb and M.Booton. Finite element models for stiffened plates under transverse loading. *Computers & Structures* 1988; **28**:361-372.
- [56] I.E.Harik and M.Guo. Finite element analysis of eccentrically stiffened plates in free vibration. *Computers & Structures* 1993; **49**:1007-1015.
- [57] T.P.Holopainen. Finite element free vibration analysis of eccentrically stiffened plates. *Computers & Structures* 1995; **56**:993-1007.
- [58] M.Barik and M.Mukhopadhyay. A new stiffened plate element for the analysis of arbitrary plates. *Thin-Walled Structures* 2002; **40**:625-639.
- [59] M.R.Barik and M.Mukhopadhyay. Free flexural vibration analysis of arbitrary plates with arbitrary stiffeners. *Journal of Vibration and Control* 1999; **5**:667-683.
- [60] T.W.Wu. Boundary element acoustics: Fundamentals and Computer codes.

Boston: WIT Press; 2000.

[61] H.A.Schenck. Improved integral formulation for acoustic radiation problems. *Journal of the Acoustical Society of America* 1968; **44**:41-58.

[62] A.F.Seybert and T.K.Rengarajan. The use of chief to obtain unique solutions for acoustic radiation using boundary integral equations. *Journal of the Acoustical Society of America* 1987; **81**:1299-1306.

[63] T.W.Wu and A.F.Seybert. A weighted residual formulation for the chief method in acoustics. *Journal of the Acoustical Society of America* 1991; **90**:1608-1614.

[64] D.J.Segalman and D.W.Lobitz. A method to overcome computational difficulties in the exterior acoustics problem. *Journal of the Acoustical Society of America* 1992; **91**:1855-1861.

[65] A.J.Burton and G.F.Miller. The application of integral equation methods to the solution of some exterior boundary-value problems. *Proceedings of the Royal Society of London. Series A, Mathematical and Physical Sciences* 1971; **323**:201-210.

[66] B.U.Koo, B.C.Lee and J.G.Ih. A non-singular boundary integral equation for acoustic problems. *Journal of Sound and Vibration* 1996; **192**:263-279.

[67] T.W.Wu and A.Dandapani. A boundary element solution for sound transmission through thin panels. *Journal of Sound and Vibration* 1994; **171**:145-157.

[68] S.Kopuz, Y.S.Unlusoy, M.Caliskan. Integrated FEM/BEM approach to the dynamic and acoustic analysis of plate structures. *Engineering Analysis with Boundary Elements* 1996; **17**:269-277.

[69] S.W.Wu, S.W.Wu. A robust formulation for solving fluid-structure interaction problems. *Computational Mechanics* 2001; **27**:69-74.

[70] W.M.Kim, J.T.Kim and J.S.Kim. Development of a criterion for efficient numerical calculation of structural vibration responses. *Journal of Mechanical Science and Technology* 2003; **17**:1148-1155.

[71] D.W.Herrin, F.Martinus, T.W.Wu and A.F.Seybert. An assessment of the high frequency boundary element and Rayleigh integral approximations. *Applied Acoustics* 2006; **67**:819-833.

- [72] H.Ahmadian, J.E.Mottershead and M.I.Friswell. Boundary condition identification by solving characteristic equations. *Journal of Sound and Vibration* 2001; **247**:755-763.
- [73] D.J.Ewins. Modal testing: Theory, Practice and Applications.2nd edition. Baldock: Research Studies Press LTD; 2000.
- [74] A.Craggs. Transient vibration analysis of linear systems using transition matrices. *N.A.S.A. Contractor report* 1968; NASA-CR-1237.
- [75] E.M.Forsyth and G.B.Warburton. Transient vibration of rectangular plates. *Journal Mechanical Engineering Science* 1960; **2**:325-330.
- [76] T.Takahagi and M.Nakai. The approximation of pressure waveforms of impact sound radiation from clamped circular plates of various thicknesses. *Journal of the Acoustical Society of America* 1985; **78**:2049-2057.
- [77] A.Craggs. The response of a simply supported plate to “N” waves at oblique incidence. *Journal of Sound and Vibration* 1971; **16**:293-307.
- [78] J.D.Quirt. Sound Transmission through Window I. Single and Double Glazing. *Journal of the Acoustical Society of America* 1982; **73**:834-844.
- [79] W.A.Utley and B.L.Fletcher. The effect of edge conditions on the sound insulation of double windows. *Journal of Sound and Vibration* 1973; **26**:63-72.
- [80] F.X.Xin and T.J.Lu. Analytical and experimental investigation on transmission loss of clamped double panels: implication of boundary effects. *Journal of the Acoustical Society of America* 2009; **125**:1506-1517.
- [81] K.K.Hodgdon, A.A.Atchley and R.J.Bernhard. Low frequency noise study. *Final report, Partner low frequency study group, Report No PARTNER-COE-2007-001* 2007;16-17.
- [82] B.Berglund, P.Hassmen and R.F.S.Job. Sources and effects of low-frequency noise. *Journal of the Acoustical Society of America* 1996; **99**:2985-3002.
- [83] M.Mukhopadhyay and S.K.Satsangi. Isoparametric stiffened plate bending element for the analysis of ships' structures. *Royal Institution of Naval Architects Transactions* 1984; **126**:144-151.

- [84] B.R.Mace. Periodically stiffened fluid-loaded plates, I- Response to convected harmonic pressure and free wave propagation. *Journal of Sound and Vibration* 1980; **73**:473-486.
- [85] B.R.Mace. Periodically stiffened fluid-loaded plates, II: Response to line and point forces. *Journal of Sound and Vibration* 1980; **73**:487-504.
- [86] R.Vaicaitis and M.Slazak. Noise transmission through stiffened panels. *Journal of Sound and Vibration* 1980; **70**:413-426.
- [87] M.Mukhopadhyay. Vibration and stability analysis of stiffened plates by semi-analytical finite difference method, part II: consideration of bending and axial displacements. *Journal of Sound and Vibration* 1989; **130**:41-53.
- [88] P.S.Nair and M.S.Rao. On vibration of plates with varying stiffener length. *Journal of Sound and Vibration* 1984; **95**:19-29.
- [89] A.H.Sheikh and M.Mukhopadhyay. Free vibration analysis of stiffened plates with arbitrary planform by the general spline finite strip method. *Journal of Sound and Vibration* 1993; **162**:147-164.
- [90] G.Aksu. Free vibration analysis of stiffened plates by including the effect of inplane inertia. *Journal of Applied Mechanics* 1982; **49**:206-212.
- [91] A.Mukherjee and M.Mukhopadhyay. Finite element free vibration of eccentrically stiffened plates. *Computers & Structures* 1988; **30**:1303-1317.
- [92] I.E.Harik and M.Guo. Finite element analysis of eccentrically stiffened plates in free vibration. *Computers & Structures* 1993; **49**:1007-1015.
- [93] J.Jiang and M.D.Olson. Nonlinear dynamic analysis of blast loaded cylindrical shell structures. *Computers & Structures* 1991; **41**:41-52.
- [94] A.H.Sheikh and M.Mukhopadhyay. Linear and nonlinear transient vibration analysis of stiffened plate structures. *Finite Elements in Analysis and Design* 2002; **38**:477-502.